H. W. Buiten

The influence of suction on the shear strength of a clay dike

The influence of suction on the shear strength of a clay dike

By

H.W. Buiten

in partial fulfilment of the requirements for the degree of

Master of Science
in Applied Earth Science

at the Delft University of Technology,
to be defended publicly on 27-08-2020

Supervisor:	Prof. Dr. C. Jommi	TU Delft (Geo-Engineering)
Thesis committee:	Dr. Ir. R.B.J. Brinkgreve	TU Delft (Geo-Engineering
	Dr. J.P. Aguilar-López	TU Delft (Hydraulic Engineering)
	Ir. P. Hopman	Waterschap Drents Overijsselse Delta
	A. Van Duinen MSc.	Deltares

Acknowledgements

After a year of researching this document finalizes my master thesis. It was a special year, with the intelligent lock down which forced everyone to stay home and to work from their home. It was a period in which I gained a lot of insight to myself. Often it was a struggle for me to finish this thesis and I am thankful to all the people who helped to reach this point.

First I would like to thank the members of my assessment committee. I would like to thank Professor C. Jommi for all her advises, remarks and endless explanations during my thesis period. This also applies to Mr. R. Brinkgreve who helped a lot with the structure, possibilities and limitations of the soil models, Plaxis and all of my work in general. I would also like to thank Mr. J. Aguilar-Lopez for the comments, advises and last minute meetings.

Furthermore I would like to thank Deltares for providing the data from the measurements in Oijen and Westervoort. I am grateful to Mr. A. van Duinen for the different insights, remarks and advises while I was working on my thesis.

Additionally I would like to thank Peter Hopman, my daily supervisor at the Waterboard Drents Overijsselse Delta, for his guidance, explanations, remarks, advices and discussions during my graduation internship. Also all the other colleagues from the WDOD, in special everyone from the department flood defense, I would like to thank for the support during my graduation internship. And of course I would like the WDOD for providing me a chance to do my graduation internship in their company.

Last but not least, I want to thank my family and friends for their support and encouragement which they gave me during my whole time as a student on the TU Delft.

The author,
Hilma Buiten

Zwolle, 19-08-2020

Abstract

Several rivers are flowing through the Netherlands and dikes next to these rivers prevent from flooding. To get insight into the flood risk of these dikes, every 12 years a safety assessment (based on soil tests and modelling) is done on the condition of the dikes. One of the tested failure mechanisms is the slope stability in case of a high water event.
This study investigates the influence of the soil suction on the shear strength of soil and therefore the slope stability of the dike is researched. The main question of this report is: What is the influence of the soil suction on the slope stability of a clay dike and how can it be modeled?
To answer this question a literature study is done, a sensitivity analysis is performed in Plaxis for the influence of the phreatic surface and the influence of the different Soil Water Retention Curves (SWRCs) from the Staring Serie. Furthermore field measurement are analyzed and the model is fitted to the field data.

From the literature study it is known the soil suction increases the effective stress, which increases the shear strength and subsequently the slope stability. The soil suction of a soil can be determined with the SWRC. The SWRC gives a relationship between the Volumetric Water Content (VWC) and the soil suction, or the degree of saturation and the soil suction (Fredlund, Rahardjo, & Fredlund, 2012). The shear strength is only affected by the effective suction of the soil suction. To calculate the effective suction, the soil suction should be multiplied with the degree of saturation (Plaxis, 2019).
Field measurements in the Maasdijk in Oijen and the IJsseldijk in Westervoort show the presence of soil suction in the dike body during the entire winter. However, the top layer of the dike reaching down to a depth of approximately 1.5 meters below surface is influenced by the weather, since no suction stresses were one meter below the surface, but soil suction stresses were measured continuously 1.7 m below surface in winter.

The shear strengths of soils during the winter season were determined with the Cone Penetration Test (CPT) en Field Vane Tests (FVT). The comparison of the measured soil suction stresses and shear strengths in winter show that the shear strength and the measured suction stress are following the same trends during the season. However, the measured shear strengths were higher than expected, which cannot only be explained with the amount of measured suction.

The SWRCs of the soils in the dike body in Oijen and in the inner toe and inner berm in Westervoort were determined with the measured VWCs and soil suction stresses. This SWRCs were compared to the SWRCs from the Staring Serie (Wösten, Veerman, de groot, & Stolte, 2001). The sensitivity analysis in Plaxis, shows that the influence of SWRC from different soils from the Staring Serie on the Factor of Safety (FoS) is minimal, as long as the chosen SWRC is from a fine grained soil. However not all SWRCs obtained from the measured field data can be compared to the SWRC from fine grained soils from the Staring Serie. A couple of the SWRCs obtained from the field data, looked more like SWRC from the sandy soils from the Staring Serie.

To conclude this study a model is fitted to the field data and extrapolated to the water level in normative (WBN) situation. This extrapolation increases the FoS from 1.54 to 1.94 with the extra strength of the dike body and from 1.54 to 2.12 with consideration of the extra strength of the hinterland.

The implementation of soil suction in models, can contribute to the assessments of dikes in the Netherlands, as it has a positive effect on the FoS and the slope stability. However, no suction stresses will be present in the top of the dike during a WBN-event as the top 1.5 m of a dike is influenced by the weather. Therefore the recommendation to the water boards is made to take the suction only into account in the zone between the phreatic surface in a dike body and 1.5 meter below the top of the dike body. This probably only applies to a dike body in a storm dominated area or relative high dike, since most of the time the phreatic surface is approximately 1.5 meter below the top of the dike.

Content

Acknowledgements 4
Abstract 5
Content 6
List of Figures 8
List of Tables 10
Abbreviations 11
1 Introduction 12
1.1 Subject 12
1.2 Problem description 12
1.3 Test Locations 14
1.4 Main- and sub questions 17
1.5 Reading Guide 18
2 Literature review 19
2.1 Current practice 19
2.2 Soil-Water Characteristics Curves 21
2.2.1 Staring data series 24
2.3 Hydraulic state 26
2.3.1 Phreatic surface in general 26
2.3.2 Hydraulic state Maasdijk Oijen 29
2.3.3 Hydraulic state IJsseldijk near Westervoort 32
2.4 Soil Suction 35
2.5 Soil models 38
2.5.1 Hardening Soil model 38
2.5.2 Mohr-Coulomb model 41
2.5.3 The Soft Soil Model 42
2.5.4 SHANSEP Concept 44
2.5.5 Undrained A 46
2.5.6 Undrained B en C 46
3 Model Configuration and parameter determination 47
3.1 Parameter Determination 47
3.2 Model 52
3.2.1 Influence mesh 53
3.2.2 Influence Tolerated Error 55
3.2.3 Influence Soil Models 55
3.2.4 Comparison D-Stability. 56
4 Results 57
4.1 Sensitivity Analysis 57
4.1.1 Influence Phreatic Surface 57
4.1.2 Influence of the Soil type 58
4.2 Field measurements 60
4.2.1 Field Measurements Westervoort 60
4.2.2 Field measurements Oijen 70
4.3 Model fit 76
4.3.1 Fit with the SHANSEP concept 76
4.3.2 Fit with the Hardening Soil model 80
4.3.3 Extrapolation to WBN situation 83
5 Interpretation 86
5.1 Sensitivity analysis 86
5.2 Field Measurements 87
5.3 Model Fit 91

6 Conclusion and recommendations 92
6.1 Conclusion 92
6.2 Recommendation for the Water Boards 95
6.3 Recommendation for further research 96
7 References 97
Appendix I. Figures Safety Factors 99
Appendix II. Slip Surfaces 101
Appendix III. Soil Test Results 106
Appendix IV. Influence Weather on the Suction and Piezometric Head 110

List of Figures

Figure 1-1: Schematized cross section of the situation of the dikes near the IJssel, with the expected shear zone. 12
Figure 1-2: Schematized cross section of the hydraulic zones in the dike body........ 13
Figure 1-3: The test location in Westervoort in the IJsseldijk (Red) and in Oijen in the Maasdijk (Purple) (Rivieren Nederland, 2020)........ 14
Figure 1-4: Location of the tensiometers, Water content reflectometers and piezometers in the IJsseldijk in Westervoort........ 15
Figure 1-5: Location of the tensiometers, Water content reflectometers and piezometers in the Maasdijk near Oijen........ 16
Figure 2-1: The structure of the WBI and the related documents........ 19
Figure 2-2: The activities and order of the four activities in the safety assessment of dikes........ 19
Figure 2-3: The pores in the soil above the phreatic surface are first filled with water (capillary fringe), after which only the small pores are filled with water (capillary fingers). The right side shows the soil water retention curve for this case. (Lu & Likos, 2004)........ 22
Figure 2-4: Left: SWRC with the different zones. (Sun, Zhou, Gao, & Shen, 2015) Right: SWRC with boundary curves and scanning curves. (Toll, et al., 2015)........ 23
Figure 2-5: Phreatic surface in a clay dike body during a WBN event according to the Waternet Creator. (Meij, Bruijn, Blinde, Schweckendiek, & Zwan, 2011) 27
Figure 2-6: The phreatic level during a high water event according to the TRWD (TAW, 2004)........ 29
Figure 2-7: Elevation map of the area around the Maasdijk near Oijen. Red arrow: location with the measurement devices. Red line: location from the height profile which will be implemented in the model (AHN, 2019) 30
Figure 2-8: Height profile and the expected phreatic surfaces in the dike body of the smaller part of the Maasdijk near Oijen. The red points give the locations of the inside toe, inside crest, outside crest and outside toe. 30
Figure 2-9: River level in the winter period near Oijen during the six high water events in the last 30 years.31
Figure 2-10: Height profile and the expected phreatic surfaces in the dike body of the IJsseldijk near Westervoort. The red points give the locations of the inside toe, inside crest, outside crest and outside toe.. 32
Figure 2-11: Elevation map of the area around the IJsseldijk near Westervoort. Red line: location from the height profile. (AHN, 2019)........ 33
Figure 2-12: River level near Westervoort during the last five high water events. 33
Figure 2-13: Graphical representation of the determination of the relevant pore water pressure $p_{active.}$ (Plaxis, 2019) 36
Figure 2-14: Left: Ranges of measured matric suction on a residual soil slope in the Jurong Formation in Singapore (Lim, Rahardjo, CHang, & Fredlund, 1996), right: The location of the sensors and sorts of cover on the soil. 36
Figure 2-15: Shear strength of a dike body above the phreatic surface. The dike body consists of a heavy clay (Staring Serie subsoil O12) with a cohesion of 5 kPa, unit weight of 18 kN/m^3 and an internal friction angle of 20 °........ 37
Figure 2-16: Hardening Soil yield contour (Plaxis, 2020)........ 38
Figure 2-17: Hyperbolic stress-strain relation in primary loading for a standard drained triaxial test........ 39
Figure 2-18: Basic idea of the linear elastic perfectly plastic model (Plaxis, 2020)........ 41
Figure 2-19: Mohr-Coulomb yield contour (Plaxis, 2020) 41
Figure 2-20: Different young's modulus' can be determined from a stress-strain graph. The location of determining the Young's modulus is important and depending of the purpose of the Young's modulus. (Plaxis, 2020) 42
Figure 2-21: Illustration of the logarithmic relation between volumetric strain and mean stress. (Plaxis, 2020) 43
Figure 2-22: Cap yield surface for SS model (Plaxis, 2020) 44
Figure 2-23: Illustration of stress paths; reality vs. Mohr-Coulomb model (Plaxis, 2020) 46

Figure 3-1: Relation between the probe resistance, local friction and the friction number. (TAW, 2001) 48
Figure 3-2: Schematisation of the subsoil below the test location on the IJsseldijk near Westervoort. 48
Figure 3-3: The failure mechanism of the safety analysis for the fine mesh. The same failure mechanism occurred in all other safety analysis. 53
Figure 3-4: The used meshes. The coarse mesh (top), the medium mesh (middle) and the fine mesh (bottom). 54
Figure 4-1: The location of the different phreatic surfaces within the dike body in Westervoort. 57
Figure 4-2: Left: The effective suction over de depth in the middle of the dike body. The suction is generated from the water table (3.3 m below surface) only, with the van Genuchten curves from the Staring Serie for each soil. Right: The Degree of saturation over de depth in the middle of the dike body. The degree of saturation is generated form the water table (3.3 m below surface) only, with the van Genuchten curves from the Staring Serie of each soil. 59
Figure 4-3: Influence of the different soils from the Staring Serie on the FoS. The Mohr-Coulomb soil model was used, with a phreatic surface 3.3 m below the surface. A fine meshing and a tolerated error of 0.01 was applied. 59
Figure 4-4: Field measurements from the outer toe in Westervoort. Top: suction and precipitation surplus, Middle: VWC, Bottom: piezometric head and precipitations surplus. 61
Figure 4-5: Field measurements from the inner toe in Westervoort. Top: suction and precipitation surplus, Middle: VWC, Bottom: piezometric head and precipitation surplus. 63
Figure 4-6: The SWRC (drying) fitted to the measured matric suction and volumetric water content 1.0 m below surface in the inner toe in Westervoort. The used data is from the period 23-03-2020 until 25-06-2020. 64
Figure 4-7: Field measurements from the inner berm in Westervoort. Top: Suction and precipitation surplus, Middle: VWC, Bottom: piezometric head and precipitation surplus. 66
Figure 4-8: The SWRC (drying) fitted to the measured matric suction and volumetric water content 1.0 m below surface in the inner berm in Westervoort. The used data is from the period 30-03-2020 until 25-06-2020. 67
Figure 4-9: The undrained shear strength derived from the CPT data and the FVT-data over the period from November until May. 69
Figure 4-10: River level in in Lith, 1.2 km downstream from Oijen. 71
Figure 4-11: The measured suction stress (upper) and volumetric water content (lower) in the crest of the Maasdijk in Oijen. The suction stress 1.0 m below surfaces increased until 104 kPa on 31 May. 71
Figure 4-12: the drying and wetting SWRC obtained from the field data measured in Oijen. 73
Figure 4-13: The undrained shear strength derived from the CPT data and the FVT-data over the period from November until May. 75
Figure 4-14: The fit from the model with the shear strength obtained from the CPT-data. The SHANSEP concept was used to fit the model. The fit is made for in the berm in Westervoort. 77
Figure 4-15: The fit from the model with the shear strength obtained from the CPT-data. The SHANSEP concept was used to fit the model. The fit is made for in the crest in Oijen. 79
Figure 4-16: The fit from the model with the shear strength obtained from the CPT-data. The Hardening Soil model was used to fit the model. The fit is made for in the berm in Westervoort. 81
Figure 4-17: The fit from the model with the shear strength obtained from the CPT-data. The tau-phi method was used to fit the model. The fit is made for in crest in Oijen. 83
Figure 4-18: Slip surfaces for the modelled dike with and without apparent cohesions according to the field data. 85
Figure 5-1: Comparison from the SWRC from the Staring Serie and the SWRC obtained from the field data. 88
Figure 5-2: Shear strengths obtained from the CPT-data, the Field Vane Test (FVT) and the measured matric suction in the crest in Oijen. 90
Figure 6-1: The dike body with phreatic level in a WBN event. If the phreatic surface is more than 1.5 m below surface, the suction can be taken into account for the part of the dike body which is above the phreatic surface, but below the 1.5 m from surface. 95

List of Tables

Table 1-1: The depth of the tensiometers and water content reflectometers in the IJsseldijk in Westervoort. 15
Table 1-2: Locations of the tensiometers and water content reflectometers in the Maasdijk near Oijen. 15
Table 2-1: Advantages and disadvantages of various designations for amount of water in soil (Fredlund, Rahardjo, & Fredlund, 2012) 22
Table 2-2: Classification of grain size according to Bakker & Schelling (1989) 24
Table 2-3: Classification of the subsoil in the Staring Serie 24
Table 2-4: Soil characteristics of the optimized parameters form the analytical equation in which the average physical soil characteristics are described. 25
Table 2-5: The characteristic points of the WC in case of clay dike, on a clay of peat layer during a WBN event. 27
Table 2-6: Information about the six high water events in the last 30 years in the Maas near Oijen. 31
Table 2-7: Statistical information about the duration of the high water events of the last 30 years near Oijen. 31
Table 2-8: Statistical information about the river level in cm of the high water events of the last 30 years near Oijen. 31
Table 2-9: Statistical analysis of the high water events the last 10 years near Westervoort 34
Table 2-10: Statistical information about the duration of the high water events of the last 10 years near Westervoort. 34
Table 2-11: Statistical information about the river level in cm of the high water events of the last 10 years near Westervoort 34
Table 2-12: Input parameters for the HS model in Plaxis 39
Table 2-13: input parameters for the MC model 42
Table 2-14: Input parameters for SS model. 44
Table 3-1: Soil classification from the probe resistance and friction number to determine the soil type used in this study. 47
Table 3-2: Used parameters for the different soils in the Mohr-Coulomb model. 49
Table 3-3: Used parameters for the different soils in the Hardening Soil Model. 50
Table 3-4: Used parameters for the different soils in the Soft Soil Model 51
Table 3-5: The calculated FoS and the number of elements for each mesh. 53
Table 3-6: The calculated Fos and the minimum number of steps for each tolerated error. 55
Table 3-7: The calculated FoS for the different soil models. 55
Table 3-8: Different Results for Plaxis and D-stability in terms of FoS. 56
Table 4-1: The calculated factors of safety (FoS) and probability of failure (Pf) for each phreatic surface ... 58
Table 4-2: The calculated FoS with and without taking into account static suctions form different soils. 58
Table 4-3: The dates on which the CPT's and FVT in the berm are performed during the winter of 2019/2020. 67
Table 4-4: The measured soil suction and VWC between the dates in the table are used to obtain the fitting parameters for the van Genuchten Equation, to obtain the SWRC for each depth. 72
Table 4-5: The dates on which the CPT's and FVT in the crest are performed during the winter of 2019/2020. 74
Table 4-6: The used apparent OCR values to fit the model shear strength to the shear strength obtained from the CPT-data for the berm in Westervoort. 77
Table 4-7: The used apparent OCR values to fit the model shear strength to the shear strength obtained from the CPT-data for the crest in Oijen 78
Table 4-8: The used apparent cohesions to fit the model shear strength to the shear strength obtained from the CPT-data for the berm in Westervoort. 80
Table 4-9: The used apparent cohesions to fit the model shear strength to the shear strength obtained from the CPT-data for the crest in Oijen. 82
Table 4-10: Results with and without apparent cohesion applied in different soil layers during a safety assessment of WBN level in terms of FoS. 84

Abbreviations

CPT	Cone Penetration Test
CSSM	Critical State Soil Mechanics
FoS	Factor of Safety
FVT	Field Vane Test
HS	Hardening Soil Model
LEPP	Linear Elastic Perfectly Plastic Model
MC	Mohr-Coulomb model
OCR	Over Consolidation Ratio
OCR*	Apparent OCR
SHANSEP	Stress History and Normalized Soil Engineering Properties
SS	Soft Soil Model
SWCC	Soil-Water Characteristics Curve
SWRC	Soil-Water Retention Curve
TRWD	"Technisch Rapport Waterspanningen bij Dijken", method to calculate the phreatic surface in a Dike Body.
VWC	Volumetric Water Content
WBI	"Wettelijk Beoordelings Instrumentarium". The WBI is a collection of legislations and guides to perform a safety assessment of flood defenses.
WBN	"Waterstand bij Norm", water level in the normative situation.
WC	Waternet Creator, tool to determine the height of the phreatic surface in a dike in case of a WBN event.

1 Introduction

1.1 Subject

Several rivers are flowing through the Netherlands. To prevent against flooding, there are dikes besides these rivers. To get insight into the flood risk of these dikes, every 12 years a safety-assessment is done for the condition of the dikes. If it turns out the condition of a dike is not sufficient, the dike has to be reinforced. One of the tested failure mechanisms of the dike is the slope stability.
In 2017 the ministry of Infrastructure and Environment published the Schematization manual slope stability (Ministerie van Infrastructuur en Milieu, 2017). In this manual, it is described how the assessment of the slope stability of a dike should be done, including the usage of lab-test and software.
At the moment the initially unsaturated zone of the dike is considered as fully saturated in the assessment and the influence of the daily unsaturated zone is not known. By taking into account this zone, the assessment of the dike can give a different outcome.

1.2 Problem description

The Waterboard Drents Overijssel Delta has a dike reinforcement project on the dikes of the IJssel between Zwolle-Olst. The dikes in this region consists in some parts of clay, with a small (0 – 2 m) layer with peat or clay underneath the dike. The dike body itself is three to five meter in height and the steepness of the slope is 1:2 until 1:3. Below the clay or peat layer there is a saturated sand layer (aquifer). In Figure 1-1 the expected shear zone of the dike with the current calculation methods is given. When high water levels occur at the river IJssel the hydraulic head of the sand layer is high. Due to this hydraulic head, the effective stress in the clay/ peat layer from the inner toe to the ditch is close to zero ($\sigma_v' = 0$ kPa), therefore the shear strength of the layer is also close to zero ($\tau = 0$ kPa). In this case most of the resistance of the shear zone, comes from inside or below the dike body.

The “Waterstand bij Norm” (WBN) is the water level in the normative situation, which is the acceptable flood risk. For every part of the dike there is a normative situation. This acceptable flood risk is determined by the government and defined as a yearly probability of flooding. For example a normative situation of 1/3000, means a situation which have a chance to happen of 1/3000th (P=0.0003) a year. The water level in this situation is called the WBN.

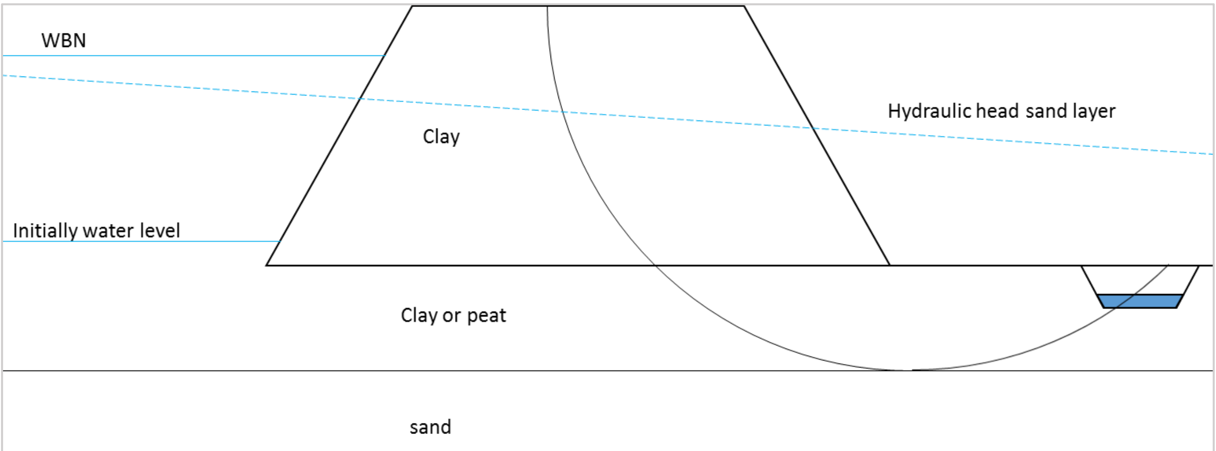

Figure 1-1: Schematized cross section of the situation of the dikes near the IJssel, with the expected shear zone.

During a WBN event, the phreatic surface in the dike and the hydraulic head in the sand layer will change. Both will rise (Figure 1-1), but the how the phreatic surface rises in time and when steady state is reached is not known. Currently the phreatic surface is calculated with the “Technisch Rapport Waterspanningen bij Dijken” (TRWD). This method calculates the phreatic surface in a steady-state or transient situation, for the WBN situation, as described in TAW (2004).

It is assumed all layers below the phreatic surface are saturated. In Figure 1-2 a more detailed, steady state, situation is drawn. In the dike body are four zones defined. Zone 4 is always below the phreatic surface, zone 3 is above the usual phreatic surface, but below the phreatic surface during high water events. Zone 2 is above the phreatic surface during high water and zone 1 is the top layer of the dike.

In Zwanenburg (2017), it is described how the strength in zone 3 should be determined. Zone 3 is in daily circumstance above the phreatic level, but in WBN circumstance below the phreatic level. The assumption is made, all layers below the phreatic level are saturated.
Above the phreatic level (zone 2), there some different hydraulic zones (Figure 1-2). First above the phreatic level there is the capillary zone. This zone is fully saturated, with a negative pore water pressure. In the funicular zone, the soil is partly saturated. The capillary rise is still there in the smaller pores, but in the bigger pores there is air. In the pendular zone the degree of saturation is mainly dependent on the infiltration (rainwater). If there is negative pore water pressure in the soil, the shear strength of the soil increases (Zwanenburg, 2017).

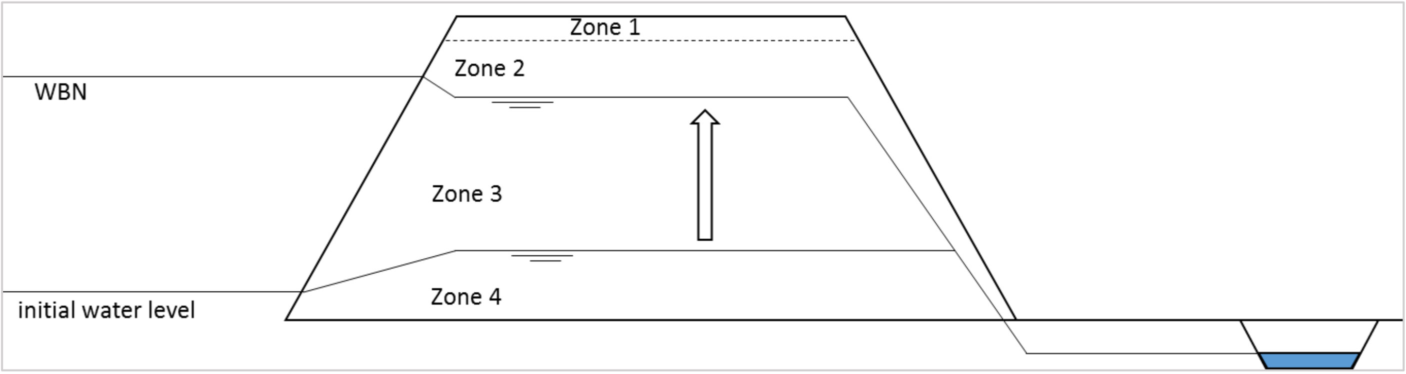

Figure 1-2: Schematized cross section of the hydraulic zones in the dike body

In case of WBN situation, the following assumption is made:
Zone 3 is initially unsaturated with capillary tensions, but changes to a zone which is saturated without capillary tensions and therefore without the higher shear strength. It is unsure if this assumption is always realistic.

Zone 2 is initially unsaturated with capillary tensions, but the water table will rise until the bottom of zone 2. Even in a WBN situation zone 2 will be above the water table and will stay a unsaturated zone, with capillary tensions.

The dike bodies near the IJssel have a quite big zone (zone 3, Figure 1-2) which is assumed to change from unsaturated with capillary tensions to saturated without capillary tensions in case of WBN situation. It is not known how big zone 3 is in reality and in what time scheme the phreatic surface rises in case of a WBN event. It is unsure how the capillary suction stresses in zone 2 and 3 influences the slope stability of a dike. Since zone 2 and 3 are quite a big part of the shear zone, the capillary tensions can have a big influence on the slope stability of the dike.

1.3 Test Locations

Deltares is performing a research about the influence of the capillary tensions on the undrained shear strength in primary dikes in the Netherlands (van Duinen, van Hoven, Visschedijk, & Wichman, 2018). At two locations, devices are installed at different depths, which measure the volumetric water content (VWC), soil suction and pore water pressure. To measure the shear strength Cone Penetration Tests (CPT) class 1 and Field Vane Tests (FVT) are performed.

Figure 1-3: The test location in Westervoort in the IJsseldijk (Red) and in Oijen in the Maasdijk (Purple) (Rivieren Nederland, 2020)

The two locations are located in Westervoort (IJsseldijk) and near Oijen (Maasdijk) (Figure 1-3). The IJsseldijk is an "old" (the exact construction time of the dike is not known) dike which consists of a clay dike body and a Holocene clay cover of about 4 meters. The water content reflectometers, tensiometers for the soil suction and piezometers are installed in the outer toe, inner toe and the inner berm (Table 1-1). The CPTs and FVTs to measure the shear strength are performed in the inner berm (Figure 1-4).

Table 1-1: The depth of the tensiometers and water content reflectometers in the IJsseldijk in Westervoort.

Sensor location	Depth [m below surface]	Depth [m+NAP]
Outer toe	1.00	9.60
Outer toe	1.50	9.12
Outer toe	2.00	8.60
Outer toe	3.00	7.60
Inner toe	1.00	10.21
Inner toe	1.50	9.67
Inner toe	2.00	9.19
Inner toe	2.40	8.81
Inner berm	1.00	9.35
Inner berm	1.50	8.86
Inner berm	2.00	8.37
Inner berm	2.55	7.88

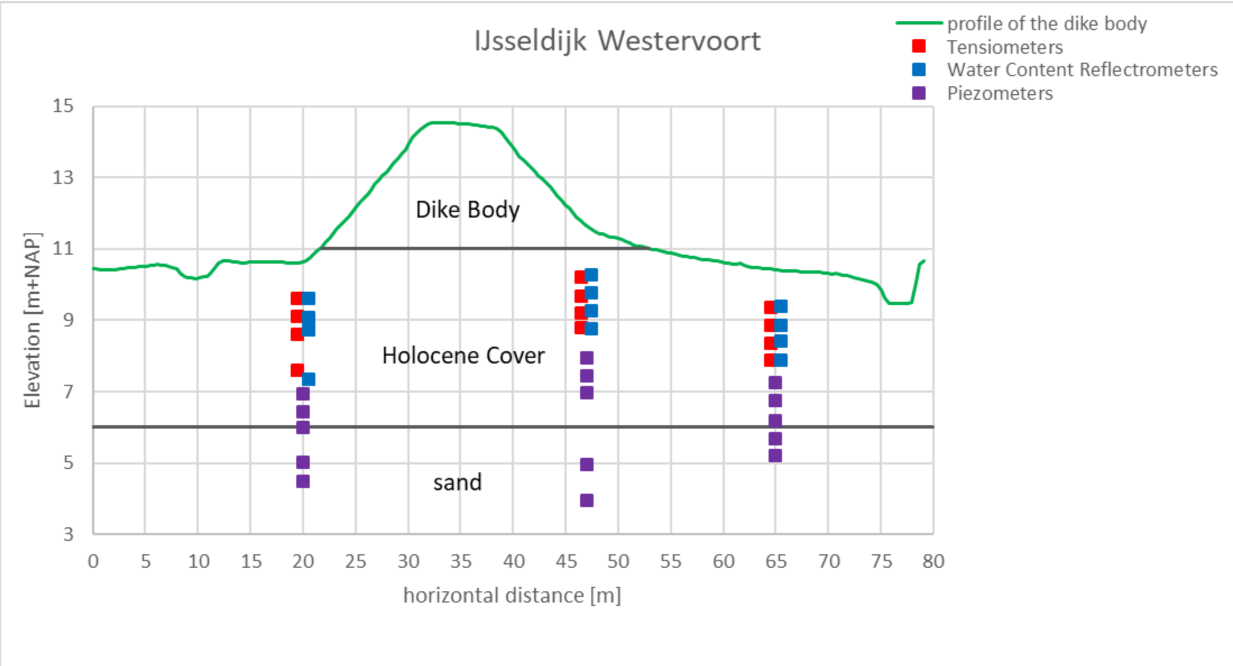

Figure 1-4: Location of the tensiometers, Water content reflectometers and piezometers in the IJsseldijk in Westervoort

The Maasdijk is a relatively new dike near Oijen. The dike consists of clay on top of a holocene clay cover which varies in thickness from 4 until 1 meter. The water content reflectrometers and tensiometers are installed in the crest (Table 1-2) and the CPTs and FVTs are also performed in the crest of the dike (Figure 1-5). The data of the above measurements will be used in this thesis to research the effect of the soil suction of the shear strength of a clay dike.

Table 1-2: Locations of the tensiometers and water content reflectometers in the Maasdijk near Oijen.

Sensor location	Depth [m below surface]	Depth [m+NAP]
Dike Body	1.00	8.30
Dike Body	1.70	7.58
Dike Body	2.40	6.95
Dike Body	3.10	6.19

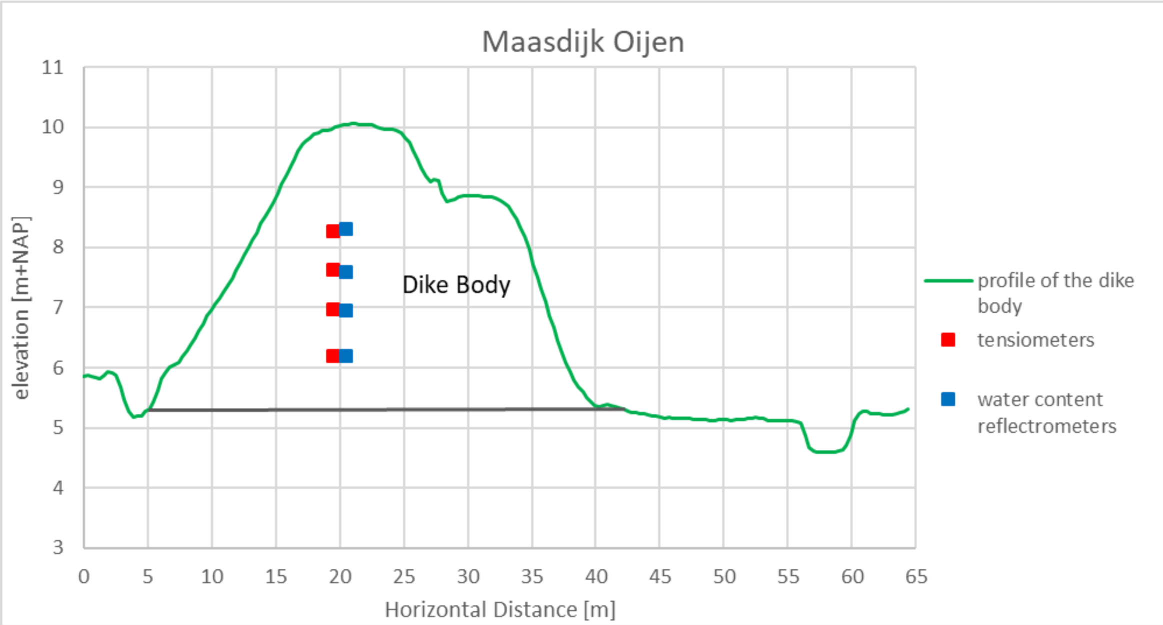

Figure 1-5: Location of the tensiometers, Water content reflectometers and piezometers in the Maasdijk near Oijen

1.4 Main- and sub questions

In the study for this thesis report an answer is sought for the following main question:

What is the influence of the soil suction on the slope stability of the dike and how can it be modelled?

Different steps were taken to answer this main question, which follow from six sub questions:

1. What is the most progressive and conservative hydraulic state of the dike in the initial state (before the start of the WBN event) and during the WBN event in steady state?
2. What is the effect of the soil suction on the shear strength of clay and the slope stability of the dike?
3. What is the maximum influence of the soil suction in the dike body on the factor of safety in case of a clay dike in the most positive and negative case?
4. Is it worthwhile to perform a time dependent analysis of the initial situation, the development of the phreatic surface and the influence on the factor of safety of slope stability of the dike?
5. How can the stability modelling of the unsaturated zone be improved by using the field data obtained by Westervoort and Oijen?
6. Should the WBI be improved according to the results of this research?

1.5 Reading Guide

The thesis outline is structured as follows:

Chapter 1, Introduction: The study background is presented, with the main- and subquestions for which an answers given in this report.
Chapter 2, Literature review: First the current practice in the assessment of dikes is described, followed with information about the Soil Water Retention Curve (SWRC), which describes the relation between soil suction stresses and VWC in a soil. Next the hydraulic states for the test location are given, afterwards the theoretical influence of soil suction on the shear strength of a dike is described. The last paragraph in the literature review gives information about the soil models used during this research.
Chapter 3, Model Configuration and Parameter Determination: In this chapter is described how the parameters are derived and what the structure of the used Plaxis model is.
Chapter 4, Results: The results of respectively the sensitivity analysis, field measurements and model fit are given and described in this chapter.
Chapter 5, Interpretation: The interpretation of the results in Chapter 4.
Chapter 6, Conclusion and Recommendations: This chapter give answers on the sub- and main questions and is concluded with a recommendation for the water boards and for further research.

2 Literature review

In this chapter an overview is given about the information known from the literature. First the current practice in the assessment of dikes will be addressed. Next the Soil-Water Characterstics Curve (SWCC), hydraulic state of the dikes and soil suction are addressed and last some information about the soil models used in this thesis are given.

2.1 Current practice

In the schematization manual slope stability (Ministerie van Infrastructuur en Milieu, 2019) is described how the safety assessment for the slope stability of primary dikes have to be performed. The schematization manual slope stability is part of the “Wettelijk Beoordelings Instrumentarium” (WBI) 2017. The WBI is a collection of legislations and guides to perform a safety assessment of flood defenses. An overview of the documents in the WBI is given in Figure 2-1.

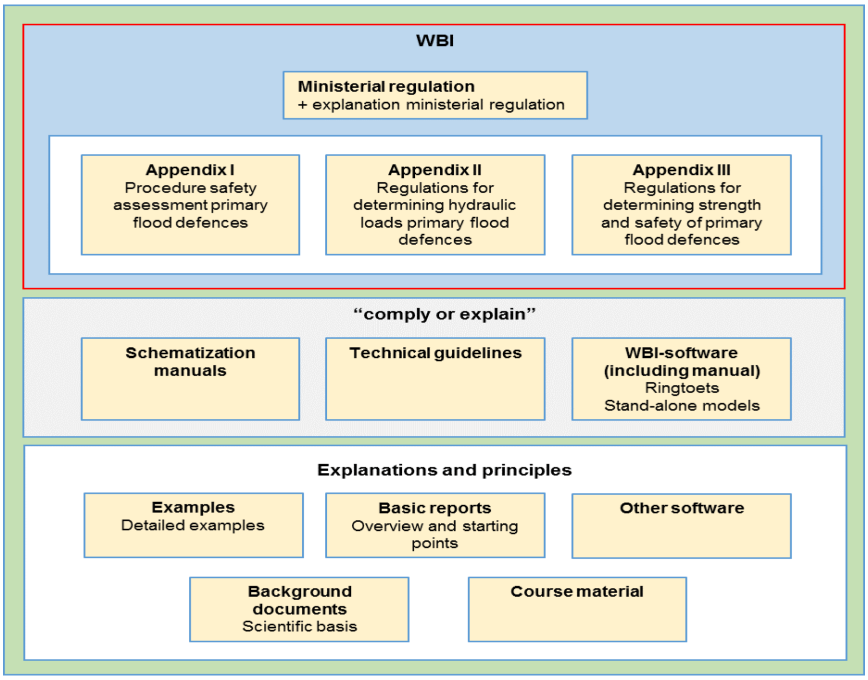

Figure 2-1: The structure of the WBI and the related documents

The safety assessment consists of four activities: data acquisition, schematization, calculating and interpretation (Figure 2-2). The whole process is in most cases an iterative process.

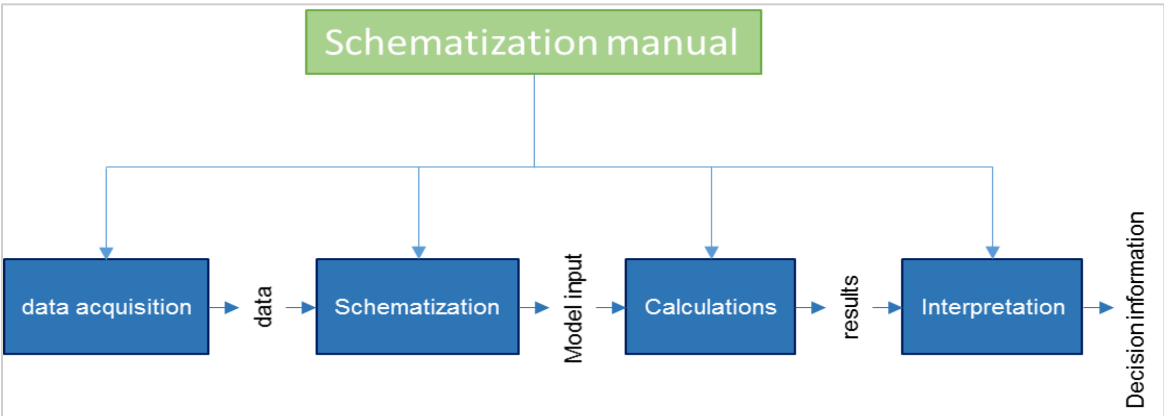

Figure 2-2: The activities and order of the four activities in the safety assessment of dikes.

In the calculations the soil is assumed to be fully saturated below the phreatic level in a WBN event and unsaturated above the phreatic level in a WBN event. The calculations below the phreatic level are performed undrained and above the phreatic level it is dependent on the soil type and Over Consolidation Cation (OCR). In case of soil with a low permeability and an OCR<3, the calculations are performed undrained, if this is not the case the calculations are performed drained.

Arcadis did a study about the change in slope stability analyses when calculating drained or undrained in D-stability. Based on default parameters there is no significant difference in the shear safety. The results based on the parameters used by the water boards were more favorable than the results with the default parameters. In the calculation with N_{kt} = 20 kPa, the results increased until 30% compared with the results from the default parameters. This results seemed too positive, therefore the calculations were repeated with N_{kt} = 60 kPa and N_{kt} = 120 kPa. The results with the corrected N_{kt}s seemed too conservative. (Arends, 2018)

The height of the phreatic level is deterimended according the TAW (2004). In most cases this is done with a steady state analysis of the phreatic surface.

2.2 Soil-Water Characteristics Curves

The Soil-Water Characteristics Curves (SWCC) uses elementary capillary theory to explain the water retention and water transmissivity for partially saturated soil. The unsaterated soil characterstics can be determined from the SWCC or the Soil Water Retention Curve (SWRC). The SWCC gives the relation between the soil suction (Ψ) and the VWC (θ) or the gravimetric water content (w). The SWRC gives the relation between the soil suction (Ψ) and the degree of saturation (S_r).

In equations (2-1) until (2-5) the formulation of the different designations for the amount of soil water are given. In Table 2-1 the advantages and disadvantages of the various designations for amount of soil water are given.

$$S_r = \frac{V_w}{V_v} = \frac{e_w}{e} = \frac{\theta}{\theta_{sat}} = \frac{w \cdot G_s}{e} \tag{2-1}$$

$$\theta = \frac{V_w}{V_v + V_s} = \frac{e_w}{1 + e} \tag{2-2}$$

$$S_r = \frac{\theta - \theta_{res}}{\theta_{sat} - \theta_{res}} \tag{2-3}$$

$$S_{eff} = \frac{S_r - S_{res}}{S_{sat} - S_{res}} \tag{2-4}$$

$$w = \frac{M_w}{M_s} \tag{2-5}$$

With:
S_r = degree of saturation [-]
θ = volumetric water content [m^3/m^3]
w = gravimetric water content [kg/kg]
V_w = Volume of water [m^3]
V_v = Volume of voids [m^3]
V_s = Volume of solids [m^3]
$e_w = \frac{V_w}{V_s}$ water ratio [-]
$e = \frac{V_v}{V_s}$ void ratio [-]
θ_{sat} = Saturated volumetric water content [-]
$G_s = \frac{\rho_s}{\rho_w}$ = Specific gravity of solids [-]
M_w = Mass of water [kg]
M_s = Mass of soil solids [kg]
S_{eff} = effective saturation [-]
θ_{res} = residual water content (the water content left in the soil after 1500 kPa suction (van Genuchten, 1980)) [m^3/m^3]
S_{sat} = saturated degree of saturation [-]
S_{res} = residual degree of saturation [-]

Table 2-1: Advantages and disadvantages of various designations for amount of water in soil (Fredlund, Rahardjo, & Fredlund, 2012)

Designation	Advantages	Disadvantages
Gravimetric water content (w)	Consistent with usage in classic soil mechanics Most common means of measurement Does not require a volume measurement Reference value is a "mass of soil" which remain constant	Does not allow differentation between change in volume and change in degree of saturation Does not yield the correct air-entry value when the soil changes volume upon drying
Volumetric water content (θ)	Is the basic form that emerges in the derivation of transient seepage and fluid storage in unsaturated soils Commonly used in databases of results obtained in soil science and agronomy	Requires a volume measurement Rigorous Definition requires a volume measurement at each soil suction Is the designation least familiar and least used historically in geotechnical engineering
Degree of saturation (S_r)	Most clearly defines the air-entry value Appears to be the variable most closely controlling unsaturated soil property functions	Requires a volume measurement Although volume measurementes are required, the degree of saturation variable does not quantify overall volume change

In the current practice it is assumed the soil above the phreatic level contains no water. In reality this is not the case. In the zone above the phreatic level, soil suction stresses occurs. Therefore all the pores in the soil above the phreatic level are filled with water, the capillary fringe. Above the capillary fringe the degree of saturation degreases with height. The dimensions of these zones are dependent of the soil. In coarse sand the capillary height is approximately 0.02 – 0.05 m and in clay it is approximately 2 - 4 m (TAW, 2001). Figure 2-3 gives an graphical representation of the zones above the groundwater table. The height of the capillary fringe is determined by the Air-Entry head.

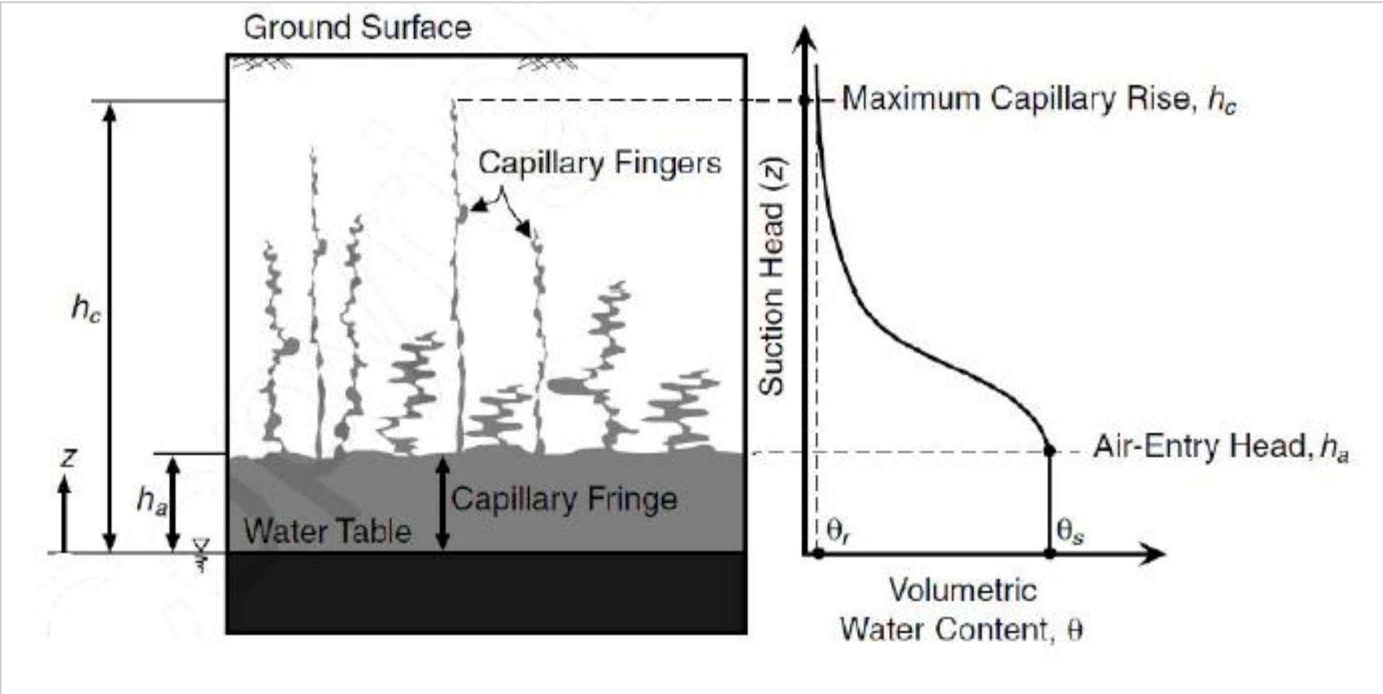

Figure 2-3: The pores in the soil above the phreatic surface are first filled with water (capillary fringe), after which only the small pores are filled with water (capillary fingers). The right side shows the soil water retention curve for this case. (Lu & Likos, 2004)

In Figure 2-4 two SWRCs are given. The SWRC is divided in three different zones. The saturated zone corresponds with the capillary fringe and the transition zone is where the water content decreases with increasing height. In the residual zone the soil has reached his most compacted state and the micropores in the soils starts to dehydrate.

In the left figure of Figure 2-4, only the initial drying curve of the soil is given. The soil only follows this curve if aggregates have not formed yet. If aggregates have formed, the initial loose state is collapsed and an irriversible decrease of water content and soil volume has occurred. Therefore, if a soil has left the primary drying curve, it can never reach his original VWC again. In that case the soil behaves like the scanning curves. The primary wetting curve is the lower boundary of the possible states of the SWRC.

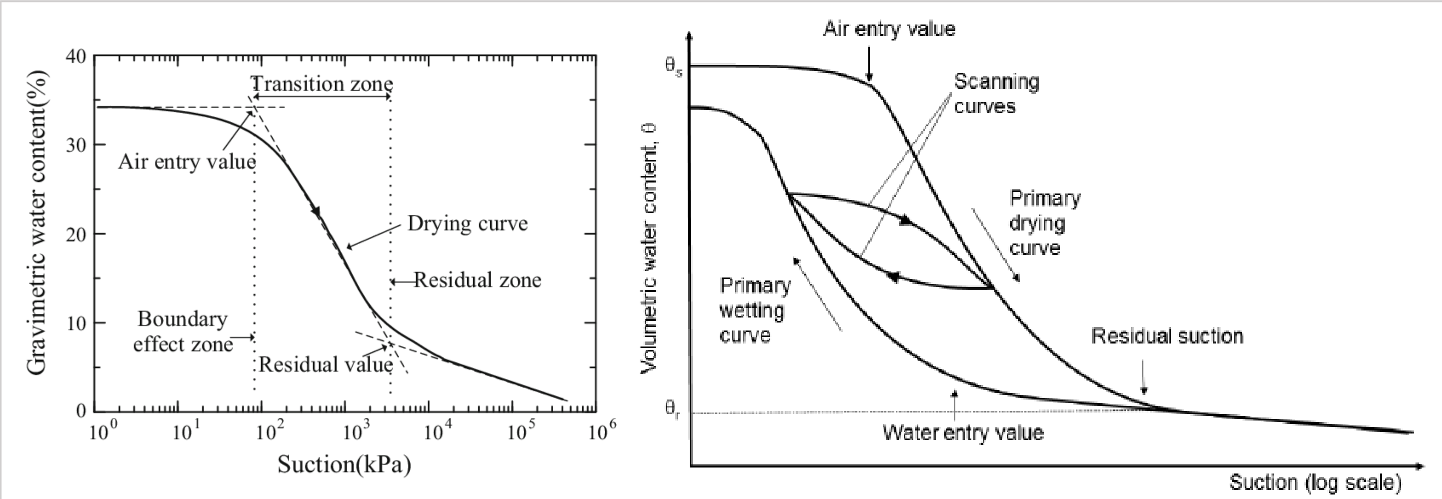

Figure 2-4: Left: SWRC with the different zones. (Sun, Zhou, Gao, & Shen, 2015) Right: SWRC with boundary curves and scanning curves. (Toll, et al., 2015)

A common way to describe the SWRC of soils is with the van Genuchten equation (equation (2-6)) (van Genuchten, 1980). With equation (2-7) the hydraulic conductivity of a soil can be calculated.

$$S_r = \frac{\theta - \theta_{res}}{\theta_{sat} - \theta_{res}} = \frac{1}{(1 + (\alpha h)^n)^m} \tag{2-6}$$

$$K(h) = \frac{K_s\left((1 + \alpha h^n)^{1-\frac{1}{n}} - \alpha h^{n-1}\right)^2}{(1 + \alpha h^n)^{\left(1-\frac{1}{n}\right)(l+2)}} \tag{2-7}$$

With:
θ = volumetric water content [cm³/cm³]
θ_{res} = residual water content [cm³/cm³]
θ_{sat} = saturated water content [cm³/cm³]
α = fitting parameter [1/cm]
n = fitting parameter
l = fitting parameter
$m = 1 - \frac{1}{n}$
K = hydraulic conductivity [cm/d]
K_s = saturated hydraulic conductivity [cm/d]
S_r = degree of saturation

2.2.1 Staring data series

In 1987 the Staring Serie was published (Wösten, Veerman, de groot, & Stolte, 2001). The Staring Serie divides the Dutch soils, from a soil map 1:50 000, in 18 topsoils and 18 subsoils. In 1994 and 2001 the series were improved, by adding new samples. The division between the soils is made according to the system of soil classification in the Netherlands (de Bakker & Schelling, 1989). The classification is made to the texture of the samples. In Table 2-2 and Table 2-3 the classification of the soils is given. The M50 value is the median grain size of the sand fraction of the soil.

Table 2-2: Classification of grain size according to Bakker & Schelling (1989)

Grain size	Classification
< 2 µm	lutum fraction
2-50 µm	loam fraction
50-105 µm	Very fine sand fraction
105-150 µm	Fine sand fraction
150-210 µm	Moderately fine sand fraction
210-420 µm	Moderately coarse sand fraction
420-2000 µm	Coarse sand fraction
2-64 mm	Gravel fraction
> 64 mm	Stone fraction

Table 2-3: Classification of the subsoil in the Staring Serie

Soil number	Soil name	Loam [%]	Lutum [%]	Organic fraction [%]	M50 [µm]	Density [g/cm^3]
O1	Non-loamy sand	0-10	-	0-3	105-210	1.4-1.8
O2	Loamy sand	10-18	-	0-3	105-210	1.4-1.7
O3	Very loamy sand	18-33	-	0-3	105-210	1.4-1.8
O4	Extremely loamy sand	33-50	-	0-3	105-210	1.4-1.7
O5	Coarse sand		-	0-3	210-2000	1.5-1.7
O6	Boulder clay	0-50	-	0-3	50-2000	1.1-1.6
O7	River loam	33-50	-	0-3	50-150	1.0-1.7
O8	Sandy loam	-	8-12	0-3	-	1.4-1.6
O9	Silt loam	-	12-18	0-3	-	1.3-1.7
O10	Clayey loam	-	18-25	0-3	-	1.3-1.5
O11	Light clay	-	25-35	0-3	-	1.3-1.6
O12	Heavy clay	-	35-50	0-3	-	1.0-1.5
O13	Very heavy clay	-	50-100	0-3	-	1.0-1.4
O14	Loam	50-85	-	0-3	-	1.0-1.6
O15	Heavy Loam	85-100	-	0-3	-	1.1-1.6
O16	Oligotrophic peat	-	-	35-100	-	0.1-0.7
O17	Eutrophic peat	-	-	35-100	-	0.1-0.6
O18	Peaty layer	-	-	15-35	-	0.8-1.4

If the soil classification is known, gives Table 2-4 the optimised parameters from the analytical equations used to describe the average physical characteristics of the soil. From these characteristics SWRC and hydraulic conductivity can be calculated with the van Genuchten equation (equation (2-6) and (2-7)).

Table 2-4: Soil characteristics of the optimized parameters form the analytical equation in which the average physical soil characteristics are described.

Soil Number	Θ_r [cm³/ cm³]	Θ_s [cm³/ cm³]	K_s [cm/d]	α [1/cm]	l [-]	n [-]
O1	0.01	0.36	15.22	0.0224	0.000	2.286
O2	0.02	0.38	12.68	0.0213	0.168	1.951
O3	0.01	0.34	10.87	0.0170	0.000	1.717
O4	0.01	0.35	9.86	0.0155	0.000	1.525
O5	0.01	0.32	25.00	0.0521	0.000	2.374
O6	0.01	0.33	33.92	0.0162	-1.330	1.311
O7	0.01	0.51	39.10	0.0123	-2.023	1.152
O8	0.00	0.47	9.08	0.0136	-0.803	1.342
O9	0.00	0.46	2.23	0.0094	-1.382	1.400
O10	0.01	0.48	2.12	0.0097	-1.879	1.257
O11	0.00	0.42	13.79	0.0191	-1.384	1.152
O12	0.01	0.56	1.02	0.0095	-4.295	1.158
O13	0.01	0.57	4.37	0.0194	-5.955	1.089
O14	0.01	0.38	1.51	0.0030	-0.292	1.728
O15	0.01	0.41	3.70	0.0071	0.912	1.298
O16	0.00	0.89	1.07	0.0103	-1.411	1.376
O17	0.01	0.86	2.93	0.0123	-1.592	1.276
O18	0.01	0.57	34.45	0.0138	-1.204	1.323

There are also different empirical equations to determine the soil characterstics, based on the classification parameters. In equation (2-8) until (2-13) equations are given to determine the soil characteristics of the clay and loam parmeters (Wösten, Veerman, de groot, & Stolte, 2001).

$$\theta_s = 0.6311 + 0.003383 \cdot c - 0.06366 \cdot \rho^2 - 0.00204 \cdot \rho \cdot C \qquad R^2 = 95\% \qquad (2\text{-}8)$$

$$K_s^* = -42.6 + 8.71 \cdot o + 61.9 \cdot \rho - 20.79 \cdot \rho^2 - 0.2107 \cdot o^2 - 0.01622 \cdot c \cdot o - 0.5382 \cdot \rho \cdot o \qquad R^2 = 31\% \qquad (2\text{-}9)$$

$$\alpha^* = -19.13 + 0.812 \cdot o + 23.4 \cdot \rho - 8.16 \cdot \rho^2 + 0.423 \cdot o^{-1} + 2.388 \cdot \ln(o) - 1.338 \cdot \rho \cdot o \qquad R^2 = 51\% \qquad (2\text{-}10)$$

$$l^* = 0.102 + 0.0222 \cdot c - 0.043 \cdot \rho \cdot c \qquad R^2 = 44\% \qquad (2\text{-}11)$$

$$n^* = -0.235 + 0.972 \cdot \rho^{-1} - 0.7743 \cdot \ln(c) - 0.3154 \cdot \ln(o) + 0.0678 \cdot \rho \cdot o \qquad R^2 = 78\% \qquad (2\text{-}12)$$

$$\frac{1}{D} = 0.6117 + 0.003601 \cdot c + 0.002172 \cdot o^2 + 0.01715 \cdot \ln(o) \qquad R^2 = 79\% \qquad (2\text{-}13)$$

With:
θ_s = saturated water content
K_s^*= saturated hydraulic conductivity (transformed model parameter) = $K_s^* = \ln(K_s)$
α^*, l^* and n^*= form fitting parameters (transformed model parameters)
$a^* = \ln(a)$ $\qquad$ $n^* = \ln(n-1)$ $\qquad$ $l^* = \ln\left(\frac{l+10}{10-l}\right)$ (only for clay and loam soils)
c = clay fraction (<2 μm) [%]
o = organic content [%]
ρ = density [g/cm³]

2.3 *Hydraulic state*

In a dike there are different hydraulic zones. For a primary dike in a daily situation, the water level in the river is approximately the same level as the phreatic level in the area behind the dike. The phreatic level in the dike is slightly higher than the river level, but can be considered as a low level in the dike. The zone in the dike, which is always below the water level, is zone 4.
In case of a high water event the water level in the river will increase. With this, the phreatic level in the dike will increase. The area which is normally above the water level, will eventually become saturated and will lie below the water level. This is zone 3.
The area above zone 3, zone 2, is always above the phreatic level. This zone can be (partly) saturated with water due to capillary tensions. The top layer of the dike, the covering layer, is zone 1. A schematization of the four zones within the dike is given in Figure 1-2.

The size of the different zones in the dike are dependent on the

- Normal water level in the river;
- Water level in case of WBN in the river;
- Geometry of the dike;
- Soil material of the dike;
- Water level behind the dike;
- Drainage present in the dike.

2.3.1 Phreatic surface in general

To determine the size of the different hydraulic zones, the height of the phreatic surface in the dike has to be determined in the daily situation and in the WBN situation. In the current situations the water pressures in the dike are calculated with the Waternet Creator (WC). The initial phreatic surface is calculated with the formula of Dupuit (equation (2-14)).

$$h = \sqrt{-\frac{N}{K}x^2 + \left(\frac{\phi_2^2 - \phi_1^2}{L} + \frac{NL}{K}\right)x + \phi_1^2}$$

(2-14)

with:
h = height of the phreatic surface with reference to the ‘impermeable boundary’ [m]
N = precipitation [m/s]
K = permeability [m/s]
x = arbitrary point in the dike [m]
$\phi_{1,2}$ = Boundary conditions at the sides of the dike, with reference to the ‘impermeable boundary’ [m]
L = width of the dike [m]

For rivers in the east of the Netherlands, the groundwater flow through the dikes is assumed to be in a steady state. Since the clay dikes in the upper region are quite sandy, the permeability in the dike bodies is higher than in the clay bodies in the lower river area.
To calculate the phreatic surface in case of a WBN situation there are two options. The TRWD (TAW, 2004) gives a safe and conservative estimation of the phreatic surface in the dike body. The WC, the software to determine the phreatic surface in the dike body from the WBI, gives a less conservative estimation. In Table 2-5 and Figure 2-5 the WC is explained.

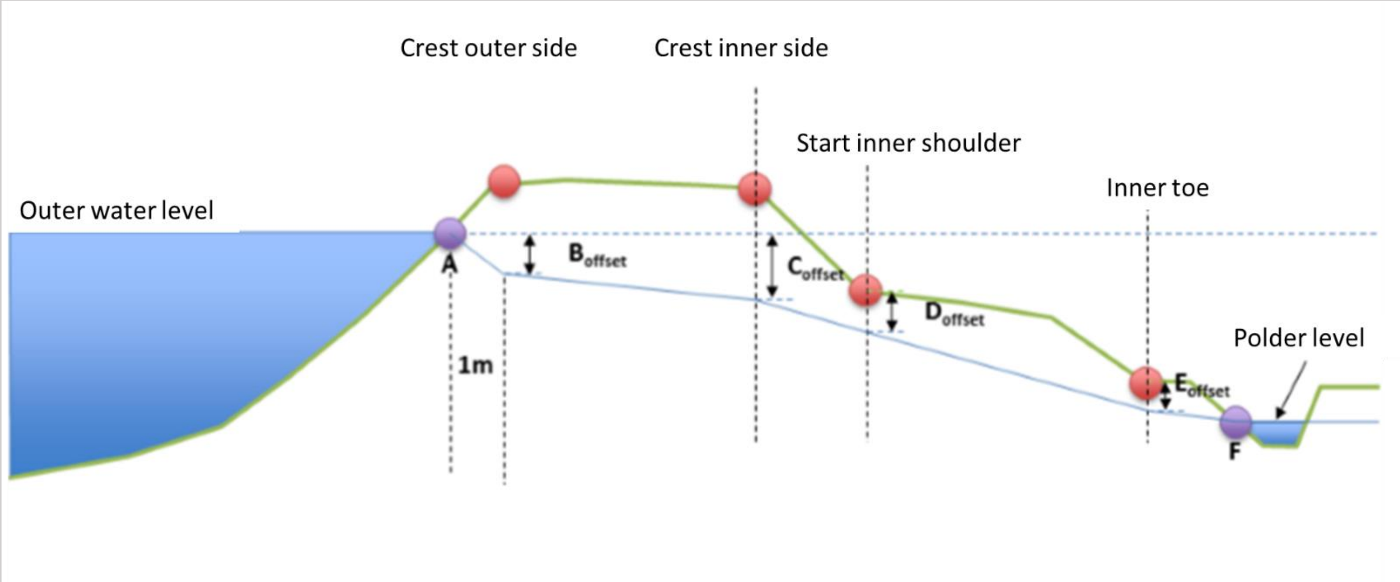

Figure 2-5: Phreatic surface in a clay dike body during a WBN event according to the Waternet Creator. (Meij, Bruijn, Blinde, Schweckendiek, & Zwan, 2011)

Table 2-5: The characteristic points of the WC in case of clay dike, on a clay of peat layer during a WBN event.

Point	**Clay-dike on clay, peat or sand layer**
A	Horizontal and vertical: Meeting point river level and outer slope of the dike
B	Horizontal: 1 meter to the right of point A. Vertical: River level minus the offset. Default offset: 1 m Minimum: initial water height point B
C	Horizontal: Below inside crest Vertical: River level minus the offset. Default offset: 1.5 m Minimum: initial water height point C
D	Horizontal: Below inner shoulder Vertical: Linear interpolation between C and E
E	Horizontal: Below inside toe Vertical: Ground level at the toe of the dike
F	Horizontal and Vertical: Meeting point polder and water level polder

The TRWD uses a different approach which is described below. In Figure 2-6 a schematic view of the calculation of the phreatic surface in the dike body is shown. The schematization consists of four points (A, B, C and D).

Point C is the height of the phreatic surface at the:
- in case of ditch, the phreatic surface of the water in the ditch
- in case of no ditch, the phreatic surface at the location of the outside toe.

Point D is the height of the phreatic surface at the:

- in case of ditch, the phreatic surface of the water in the ditch
- in case of no ditch, the phratic surface of the water at the location of the inner toe.

Point A is below the inner crest of the dike body. The height of point A is determined with equation (2-15), with a maximum of 0.3 m below the crest of the dike. In case of the TRWD, the height of point A is not dependent of the outer water level. This means the height of point A in a WBN event is equal to point A in the daily initial level. This is a realistic case for the dikes in the western part of the Netherlands, but less realistic for dikes in the eastern areas. Therefore, the TRWD is in this case only used to desbribe the phreatic surface with a WBN event.

$$A_{height} = \text{Minimum}(C_{height} + \frac{L}{X} \text{ or } D_{height} + \frac{L}{X}) \tag{2-15}$$

With:
A_{heigth} = height of point A
C_{height} = height of point C
D_{height} = height of point D
L = distance between point C and point D
d = thickness of clay or peat layer below the dike body [m]
X = 12 if d = 0.0 m
X = 10 if 0.0 m < d < 4.0 m
X = 8 if d > 4.0 m

The height of point B is equal to the height of point A. The horizontal location of point B is dependent on the penetration depth, which is dependent on the outer water level. The penetration depth I can be determined with equation (2-16).

$$I = \sqrt{\frac{2k_z H_o t}{n_z}} \tag{2-16}$$

With:
I = penetration depth [m]
k_z = hydraulic conductivity of the dike body material [m/s]
H_0 = Water depth relative to the low permeable layers [m]
t = duration of the high water [s]
n_z = porosity of the dike body material [-]

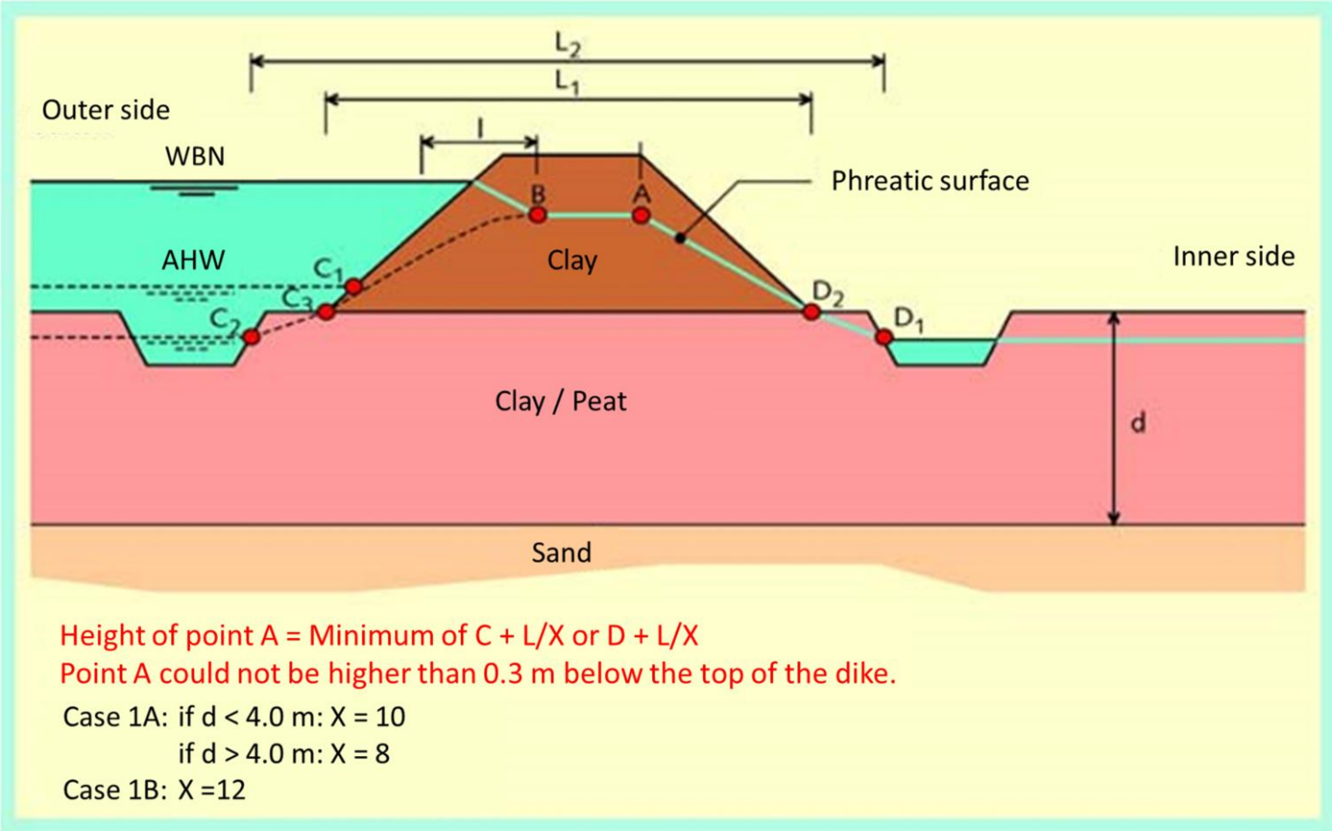

Figure 2-6: The phreatic level during a high water event according to the TRWD (TAW, 2004).

For the two test locations the WBN are quite different. The Maasdijk near Oijen has a WBN of 8.5 m +NAP, the dike has a height of around 9.7 m +NAP and the ground level is around 5.5 m +NAP. This means that approximately two meter below the top of the dike is above the phreatic level according to Table 2-5.
The IJsseldike near Westervoort has a WBN of 14.5 m +NAP, the dike height is around 14.5 m +NAP and the ground level is around 10 m +NAP. This means approximately one meter below the top of the dike is above the phreatic surface according to Table 2-5.

2.3.2 Hydraulic state Maasdijk Oijen

In Figure 2-7 the contour map of the area around the Maasdijk in Oijen is shown. The actual location of the measurement devices is on a dike which has a quite wide crest. The width of the crest of the dike is due to the construction of a ‘new’ dike around 1950. The old dike was following the road on the right side as can be seen in Figure 2-7, whereas the new dike was constructed parallel to the river. The space in between is filled with clay. Since the width of the dike around the measurement devices is not representative for the width of the total dike, the modelling is done with a smaller part of the dike about 150 m North of the location of the measurement devices.

During the winter the water level is mostly constant, except in case of heavy rainfalls in the Belgan Ardennes. Figure 2-9, shows the water level of six high water events in the river during the winter periods. It can be seen that this height is about 4.9 m+NAP in the neighbourhood of Lith. The measurepoint of this water heigth is 1.2 km downstreams from the test location. Another measurepoint of the water level is 3.5 km upstream. Over here the average water level is also around the 4.9 m+NAP. Therefore an average river water level of 4.9 m+NAP is assumed for the measure location near Oijen. The water level at the inner side of the dike is determined by the waterboard Aa en Maas. The water level in summer is 3.8 m+NAP and in winter it is 3.55 m+NAP. For the high water events a water level at the inner side of the dike of 5 m+NAP is assumed.
During a WBN event the water level is 8.5 m+NAP. In Figure 2-8 the expected phreatic surfaces according of the different methods are given.

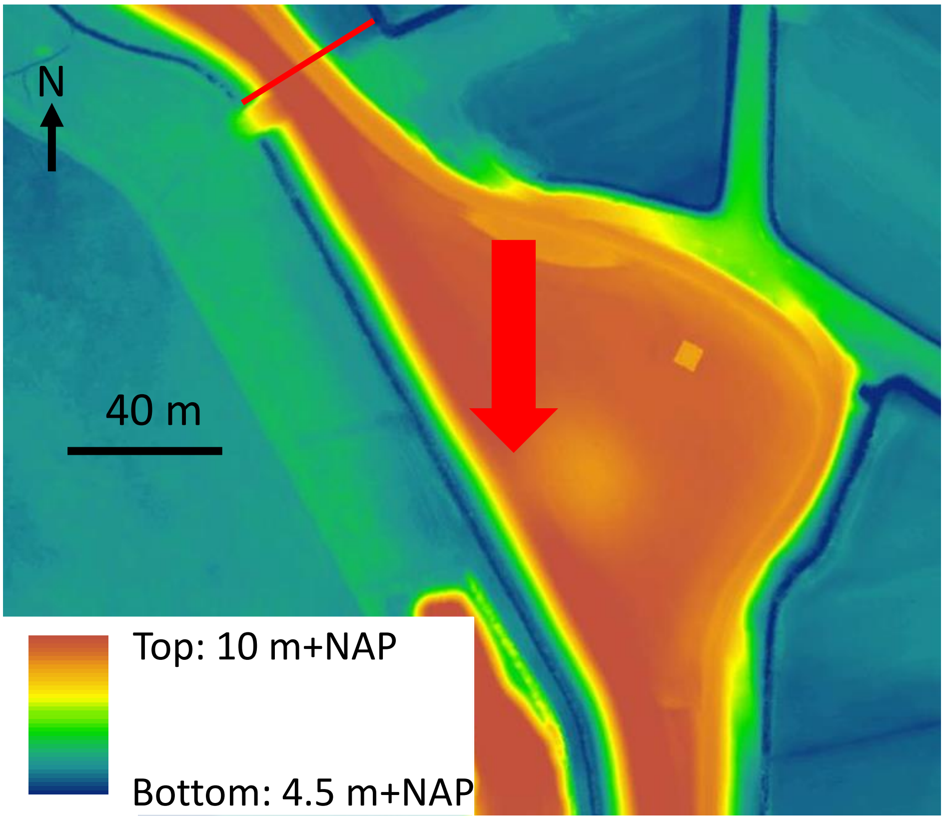

Figure 2-7: Elevation map of the area around the Maasdijk near Oijen. Red arrow: location with the measurement devices. Red line: location from the height profile which will be implemented in the model (AHN, 2019)

The high waters during the last 30 years had a duration of 3-19 days. A high water is defined as 500 cm+NAP and higher. Further analyzing of the results is done and the results are shown in
Table 2-6 until Table 2-8. The highest peak did not happen during the longest high water event.

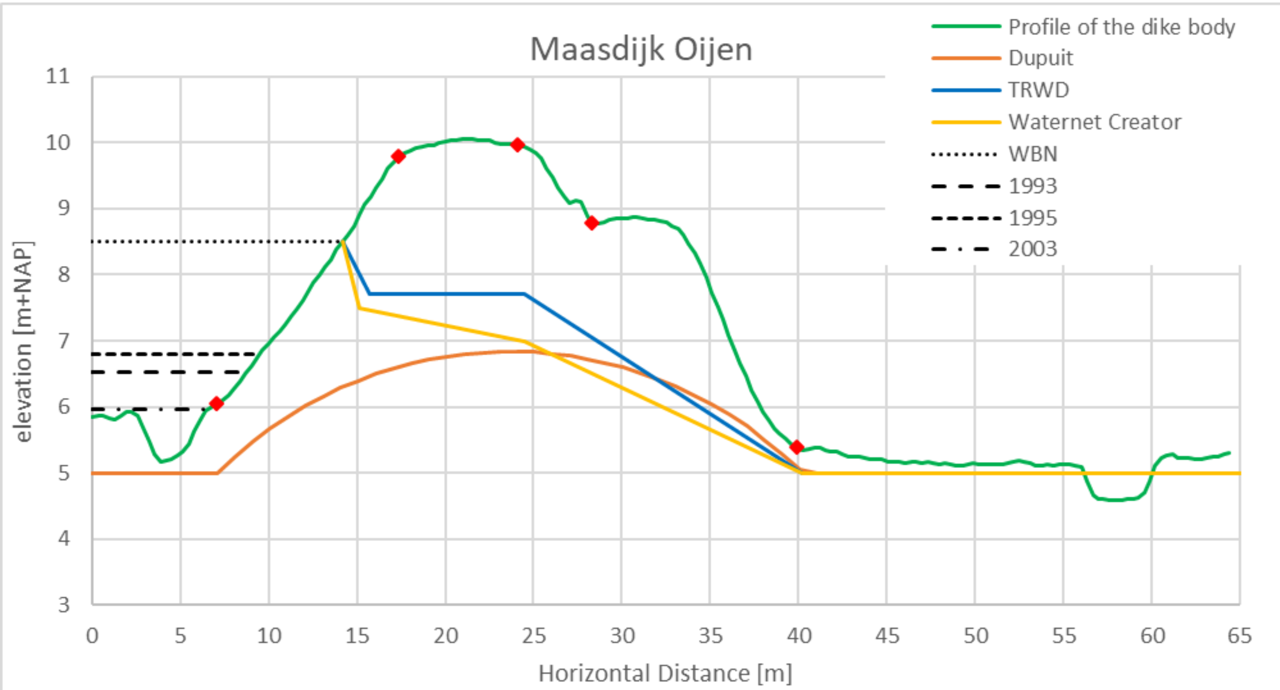

Figure 2-8: Height profile and the expected phreatic surfaces in the dike body of the smaller part of the Maasdijk near Oijen. The red points give the locations of the inside toe, inside crest, outside crest and outside toe.

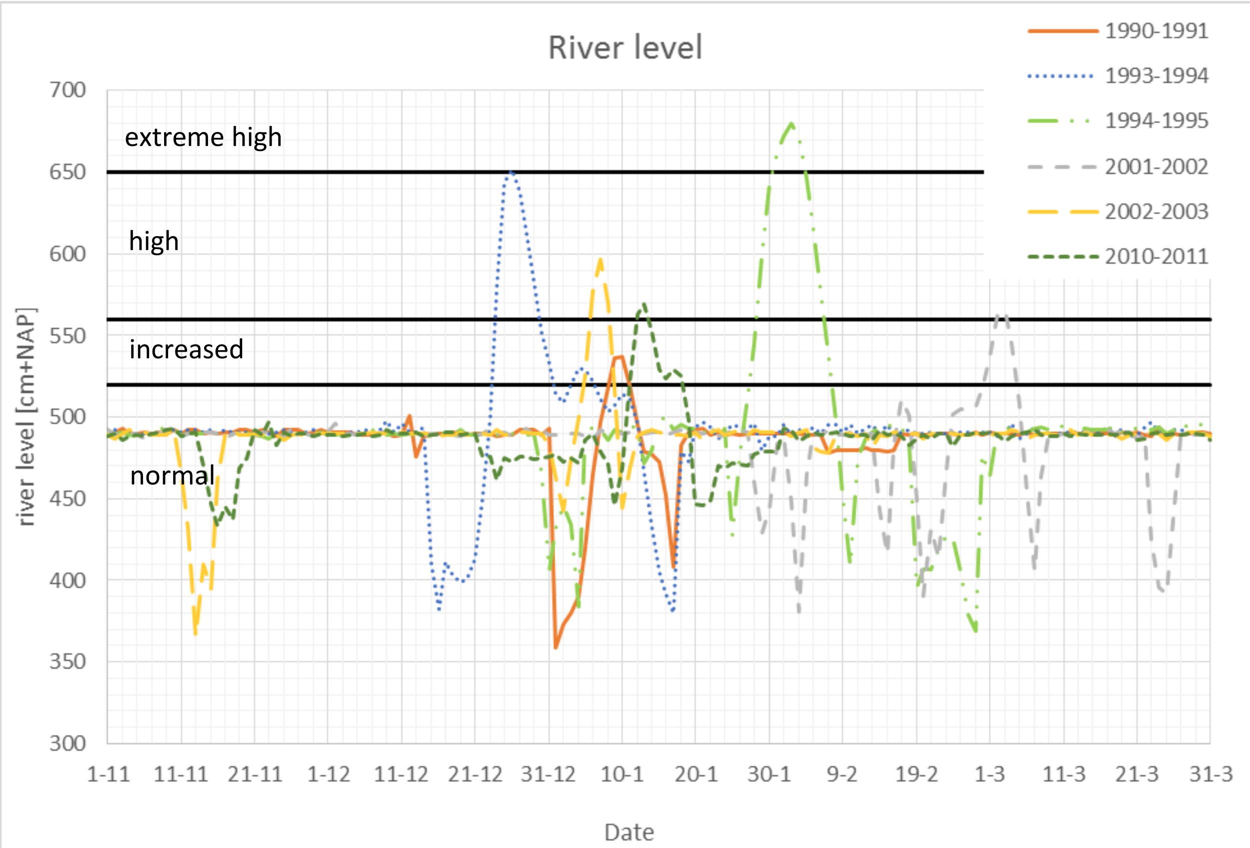

Figure 2-9: River level in the winter period near Oijen during the six high water events in the last 30 years.

Table 2-6: Information about the six high water events in the last 30 years in the Maas near Oijen.

Start date	End date	#Days	Day peak	Peak [cm]
8-1-1991	11-1-1991	3	10-1-1991	537
23-12-1993	11-1-1994	19	26-12-1993	652
16-1-1995	7-2-1995	11	2-2-1995	680
24-2-2002	5-3-2002	9	3-3-2002	565
5-1-2003	9-1-2003	4	7-1-2003	597
11-1-2011	18-1-2011	7	13-1-2011	569

Table 2-7: Statistical information about the duration of the high water events of the last 30 years near Oijen.

Average	St.dev.p	Min. (95%)	Max. (95%)
9	5	0	19

Table 2-8: Statistical information about the river level in cm of the high water events of the last 30 years near Oijen.

average	st.dev.p	min. (95%)	max. (95%)
600	50	500	700

2.3.3 Hydraulic state IJsseldijk near Westervoort

In Figure 2-10 the height profile of the IJsseldijk near Westervoort is shown and in Figure 2-11 the view from above can be found. At both sides of the dike there is a ditch. At the outer side of the dike, there is a ditch with a depth of 10 m+NAP and on the inner side there is ditch with a depth of 9.3 m +NAP.

The high water events in the IJssel can be caused by two reasons, the melting water from the Alps in Spring and heavy rain in the Rhine basin, or a combination of these two events. In Figure 2-12 the recorded water levels in the IJssel, near the test location, during high water events are shown. During the winter period the starting water level in the river is around 8 m+NAP. There is no fixed water level behind the dike, therefore a ground water level of 10 m+NAP is assumed on the inner side of the dike.
An event is called a high water event if the water level raises at least be above the 11 m+NAP. The duration of the high water event is from the day the water level is above the 9 m+NAP until the day it is below the 9 m+NAP.
During a WBN event the water level is 14.5 m+NAP. Since this is the same as the top of the dike, a WBN event of 14 m+NAP is assumed to be the WBN event. The expected conservative (TRWD) and les concervative (WC) phreatic surface are shown in Figure 2-10.

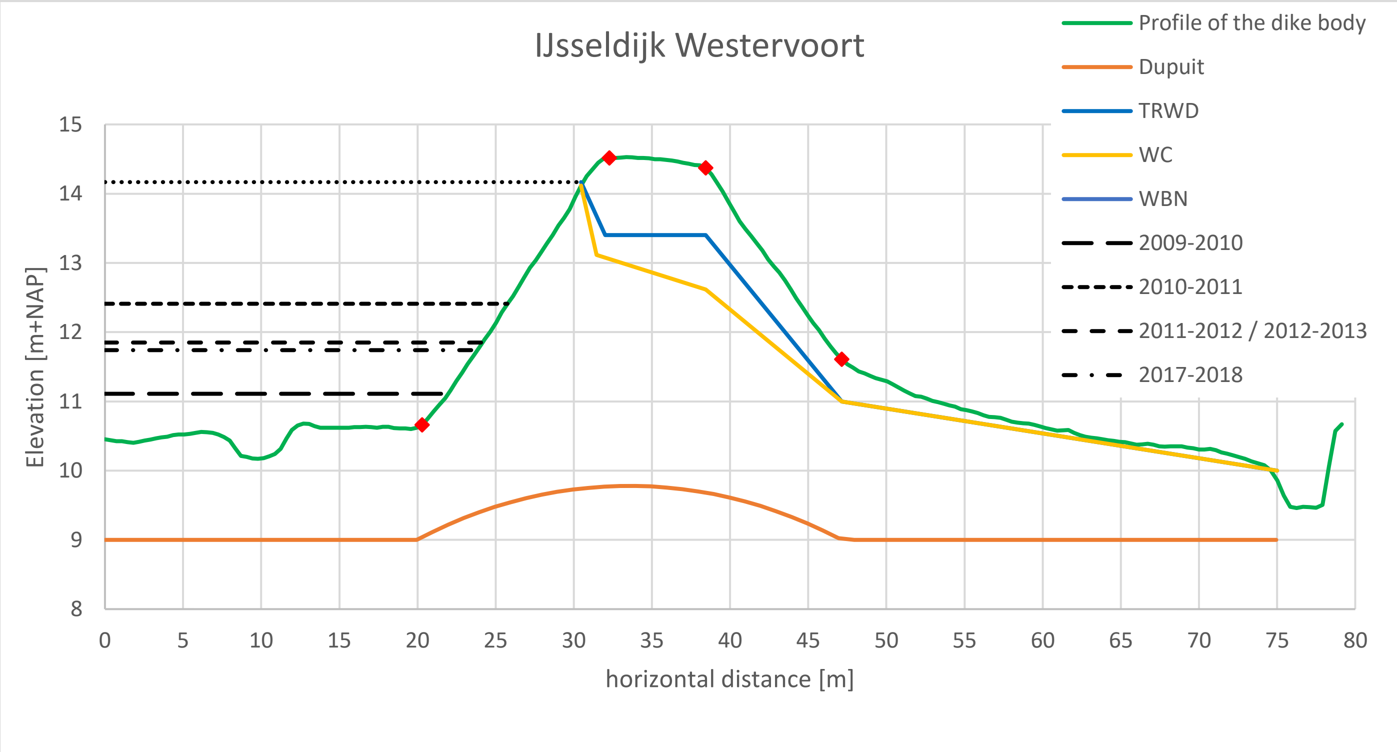

Figure 2-10: Height profile and the expected phreatic surfaces in the dike body of the IJsseldijk near Westervoort. The red points give the locations of the inside toe, inside crest, outside crest and outside toe.

The highest recorded high water in the last ten years is 12.4 m+NAP. In December 1993 and January 1995 high water events occurred. These high water events were not recorded near Westervoort, but according to the report the maximum high water in 1995 was around 13.3 m+NAP near Westervoort (TAW, 1995).

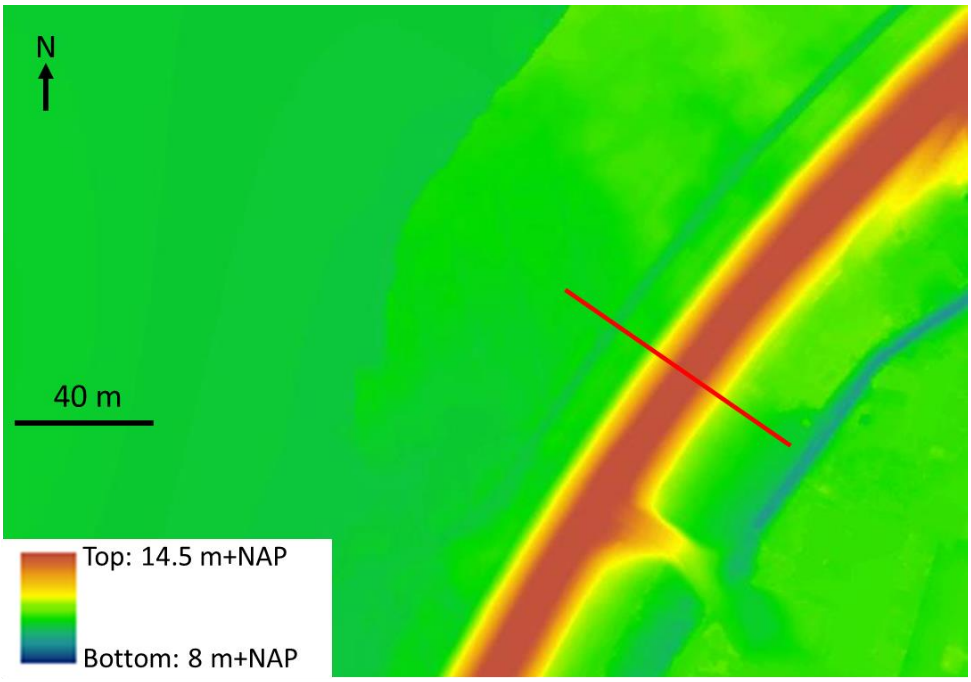

Figure 2-11: Elevation map of the area around the IJsseldijk near Westervoort. Red line: location from the height profile. (AHN, 2019)

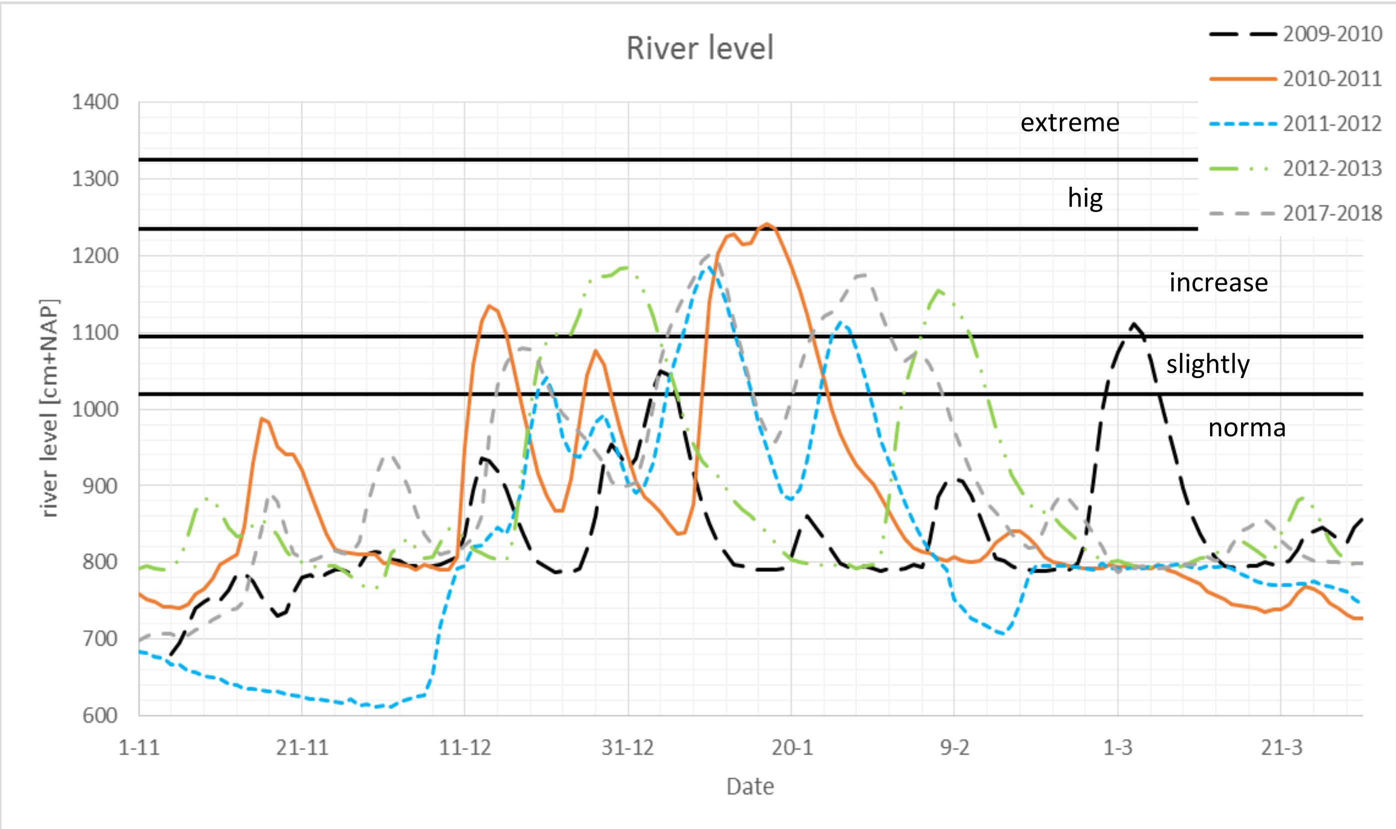

Figure 2-12: River level near Westervoort during the last five high water events.

In Table 2-9 until Table 2-11 a statistical analysis for the high water events of the last 10 years near Westervoort is given. To be characterized as an high water event the water has to be higher than 9 m+NAP, with a peak above the 11 m+NAP and a duration of at least 5 days.

Table 2-9: Statistical analysis of the high water events the last 10 years near Westervoort

Start date	End date	#Days	Day peak	Peak [cm]
26-2-2010	8-3-2010	10	3-3-2010	1111
11-12-2010	1-1-2011	21	14-12-2010	1134
9-1-2011	30-1-2011	21	17-1-2011	1241
19-12-2011	2-2-2012	45	21-12-2011	1184
18-12-2012	11-1-2013	24	31-12-2012	1185
2-2-2013	16-2-2013	14	7-2-2013	1154
31-12-2017	11-2-2018	42	29-1-2018	1174

Table 2-10: Statistical information about the duration of the high water events of the last 10 years near Westervoort.

Average	St.dev.p	Min. (95%)	Max. (95%)
25	12	0	61

Table 2-11: Statistical information about the river level in cm of the high water events of the last 10 years near Westervoort

Average	St.dev.p	Min. (95%)	Max. (95%)
1169	39	1052	1286

2.4 Soil Suction

In Chapter 2.2 information about the SWCC is given. The SWCC shows the relationship between the soil suction and the VWC or degree of saturation.
The soil suction (Ψ) consists of the matric suction (Ψ_m) and the osmotic suction (π). The matric suction consists of two parts the capillary suction (Ψ_c) and the adsorption component (Ψ_{AD}). Osmotic suction is related to the salt content present in the soil water. The osmotic suction may only be significant in cases where chemical contamination change the salt content of the pore water, or construction occurs in saline soils or marine conditions. In the case of soil water in the neighborhood of rivers and dikes in the upper river area, the osmotic suction is negligible (Rowe, 2011).
The soil suction is measured as the negative pore water pressure, but only the capillary component influences the shear strength. The adsorption component influence the water in the micro pores, which does not influence the effective stress and therefore the shear strength of the soil (van Duinen, van Hoven, Visschedijk, & Wichman, 2018).
The capillar component of the soil suction influences the shear strength. The maximum possible shear stress according to the Mohr-Coulomb model can be determined with equation (2-17). If the shear stress exceeds this maximum, failure will occur.

$$\tau_f = c' + \sigma' \tan(\phi) \tag{2-17}$$

With:
τ_f = shear strength [kPa]
c = cohesion [kPa]
σ' = effective vertical stress [kPa]
ϕ = friction angle [°]

The effective stress of a soil is dependent from the total stress on top of the soil and the pore water pressure (or pore water suction).
Soil consists of two or more phases. One of the phases is the grains, which form a skeleton. In between the grains are pores, these pores can be filled with a fluid, usually water. The effective stress can be calculated according to equation (2-18).

$$\sigma' = \sigma - u \tag{2-18}$$

With:
σ' = effective stress [kPa]
σ = total stress [kPa]
u = pore water pressure [kPa]

A negative pore water pressure will lead to a higher effective stress and therefore a higher maximum shear strength. Since the pores above the water table are not completely filled with water, the suction has to be multiplied with the matric suction coefficient, as a simplification the degree of saturation (S_r) can be used. Equation (2-19) gives the total equation with the degree of saturation (S_r).

$$\tau_f = c' + \sigma \tan(\phi') - S_r u \tan(\phi') \tag{2-19}$$

In case of a negative pore water pressure, water suction, the effective stress will increase. The negative pore water pressure is present in the soil above the phreatic level, the capillary and funicular zone. The dimensions of soil above the phreatic surface where suction is present are mainly dependent on the size of the pores and therefore on the soil type. The smaller the soil grains, the smaller the pores, the higher the capillary and funicular zone.

Below the phreatic level the water pressures are positive, above the phreatic level, there are suction stresses and therefore a negative pore water pressure. The theoretical hydrostatic line above the phreatic level will increase linear. But since the degree of saturation above the hydrostatic line is not 100% until the top, the actual pore water pressure (p_{active}) will decrease to zero (Figure 2-13).

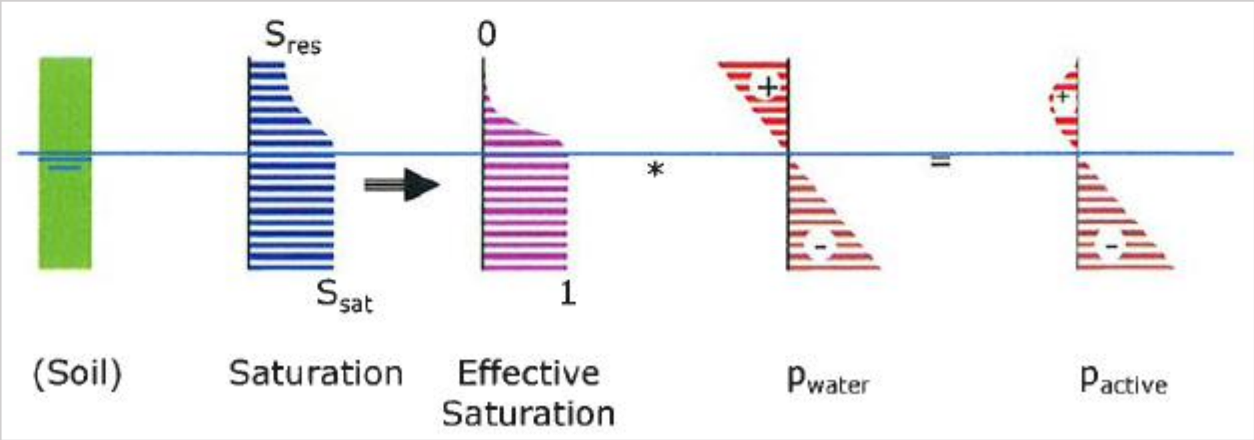

Figure 2-13: Graphical representation of the determination of the relevant pore water pressure p_{active}. (Plaxis, 2019)

Beside the influence of the effective saturation, the precipitation also influences the suction in the top layers of the soil. Lim et al. (1996) performed a research on the infiltration of precipitation on a slope. They installed tensiometers on top of the slope (R1), halfway the slope (R2 and R3) and at the bottom of the slope (R4). Furthemore, they divided the slope in three parts. The first part covered with canvas (P1), the second part without any cover (P2) and the third part covered with grass (P3). Figure 2-14 shows the difference in suction measured during the test period. In case the water infiltrates in the soil, the suction in the top layer will disappear. In a grass-covered dike the influence of the precipitation on the soil suction is approximately until one meter below surface (Figure 2-14).

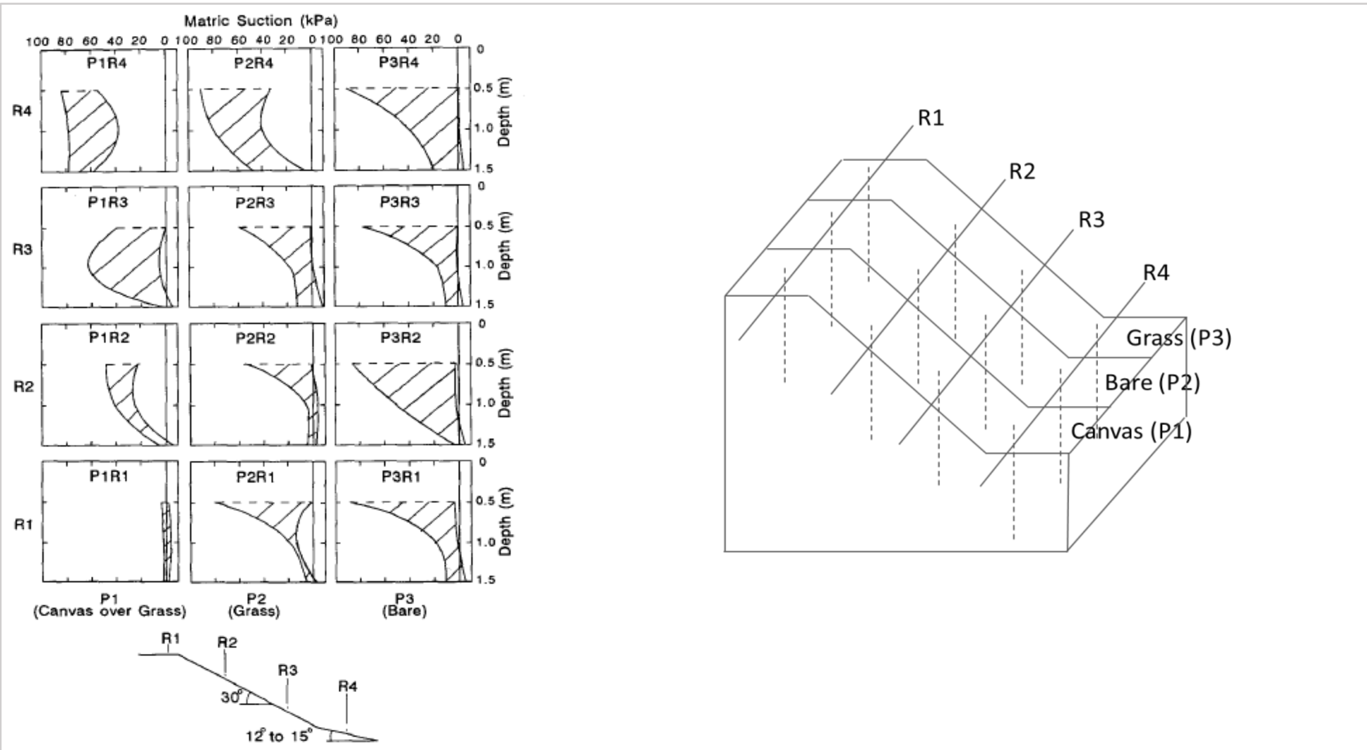

Figure 2-14: Left: Ranges of measured matric suction on a residual soil slope in the Jurong Formation in Singapore (Lim, Rahardjo, CHang, & Fredlund, 1996), right: The location of the sensors and sorts of cover on the soil.

For example, think of a dike body with a height of five meters, with a phreatic surface during the WBN event three meter below the top. The dike body consists of heavy clay (Staring Serie subsoil O12). The cohesion of the soil is 5 kPa, the unit weight 18 kN/m^3 and the internal friction angle 20°. Figure 2-15 shows the shear strength for the dike body, assuming the top of the dike is at 10 m+NAP, with and without taking into account the suction. In reality the suction until one meter below the top of the dike body should not be taken into account, since the precipitation influences these part. Therefore the maximum difference between the shear strength with and without suction is at a height above the phreatic level of two meters. The shear strength with suction is theoretical 54 % higher than without suction.

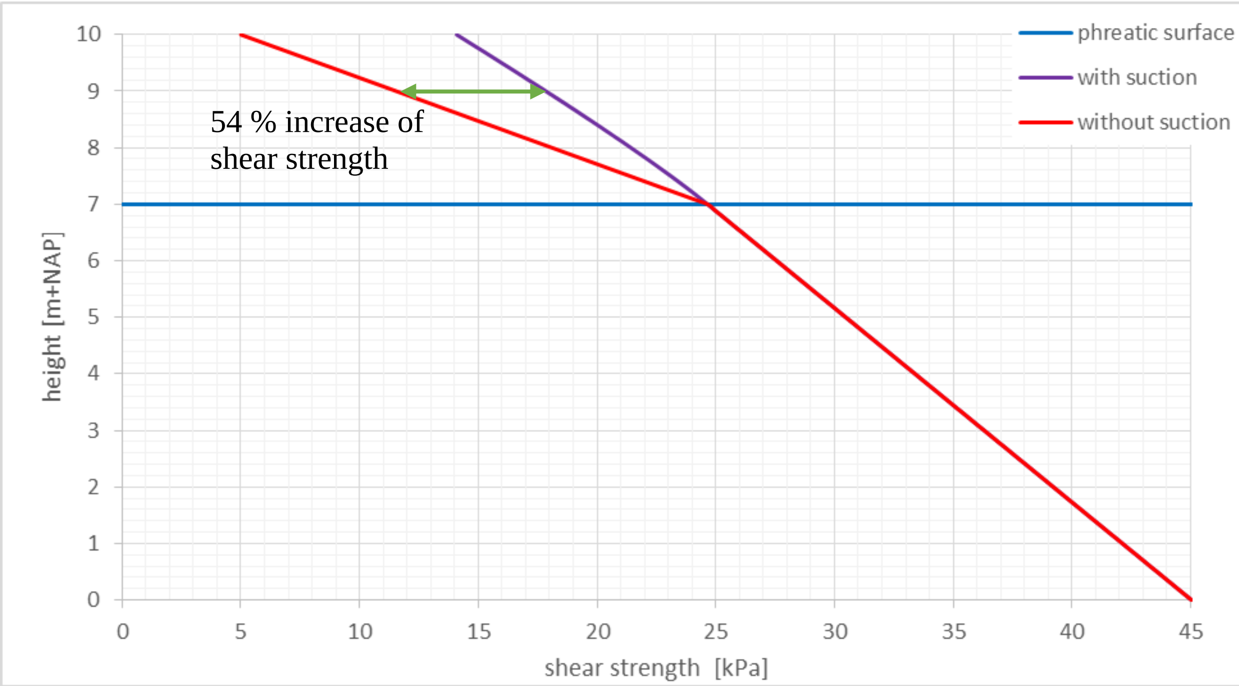

Figure 2-15: Shear strength of a dike body above the phreatic surface. The dike body consists of a heavy clay (Staring Serie subsoil O12) with a cohesion of 5 kPa, unit weight of 18 kN/m^3 and an internal friction angle of 20 °.

2.5 Soil models

In the WBI 2017 the Critical State Soil Mechanics (CSSM) concept is used in the assessment of the slope stability. To model the qualitative effects of the soil suction the Mohr-Coulomb (MC) model is used and for the quantitative effects, furthermore the Hardening Soil (HS), Soft Soil (SS) model and SHANSEP concept are used. In the end some information is given about the different methods to make a undrained calculation in Plaxis.

2.5.1 Hardening Soil model

The Hardening Soil (HS) model is different from the MC model in describing the yield surface and the stress-dependency of stiffness. In the HS model the yield surface can expand due to plastic straining, called hardening. There are two types of hardening in the HS model: shear hardening and compression hardening. Shear hardening is used to model irreversible strains due to primary deviatoric loading and Compression hardening is used to model irreversible strains due to primary compression in oedometer loading or isotropic loading.

The HS model is based on the Duncan-Chang or hyperbolic model and has the following basic characteristics:

- Stress dependent stiffness according to a power law;
- Plastic straining due to primary deviatoric loading;
- Plastic straining due to primary compression;
- Elastic unloading/reloading;
- Failure according MC criterion.

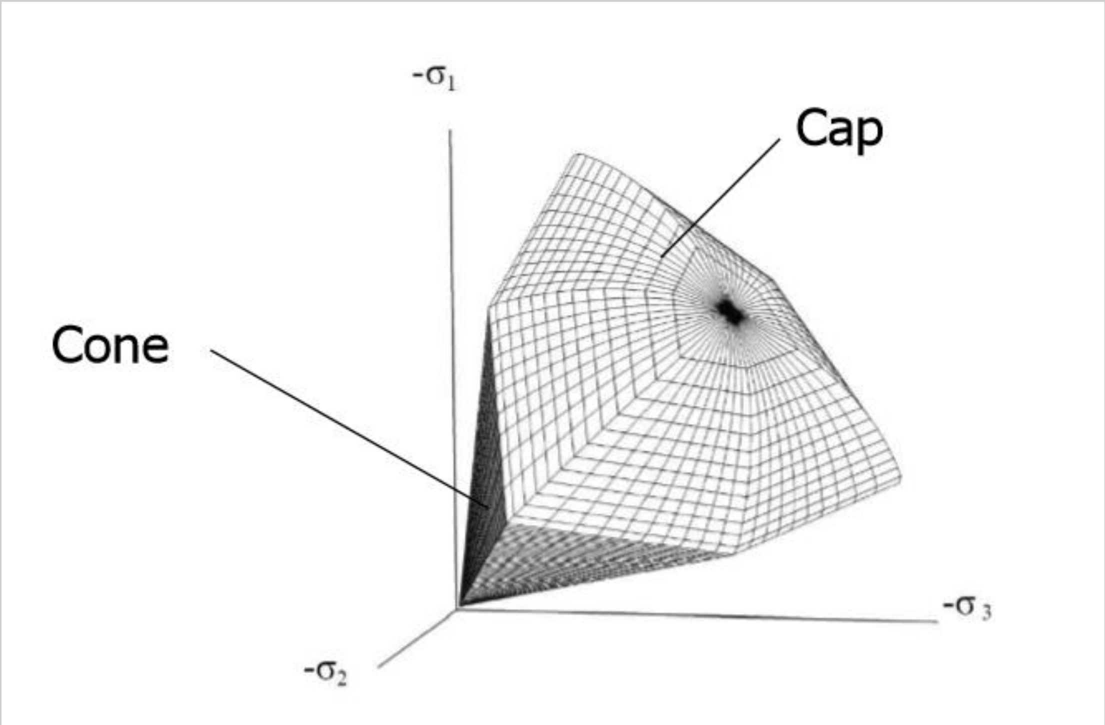

Figure 2-16: Hardening Soil yield contour (Plaxis, 2020)

The basic characteristic of the HS model is the stress dependency of the soil stiffness. Therefore, the input parameters for the HS model are different reference values for the soil stiffness (Table 2-12). Figure 2-20 gives a graphical representation of the different stiffness parameters.

Table 2-12: Input parameters for the HS model in Plaxis

Symbol	Parameter	Unit	Default value
Failure parameters as In MC model			
c	Effective cohesion	kN/m^2	
φ	Effective angle of internal friction	°	
ψ	Angle of dilatancy	°	
σ_t	Tension cut-off and tensile strength	kN/m^2	
Basic parameters for soil stiffness			
E_{50}^{ref}	Secant stiffness in standard triaxial test	kN/m^2	
E_{oed}^{ref}	Tangent stiffness for primary oedometer loading	kN/m^2	
E_{ur}^{ref}	Unloading/reloading stiffness	kN/m^2	$E_{ur}^{ref} = 3E_{50}^{ref}$
m	Power for stress-level dependency stiffness		
Advanced parameters (it is advised to use the default settings)			
ν_{ur}	Poisson's ratio for unloading-reloading		0.2
p^{ref}	Reference stress for stiffness	kN/m^2	100
K_0^{nc}	K_0- value for normal consolidation		$K_0^{nc} = 1 - \sin(\varphi)$
R_f	Failure ratio q_f / q_a		0.9
$\sigma_{tension}$	Tensile strength	kN/m^2	0
c_{inc}	As in MC model	kN/m^3	0
Alternative parameters			
C_c	Compression index		
C_s	Swelling index or reloading index		
e_{init}	Initial void ratio		

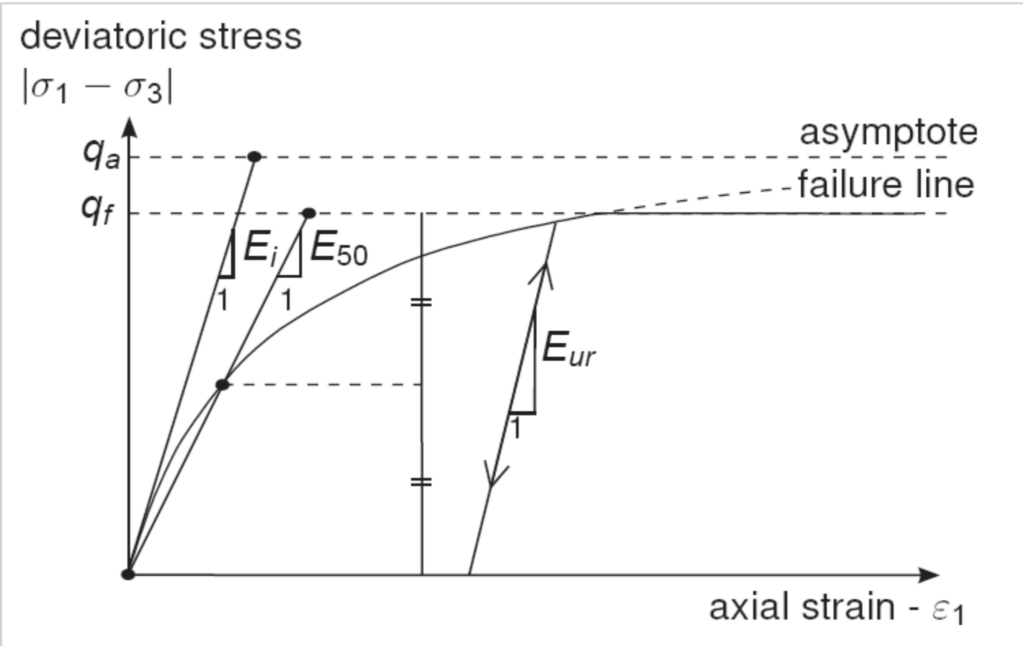

Figure 2-17: Hyperbolic stress-strain relation in primary loading for a standard drained triaxial test

In Figure 2-17 the hyperbolic relationship between the axial strain (ε_1) and the deviatoric stress (q) is given. The yield curve for primary triaxial loading can be described by equation (2-20).

$$q = -\frac{\varepsilon_1}{\frac{1}{E_i} - \frac{\varepsilon_1}{q_a}} \qquad \text{for: } q < q_f \tag{2-20}$$

With:
q = deviatoric stress [kPa]
ε_1 = axial strain
E_i = initial stiffness [kPa]
q_a = asymptotic value of the shear strength [kPa]

The initial stiffness E_i is related to E_{50} by equation (2-21).

$$E_i = \frac{2E_{50}}{2 - R_f} \qquad E_{50} = E_{50}^{ref}\left(\frac{c\cos(\varphi) - \sigma_3' \sin(\varphi)}{c\cos(\varphi) + p^{ref}\sin(\varphi)}\right)^m \tag{2-21}$$

With:
E_{50} = secant stiffness modulus [kPa]
R_f = failure ratio (default value 0.9)
E_{50}^{ref} = reference stiffness modulus corresponding to the reference stress p_{ref} [kPa] (p_{ref} is as default 100 kPa)
c = cohesion [kPa]
φ = internal friction angle [°]
σ_3' = principal horizontal effective stress [kPa]
m = amount of stress dependency (0.3 – 1)

The ultimate deviatoric stress (q_f) and the asymptotic value of the shear strength (q_a) are defined by equation:

$$q_f = \frac{2\sin(\varphi)}{1 - \sin(\varphi)}\left(c\cot(\varphi) - \sigma_3'\right) \qquad q_a = \frac{q_f}{R_f} \tag{2-22}$$

With:
q_f = ultimate deviatoric stress [kPa]
φ = internal friction angle [°]
c = cohesion [kPa]
σ_3' = principal horizontal effective stress [kPa]
R_f = failure ratio (default value 0.9)
q_a = asymptotic value of the deviatoric stress [kPa]

Although there are benefits to the HS model, there are also some limitations. The HS model does not distinguish between peak strength and residual strength, which means that it does not include softening behavior. There is no accumulation of strain or pore pressure in cyclic loading. Creep behavior is not included in the model and it is an isotropic model. The model is not recommended for very soft soils (ratio E_{50}^{ref} over E_{oed}^{ref} larger than two).

2.5.2 Mohr-Coulomb model

The Mohr-Coulomb (MC) model, also called the Linear Elastic Perfectly Plastic (LEPP) model with a Mohr-Coulomb failure criterion, is a very simplified model of the behavior of soil. In reality, the soil stiffness depends of the stress subjected to the soil, the stress path and the strain level. The MC model gives a good first approximation. The strain in the MC model consists of two parts, the elastic part and the plastic part (equation (2-23)). The linear elastic part is based on Hooke's law of isotropic elasticity and the perfectly plastic part is based on the Mohr-Coulomb failure criterion. (Plaxis, 2020)
In Figure 2-18 the basic idea of the LEPP model is shown. If the stress acting on a surface is increasing, the material, in this case the soil, will strain. If the stress is removed, the material will go back to its old dimensions. This part is called the elastic strain. Plastic strain occurs after the elastic strain, and is a permanent deformation. If the stress is removed, the plastic part of the strain will be left.

$$\varepsilon = \varepsilon^e + \varepsilon^p \tag{2-23}$$

Plastic strains are irreversible. To evaluate if plastic strains are occurring, there is a yield function *f*. If the yield function becomes equal or bigger than zero, plastic strains are occurring. Figure 2-19 shows the six yield functions of the MC model in the principal stress plain.

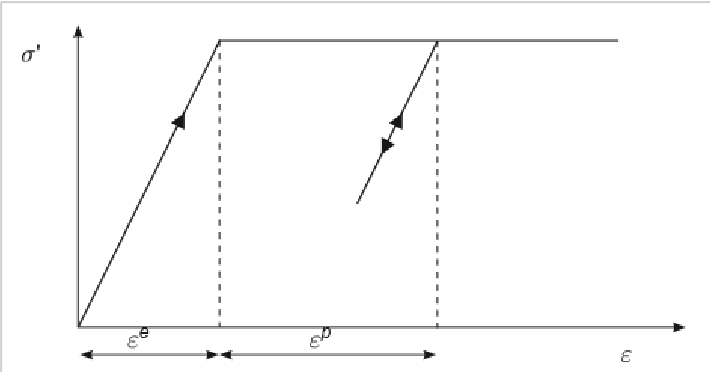

Figure 2-18: Basic idea of the linear elastic perfectly plastic model (Plaxis, 2020)

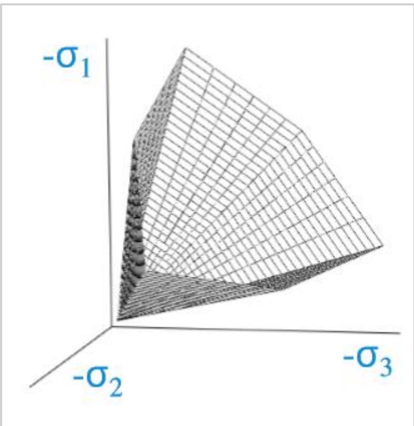

Figure 2-19: Mohr-Coulomb yield contour (Plaxis, 2020)

The basic parameters for the MC model are given in Table 2-13. The Young's modulus *E* can be determined in different ways. In Figure 2-20 the different ways are graphically shown. In this case the E_{50} value of the Young's modulus is used. Since the undrained parameters are used, the Young's modulus has the meaning of the effective Young's modulus.
With the advanced parameters a depth dependent Young's modulus can be used. The increment of stiffness per meter is given through the E'_{inc} parameter. The stiffness for each depth is calculated with equation (2-24).

$$E(y) = E_{ref} + (y_{ref} - y)E_{inc} \qquad (y < y_{ref}) \tag{2-24}$$

Table 2-13: input parameters for the MC model

Symbol	Parameter	Unit
Basic parameters		
E	Young's modulus	kN/m^2
ν	Poisson's ratio	-
c	Cohesion	kN/m^2
φ	Friction angle	°
Ψ	Dilatancy angle	°
σ_t	Tension cut-ff and tensile strength	kN/m^2
Advanced parameters		
E'_{inc}	Depth dependency of the young's modulus	kN/m^2/m
y_{ref}	Reference depth of the young's modulus	m
c'_{inc}	Depth dependency of the cohesion	kN/m^2/m
y_{ref}	Reference depth of the cohesion	m

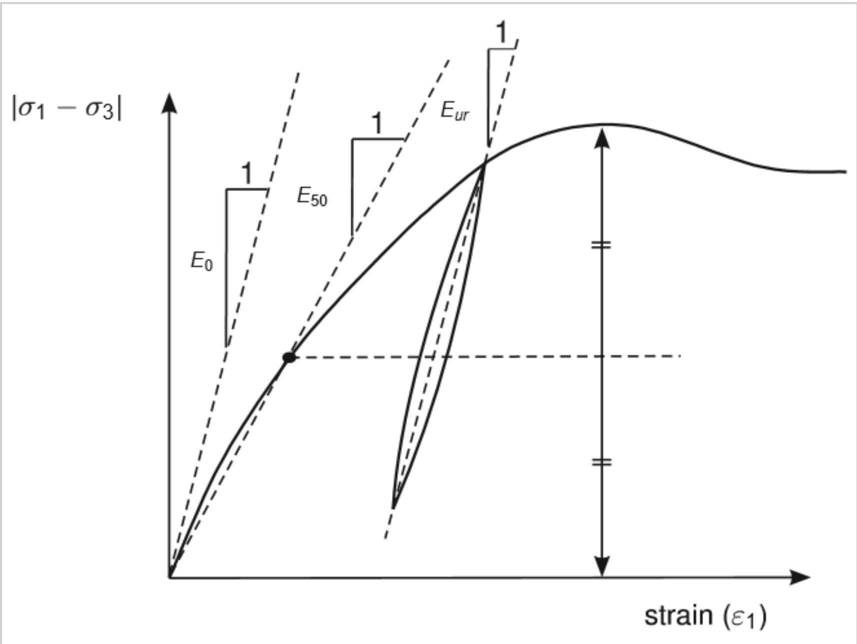

Figure 2-20: Different young's modulus' can be determined from a stress-strain graph. The location of determining the Young's modulus is important and depending of the purpose of the Young's modulus. (Plaxis, 2020)

2.5.3 The Soft Soil Model

The Soft Soil Model (SS) is an advanced constitutive model to simulate the behavior of normally consolidated soft soils, for example clays and peats. The characteristics of the SS model are listed below:

- Stress dependent stiffness behavior;
- Distinction between primary loading and unloading-reloading;
- Memory for pre-consolidations stress;
- Failure behavior according to the MC criterion.

The model assumes a logarithmic relation between the volumetric strain (ε_v) and the mean effective stress (p'). During isotropic virgin compression this relation is described according to equation (2-25) and the relationship during unloading and reloading is given in equation (2-26). The graphical representation of the swelling and compression index is given in Figure 2-21. (Plaxis, 2020)

$$\varepsilon_v - \varepsilon_v^{e0} = -\lambda^* \ln\left(\frac{p' + c\,cot(\varphi)}{p^0 + c\,cot(\varphi)}\right)$$

(2-25)

With:
ε_v = volumetric strain
ε_v^{e0} = initial volumetric strain
λ^* = modified compression index
p' = mean effective stress [kPa]
p^0 = initial value of the mean effective stress [kPa]

$$\varepsilon_v^e - \varepsilon_v^{e0} = -\kappa^* \ln\left(\frac{p' + c\,cot(\varphi)}{p^0 + c\,cot(\varphi)}\right)$$

(2-26)

With:
ε_v^e = volumetric elastic strain
ε_v^{e0} = initial volumetric strain
κ^* = modified swelling index
p' = mean effective stress [kPa]
p^0 = initial value of the mean effective stress [kPa]

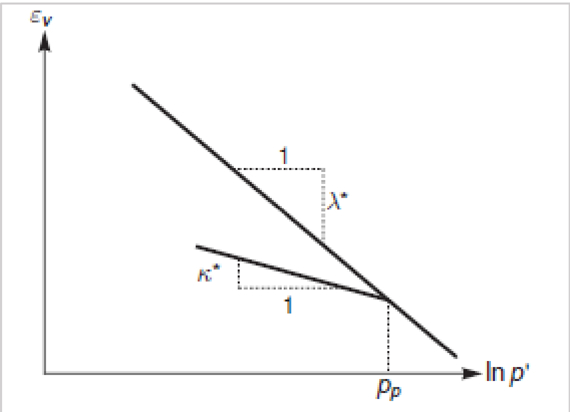

Figure 2-21: Illustration of the logarithmic relation between volumetric strain and mean stress. (Plaxis, 2020)

$$f_c = \frac{q^2}{M^2(p' + c\cot(\varphi))} + p'$$

(2-27)

f_c = yield surface cap hardening
q = deviatoric stress [kPa]
M = steepness parameter (determined automatically by PLAXIS)
p' = mean effective stress [kPa]

In Figure 2-22 the cap yield surface is shown. The parameter M determines the shape and steepness of the yield surface, but it is not a direct input parameter. M is calculated internally from the input parameters (K_0^{NC}, ν_{ur} and λ^*/κ^*).

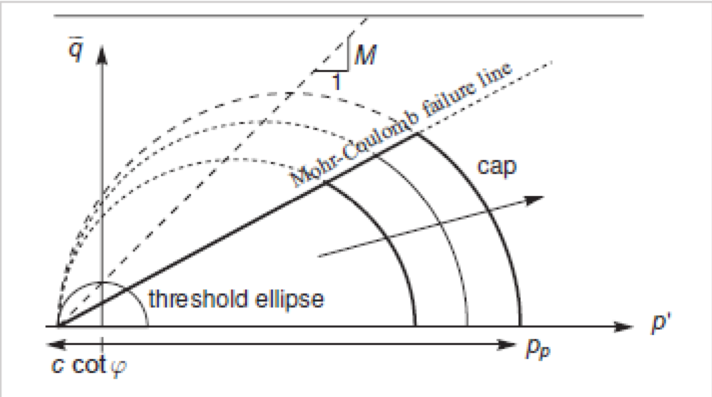

Figure 2-22: Cap yield surface for SS model (Plaxis, 2020)

Table 2-14: Input parameters for SS model.

Symbol	**Parameter**	**Unit**
Basic parameters:		
λ^*	Modified compression index	
κ^*	Modified swelling index	
c	Effective cohesion	kN/m^2
φ	Friction angle	
ψ	Dilatanct angle	
σ_t	Tensile strength	kN/m^2
Advanced parameters (use default setings):		
ν_{ur}	Poisson's ratio for unloading/ reloading	
K_0^{NC}	Coefficient of lateral stress in normal consolidation	
M	Dependent of K_o^{NC}	

2.5.4 SHANSEP Concept

The Stress History and Normalized Soil Engineering Properties method (SHANSEP) concept is a way to calculate the undrained shear strength of a soil, based on the effective stress state of a soil. In case of undrained behavior, the water pressures are generated in the soil, when sheared. Therefore the effective stress of the soil and the shear stress of the soil decreases. Since the assumption is made that the slope failure of primary dikes occurs in a short time, undrained behavior is assumed to be representative in case of soil layers with a low permeability. In case of undrained behavior the SHANSEP method is used to determine the shear strength. The shear strength is dependent on several factors, including the stress history and current stress conditions of the soil. The undrained shear strength can be determined with the SHANSEP method as follows:

$$s_u = S\sigma'_{vi}(OCR)^m \qquad \text{with } OCR = \frac{\sigma'_{vy}}{\sigma'_{vi}}$$

(2-28)

With:
s_u = mobilized undrained shear strength [kPa]
σ'_{vi} = effective normal stress [kPa]
$S = \frac{s_u}{\sigma'_{vc}}$ for a normally-consolidated soil (*OCR* =1)
OCR = over consolidation ratio
m = magnitude

In the SHANSEP NGI-ADP model in Plaxis, the OCR is based on the largest principal effective stress σ_1 (equation (2-29)).

$$OCR = \frac{\sigma_{1,max}}{\sigma_1}$$

(2-29)

With:
OCR = over consolidation ratio
σ_1 = largest principal effective stress [kPa]
$\sigma_{1,max}$ = largest principal effective stress the soil experienced, based on the OCR or based on the calculations in the model. [kPa]

In Plaxis equation (2-30) is used to calculate the undrained shear strength with the SHANSEP concept.

$$s_u = \alpha\sigma_1\left(\frac{\sigma_{1,max}}{\sigma_1}\right)^m$$

(2-30)

With:
S_u = undrained shear strength [kPa]
$\alpha = \frac{S_u}{\sigma'_{vc}}$ for a normally-consolidated soil (*OCR* =1)
σ_1 = largest principal effective stress [kPa]
$\sigma_{1,max}$ = largest principal effective stress the soil experienced, based on the OCR or based on the calculations in the model. [kPa]
m = magnitude

Another way to calculate the undrained shear strength is with the data from a CPT test. To derive the shear strength from the CPT data the empirical equation (2-31) is used (Ministerie van Infrastructuur en Milieu, 2019). The empirical correlation factor (N_{kt}) is chosen, by comparing the CPT-data to the FVT data from the same day.

$$S_u = \frac{q_c - \sigma_v'}{N_{kt}}$$

(2-31)

With:
S_u = undrained shear strength [kPa]
q_c = Cone resistance [kPa]
σ_v' = effective vertical stress [18 kPa]
N_{kt} = empirical correlation factor

2.5.5 Undrained A

To model the soil suction, an undrained calculation is necessary. Plaxis gives different options for undrained calculations. With the option undrained A, the effective stress parameters are used and should be entered in the material parameters. If the drainage type is set to undrained A, Plaxis will add the stiffness of the water to the stiffness matrix in order to distinguish between effective stresses and (excess) pore pressures. The advantage of this method is the increased shear strength after consolidation if a load is applied on the soil. In Figure 2-23 the stress paths in different scenarios are shown. In case the undrained MC model is used, the mean effective stress *p*' remains constant until failure (stress path (1)). In case consolidation occurs, the mean effective stress will increase during the consolidation, which will result in a higher shear strength when a new load is applied (stress path (3) and (4)). In case of soft soils (normally consolidated clays and peats), the mean effective stress will decrease due to the shear induced pore pressure (stress path (2)).

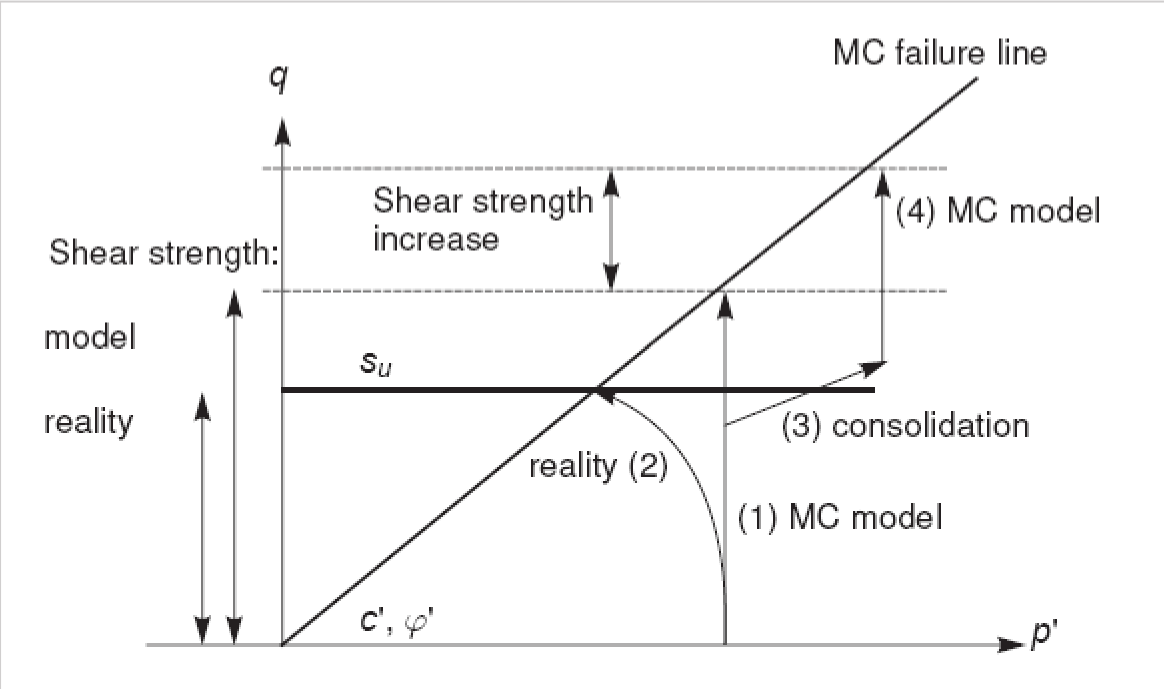

Figure 2-23: Illustration of stress paths; reality vs. Mohr-Coulomb model (Plaxis, 2020)

2.5.6 Undrained B en C

Other options to model undrained behavior in Plaxis are with the undrained B or C option. The undrained B option can be used if the undrained shear profile for a soil over depth is known. In that case a direct input of the shear strength of the soil is used. Due to the undrained shear strength increasing with depth most of the time, it is possible to specify an increase of the undrained shear strength with depth (Plaxis, 2020).

The undrained C option is used, when a conventional total stress analysis is performed, with all parameters specified as undrained. On top of that, for this option the undrained shear strength is a direct input parameter. The difference with undrained B is that there is no distinction between total stresses and effective stresses in the undrained C option. All stresses have to be interpreted as total stresses and the pore pressure is always zero (Plaxis, 2020).

Since the purpose of this study is to look for a way to calculate the undrained shear strength with effective shear strength parameters the pore water pressure should be taken into account. Therefore the undrained B and C cannot be used for the purpose of this study.

3 Model Configuration and parameter determination

In Plaxis a model is built to determine the influence of the different variables and to make a model which represents the measurement data. In chapter 3.2 the model is described and in chapter 3.1 the different parameters for the soil models are derived.

An important note for the model is, that from two test locations, one model has been build. To build a model of a dike information is needed from the foreland, dike body, below the dike body and the hinterland. As can be seen in Figure 1-4, in Westervoort measurements are performed in the outer toe, inner toe and inner berm and CPTs are performed every two to four weeks in the inner berm. Therefore enough information is known about the fore- and hinterland. Furthermore in the end of October two CPTs were performed in the outer toe and inner toe and one CPT was performed in the crest. Therefore the layering of the fore- and hinterland can be determined. The soil layering for the dike body was not reliable with only one CPT. In Figure 1-5 it is shown in Oijen measurements are performed in the crest only. Therefore only information is available from the dike body and not from the fore- and hinterland.
So from Westervoort detailed information was known for the fore- and hinterland and from Oijen only information was known from the dike body. Therefore one model is built with the dike body from Oijen and the fore- and hineterland from Westervoort. In Figure 3-2 the area within the red lines is based on the test location in Oijen, the rest of the model is based on the test location in Westervoort.

3.1 Parameter Determination

Different soil models are used to model the behavior of the soils in the dikes. In chapter 2.5 the differences between the soil models are explained. In this chapter first is explained how the different layers are determined, after that the parameter determination of the MC model, HS model, SS model and the SHANSEP concept are described respectively.

In Westervoort CPTs were performed in the outer toe, crest, inner toe and inner berm. Furthermore soil samples from the inner berm were taken until a depth of 4.25 m below the surface. From the CPTs a classification is made with Figure 3-1. In the model a distinction is made between the soil types according to the CPT data as described in Table 3-1.

Table 3-1: Soil classification from the probe resistance and friction number to determine the soil type used in this study.

Soil type	Probe resistance q_c [MPa]	Friction number
Sand	>6	<1
Sandy Clay	3-6	0-2
Silty Clay	0-1	0-3
Clay	0-1	3-5
Peat	0-2	>6

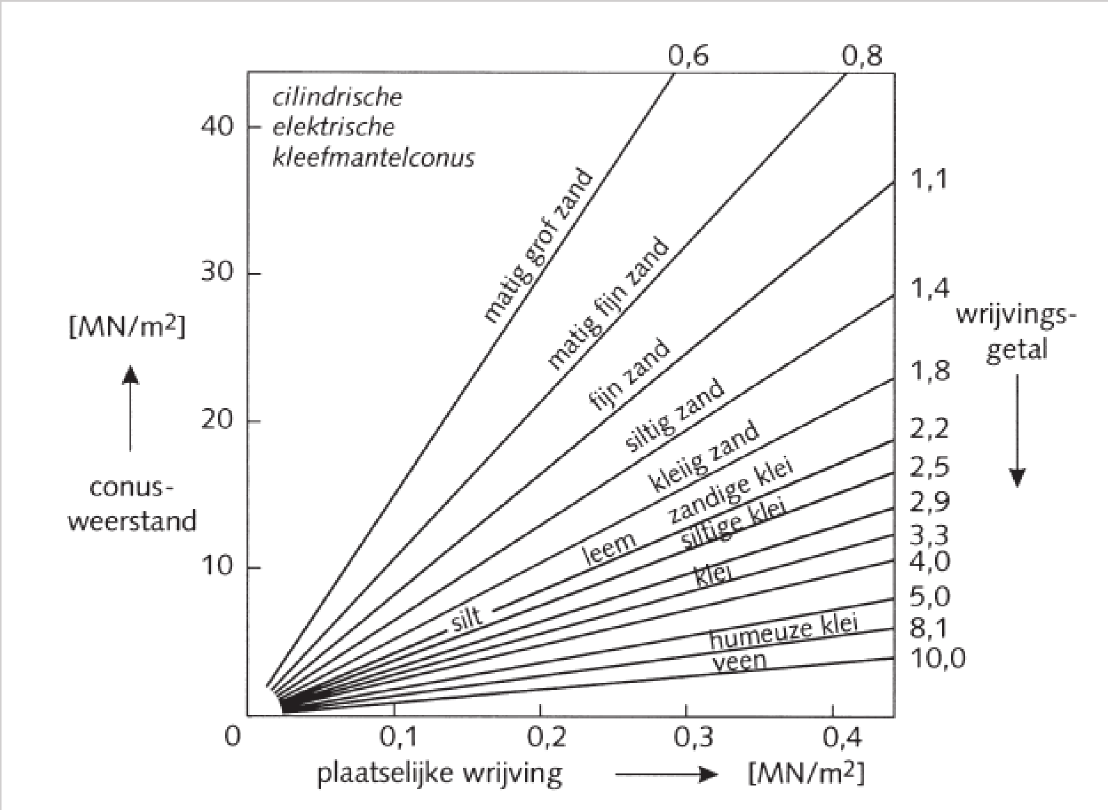

Figure 3-1: Relation between the probe resistance, local friction and the friction number. (TAW, 2001)

From the CPTs, the soil schematization from Figure 3-2 is assumed.

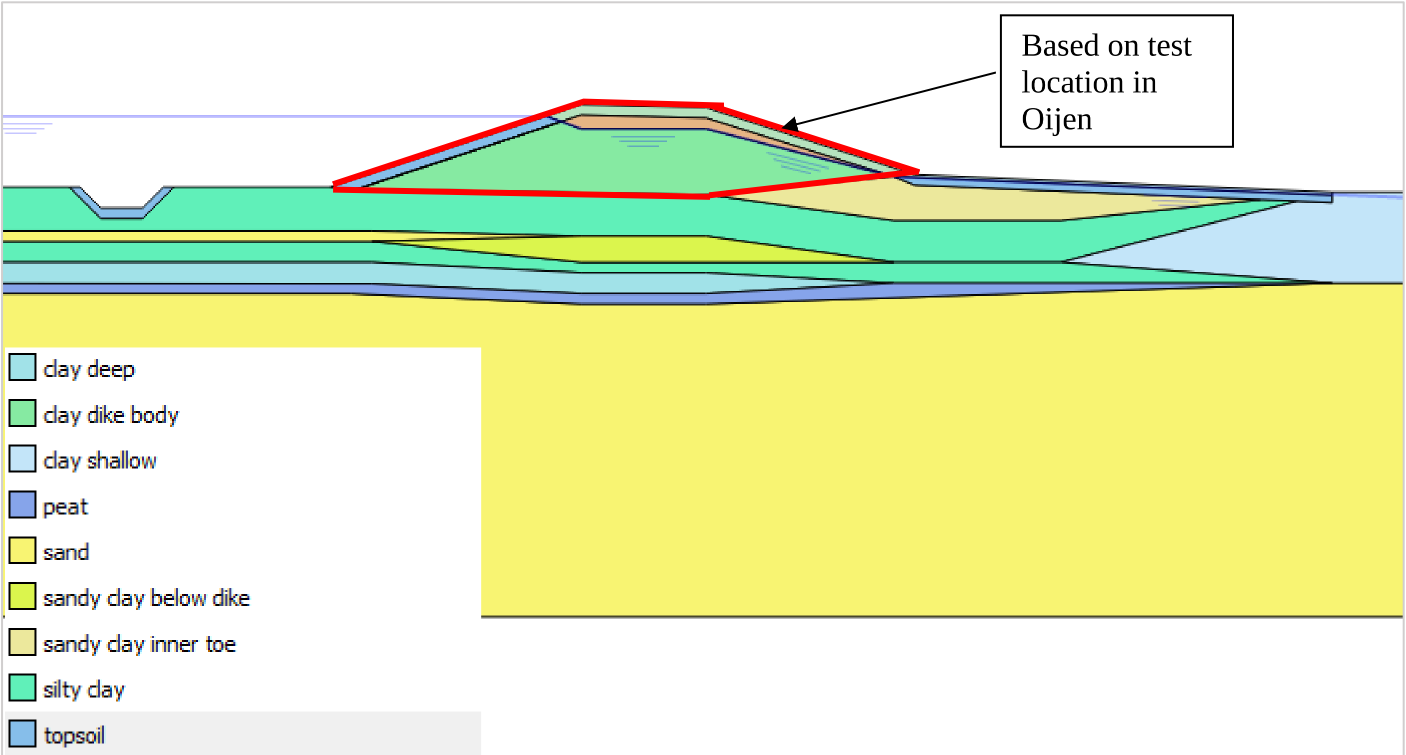

Figure 3-2: Schematisation of the subsoil below the test location on the IJsseldijk near Westervoort.

In Table 2-13 the necessary input parameters for the MC model are given. The shear strength parameters, the friction angle (φ) and the cohesion (c), are derived from the schematization manual macro stability (Ministerie van Infrastructuur en Milieu, 2019). The cohesion is always zero, since the critical state concept is used. Only the topsoil does have some cohesion, to prevent micro-instability near the surface of the dike body. The default value for the dilatancy angle is also zero due to the critical state concept.
The Young's modulus (E) and the Poisson's ratio are determined from the Eurocode 7 (Normcommissie 351006 'Geotechniek', 2019). To determine the soil unit weight the results from the soil tests from Wiertsema and Partners (Appendix III) where used and older assessment and reinforcement reports (Heidemij - adviesbureau, 1986).
To determine the soil suction profile, the soils are linked to a Staring Serie. To link the soils to the Staring Serie, the grain size distribution was needed. From a borehole in the inner berm in Westervoort and from the crest in Oijen the grain size distribution of the soils (Appendix III) and the corresponding Staring Serie were determined (Wösten, Veerman, de groot, & Stolte, 2001). The parameters used in the MC model are given in Table 3-2.

Table 3-2: Used parameters for the different soils in the Mohr-Coulomb model.

Soil	**Drained/ Undrained**	γ_{dry} **[kN/m³]**	γ_{sat} **[kN/m³]**	***E*** **[kPa]**	ν **[-]**	***c*** **[kPa]**	φ **[°]**	ψ **[°]**	**Staring Serie**
Sand	drained	17	19	45000	0.35	0	30	0	O1
Sandy clay below dike	undrained	19	19	3500	0.25	0	32	0	O9
Sandy clay inner toe	undrained	17	17	3500	0.25	0	32	0	O8
Silty clay	undrained	18.5	18.5	3500	0.3	0	32	0	O9
Clay berm	undrained	17.2	17.2	2500	0.4	0	32	0	O11
Clay deep	undrained	18	18	3000	0.4	0	32	0	O12
Clay dike body	undrained/drained	18.8	18.8	3000	0.4	0	32	0	O13
Peat	undrained	10	12	500	0.15	0	35	0	O18
Topsoil	undrained/ drained	18.8	18.8	3000	0.4	5	25	0	O13

The parameters of the HS model are different from the MC parameters. The difference between the MC parameters and the HS parameters are the Young's modulus'. Where in the MC model only one Young's modulus is an input parameter, there are three in the HS model. The three Young's modulus' are the Secant stiffness in drained triaxial test (E_{50}^{ref}), the Tangent stiffness for primary oedometer loading (E_{oed}^{ref}) and the Unloading/reloading stiffness (E_{ur}^{ref}). The reference vertical stress is 100 kPa. Since the Young's modulus is dependent of the stress level in the HS model, the Young's modulus' were the same for all the clay and silty clay layers. The exponent m is one for all clayey and peat layers and 0.5 for the sand layer. The shear strength parameters are the same as in the MC model.
The K_0^{nc}-value is determined from the Poisson ratio from the MC model according to equation (3-1). Table 3-3 give the parameters for the HS model.

$$K_0^{NC} = \frac{\sigma_h'}{\sigma_v{}'} = \frac{v}{1-v}$$

(3-1)

With:
K_0^{NC} = earth pressure coefficient [-]
σ_h' = horizontal effective stress [kPa]
$\sigma_v{}'$ = vertical effective stress [kPa]
v = poisson's ratio [-]

Table 3-3: Used parameters for the different soils in the Hardening Soil Model.

Soil	Drained/ Undrained	γ_{dry} [kN/m^3]	γ_{sat} [kN/m^3]	E_{50}^{ref} [kPa]	E_{oed}^{ref} [kPa]	E_{ur}^{ref} [kPa]	*m*	c'_{ref} [kPa]	φ' [°]	ψ [°]	K_0^{NC}	Staring Serie
Sand	drained	17	19	45000	45000	135000	0.5	0	30	0	0.5385	O1
Sandy clay below dike	undrained	19	19	3500	3500	12500	1	0	32	0	0.3333	O9
Sandy clay inner toe	undrained	17	17	3500	3500	12500	1	0	32	0	0.3333	O8
Silty clay	undrained	18.5	18.5	2500	2500	12500	1	0	32	0	0.6667	O9
Clay berm	undrained	17.2	17.2	2500	2500	12500	1	0	32	0	0.6667	O11
Clay deep	undrained	18	18	2500	2500	12500	1	0	32	0	0.6667	O12
Clay dike body	undrained/ drained	18.8	18.8	2500	2500	12500	1	0	32	0	0.6667	O13
Peat	undrained	10	12.5	1000	500	2000	1	0	35	0	0.2720	O18
Topsoil	undrained/ drained	18.8	18.8	2500	2500	12500	1	5	25	0	0.6667	O13

The shear strength parameters from the SS model are the same as the for the MC and the HS model. The difference is in the stiffness parameters. Where the MC and the HS model use the Young's modulus for the stiffness parameters, uses the SS model the modified compression index (λ*) and the modified swelling index (κ*). The stiffness parameters can be obtained from a one-dimensional compressions test with equation (3-2) and (3-3) (Plaxis, 2020).

$$\lambda^* = \frac{C_c}{2.3(1+e)}$$

(3-2)

$$\kappa^* = \frac{2C_s}{2.3(1+e)}$$

(3-3)

With:
λ^* = Modified compression index [-]
κ^* = Modified swelling index [-]
C_c = one-dimensional compression index [-]
C_s = one-dimensional swelling index [-]
e = void ratio [-]

From the soil test executed by Inpijn-Blokpel Ingenieursbureau for Water Board Rijn en IJssel, the recompresson ratio and compression ratio from the NEN-Bjerrum method are known (van Heerebeek, 2017). With equation (3-4) and (3-5) the one-dimensional compression and swelling index can be calculated. Since the only information for this parameters was from silty clays and the stiffness parameters do not have much influence on the shear strength, the same values are assumed for all clayey soils.

$$RR = \frac{C_s}{1 + e_0} \tag{3-4}$$

$$CR = \frac{C_c}{1 + e_0} \tag{3-5}$$

With:
RR = recompression ratio
CR = Compression ratio

Table 3-4 shows the used parameters for the Soft-Soil model.

Table 3-4: Used parameters for the different soils in the Soft Soil Model

Soil	**Drained/ undrained**	γ_{dry} **[kN/m³]**	γ_{sat} **[kN/m³]**	λ^*	κ^*	c'_{ref} **[kPa]**	φ' **[°]**	ψ **[°]**	K_0^{NC}	**Staring Serie**
Sandy clay below dike	undrained	17	19	0.12	0.03	0	32	0	0.3333	O9
Sandy clay inner toe	undrained	19	17	0.12	0.03	0	32	0	0.3333	O8
Silty clay	undrained	18.5	18.5	0.12	0.03	0	32	0	0.5953	O9
Clay berm	undrained	17.2	17.2	0.12	0.03	0	32	0	0.5953	O11
Clay deep	undrained	18	18	0.12	0.03	0	32	0	0.5953	O12
Clay dike body	Undrained/ drained	18.8	18.8	0.12	0.03	0	32	0	0.5953	O13
Peat	Undrained	10	12.5	0.12	0.03	0	35	0	0.1765	O18
Topsoil	Undrained/ drained	18.8	18.8	0.12	0.03	5	25	0	0.6667	O13

Another method to calculate the shear strength, is with the SHANSEP concept (chapter 2.5.4). For the SHANSEP concept the ratio between the undrained shear strength and the effective vertical stress in normally consolidated soil (α in Plaxis, *S* in the literature) and the power *m* are needed as input parameters. For both values the expectation values from the Schematization Manual Macro Stability (Ministerie van Infrastructuur en Milieu, 2019) are chosen. Therefore the α for the dike body is 0.31 and for the other silty clays it is 0.30. the power exponent *m* is 0.9 as the default value.

3.2 Model

To model the behavior of the dike in case of a high water event, a model is built in Plaxis. The model consists of an initial calculation phase with three phases afterwards.
In the initial calculation phase a K_0 procedure is performed to set the characteristic critical state parameters. After that the first phase takes place. This a nill-step with plastic deformation to determine the start situation of the dike. In these phases the river level is at daily level.
The second phase is the high water event. The river is at WBN-event level and the phreatic surface in the dike body is higher dan during the initial situation. The soil layers above the phreatic surface are modelled to behave drained and below the phreatic surface they model undrained. The third and last phase is the safety calculation to determine the Safety Factor of the situation.
For the model fit to the measured data, the model was the same. Only instead of the phase with the river lever during WBN-event a phase with the water conditions during a specific moment was implemented in the model and no safety analysis was performed.

To determine the influence of the different variables of the model, different sensitivity analyses where performed. In this sensitivity analysis different soil models, tolerated errors and meshing where used. To compare the different variables, the same standard situation is used every time.

- Mohr Coulomb soil model
- Phreatic surface according to the TRWD
- Fine meshing
- Suction is not taken into account in the calculation
- Tolerated error of 1%

The comparison will be done by comparing the safety factor of the safety analysis of the model. To determine the safety factor Plaxis uses a strength reduction method. The shear strength parameters are lowered with each step according to equation (3-1), until failure occurs. If failure occurs the shear strength parameter reduction stops and the strength reduction multiplier becomes constant.

$$\sum Msf = \frac{\tan(\varphi_{input})}{\tan(\varphi_{reduced})} = \frac{c_{input}}{c_{reducted}} = \frac{s_{u,input}}{s_{u,reduced}} \qquad (\ 3\text{-}1\ )$$

With:
$\sum Msf$ = Total multiplier = global safety factor (if constant during the last steps)
φ = friction angle [°]
c = cohesion [kPa]
s_u = Undrained shear strength [kPa]

The safety factors will be shown in a graph with on the vertical axis the strength reduction multiplier Msf and on the horizontal axis the steps. If the strength reduction multiplier becomes constant, is that value equal to the global safety factor. (Plaxis, 2020)

Furthermore the safety factors obtained with the Plaxis model are compared to the results obtained with the D-stability model, which is normally used in the assessments of the dikes. Since D-stability works only with the tau-phi method in drained situation, the total dike was set on drained for this comparison.

3.2.1 Influence mesh

A finer mesh normally stands for a more accurate and more precise calculation, however the calculation time increases when a finer mesh is used. To determine the influence of the mesh, one model is calculated several times with different meshes. Appendix I, Figure I-1 shows the results of the safety factors calculated with Plaxis which are summarized in Table 3-5. Appendix II, Figure II-1 shows the failure surfaces for the different meshes. Figure 3-4 and Figure 3-3 are showing the used mesh, mesh quality and the failure mechanism. The influence of the mesh on the calculated safety factor and the failure surface is small. The medium mesh gives the highest safety factor and the fine mesh the lowest, but the difference between these two is only 0.02. This difference is very small and not significant. Also the differences in the failure surfaces are minimal.
In Figure 3-4 the mesh quality is shown, the more red an area, the worse the mesh quality, which lead to inaccurate or non-precise results. In the coarse mesh there are a couple of big red areas, where there in the medium and fine mesh each less and smaller red areas are showing.
Since the Factor of Safety (FoS) and the failure surface did not change significant, but the mesh quality of the fine mesh is better, a fine mesh is used in the final model.
The very fine mesh is not calculated since the initial state does not reach the accuracy condition in the last step.

Table 3-5: The calculated FoS and the number of elements for each mesh.

Mesh	**FoS**	**#Elements Total**	**#Elements Dike Body**
Coarse	1.29	2417	362
Medium	1.30	2955	464
Fine	1.28	4095	754

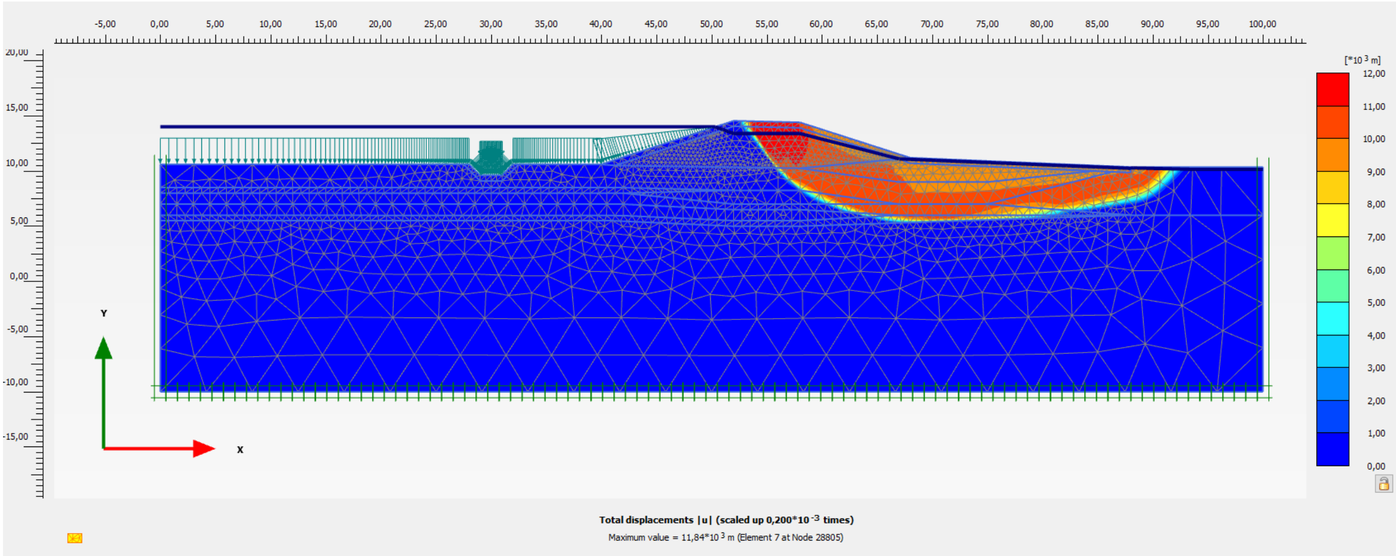

Figure 3-3: The failure mechanism of the safety analysis for the fine mesh. The same failure mechanism occurred in all other safety analysis.

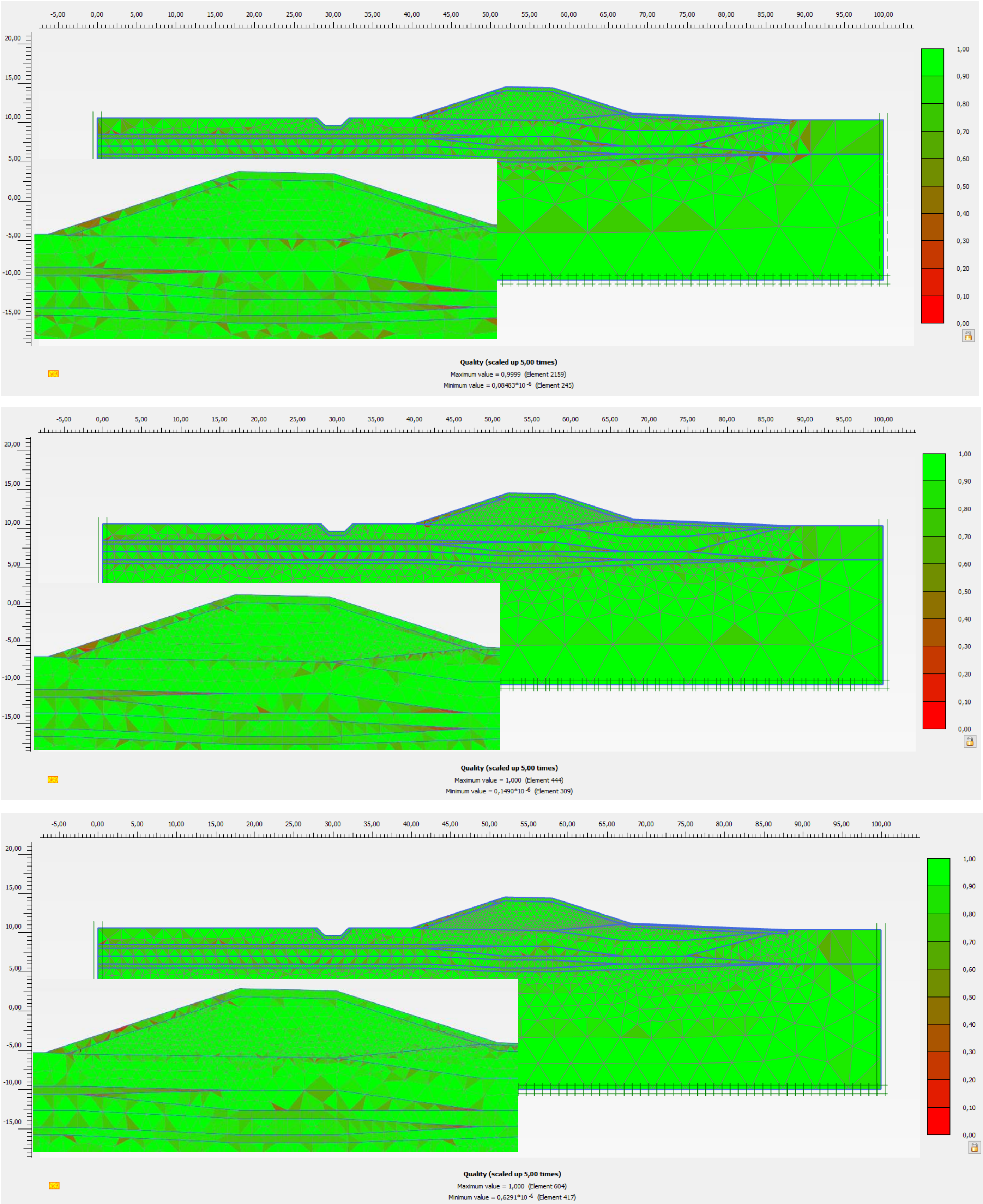

Figure 3-4: The used meshes. The coarse mesh (top), the medium mesh (middle) and the fine mesh (bottom).

3.2.2 Influence Tolerated Error

The tolerated error has also influence on the factor of safety. The lowest tolerated error of 0.001 gives the lowest factor of safety, while a higher tolerated error gives a higher safety factor. Table 3-6 shows that the difference in FoS is maximum 0.03 (Appendix I, Figure I-2). The difference in failure surfaces are minimal (Appendix II, Figure II-2). The number of steps needed have an influence on the calculation time. The more steps needed, the more time the calculation will need. The tolerated error of 0.001 needs 2.5 times as many steps than the tolerated errors of 0.005 and 0.01, which means the calculation will be significant longer. Since the difference in FoS is only 0.03, the difference in slip surface is minimal and the difference in calculation steps and therefore calculation time is quite big, a tolerated error of 0.005 is used in the final model.

Table 3-6: The calculated Fos and the minimum number of steps for each tolerated error.

Tolerated error	FoS	#Steps minimum
0.001	1.25	241
0.005	1.28	95
0.01	1.28	93

3.2.3 Influence Soil Models

Three soil models are compared to look into the differences. First the MC model was used to give a first impression of the safety factor. After that the HS model and the SS model were used to model the behavior of the soil layers. In Table 3-7 (Appendix I, Figure I-3) the results are shown in terms of the effect from the different soil models on the FoS in a WBN situation. The SS model gives the highest FoS, the MC the lowest FoS.

Table 3-7: The calculated FoS for the different soil models.

Soil Model	FoS
Soft Soils	1.46
Hardening Soil	1.36
Mohr Coulomb	1.28

When looking at the HS, SS and MC model, the shear stress is calculated in the same way, with the shear strength parameters, c' and φ'. In all models these parameters where the same. Also the other parameters which influence the shear strength of the soils, where comparable (Chapter 3.1). Since the shear stress parameters where the same, the expected result where comparable FoSs. However, this is not the case. In Appendix II, Figure II-3 the failure surfaces of the different models are shown. In the MC model the failure surface goes through the clay in the inner berm for a longer time than with the HS and the SS model. This can explain part of the lower FoS for the MC model.

When the models are compared in a total drained calculation, as done in Chapter 3.2.4, the differences in FoS are only 0.01 (Table 3-8). Therefore the difference in FoS comes probably from the generation of pore water pressures during the failure. Assumed is the soil behaves undrained during the failure, since the failure occurs fast. The exact reason for the difference between the soil models in the safety calculation in a undrained situation, is unknown.

According the POV Macrostabiliteit (2018) the HS model in combination with the SS model has to be used in a Plaxis calculation. Therefore these models are used in further calculations.

3.2.4 Comparison D-Stability.

In the assessments of the dikes, the soil body normally is modelled and tested in D-stability (Deltares, 2019). In D-Stability the only choice between soil models to be made is between drained and undrained. For clayey and silty soils the program calculates the undrained shear stress with the SHANSEP concept and the drained shear stress according to equation (2-17), without taking the suction into account. Furthermore in D-Stability a failure mechanism has to be chosen: Bisshop, LiftVan or Spencer. The results from the calculation in D-stability are compared to the results from the different soil models calculated with Plaxis in Table 3-8.
In a drained calculation the SS, HS and the MC model give more or less the same FoS, which is more or less the same as the model in D-stability. Also the shear zones in both models are comparable (Appendix II, Figure II-3 and Figure II-4), only the shear zone in D-stability, Spencer method, goes not through the Peat layer, but through the Silty Clay layer above. However, this difference has a minimal effect on the FoS.

Table 3-8: Different Results for Plaxis and D-stability in terms of FoS.

Model	**FoS**
D-Stability Bishop	1.43
D-Stabilty LiftVan	1.38
D-Stability Spencer	1.40
Plaxis MC	1.44
Plaxis HS	1.45
Plaxis SS	1.44

After the interpretation of the measured suction stresses, measured water contents and performed CPT-data a safety analysis will be performed with changes in the parameters according to the results (Chapter 4). For this model a fine mesh will be used, with a tolerated error of 0.005 and a mixture of the HS and SS model, according to the POV Macrostabiliteit (2018).

4 Results

The results from the different parts of the research will be shown in this chapter. First the results from the sensitivity analysis in Plaxis will be shown, after that the results of the field tests and last the results of the model fit to the field data and an extrapolation to the WBN-situation.

4.1 Sensitivity Analysis

The influence of the suction on the shear strength and therefore the slope stability of the dike is dependent of different parameters. The influence of the suction profile and phreatic surface are determined. To determine the influence of these parameters, one of the parameters is changed from the "starting" situation every time. The starting situation consists of the following:

- Mohr Coulomb soil model
- Phreatic surface according to the TRWD
- Fine meshing
- Suction is not taken into account in the calculation
- Tolerated error of 1%

The comparison will be done by comparing the safety factor of the safety analysis of the model. To determine the safety factor Plaxis uses a strength reduction method as explained in chapter 3.2.

4.1.1 Influence Phreatic Surface

The higher the water table in the dike body, the lower the effective vertical stress in the dike body and therefore a lower shear strength. Due to the lower shear strength a lower FoS can be expected. Figure 4-1 shows the location of the phreatic surfaces modelled within the dike body. The results can be found in Table 4-1 and Appendix I, Figure I-4. The maximum difference in safety factor is 0.27. Even at the realistic phreatic surfaces in the dike body (1.1 m below surface (TRWD) and 1.6 m below surface (WC)), the FoS differs with 0.1, which is a significant improvement. The change in phreatic surface does not change the slip surface (Appendix II, Figure II-5).

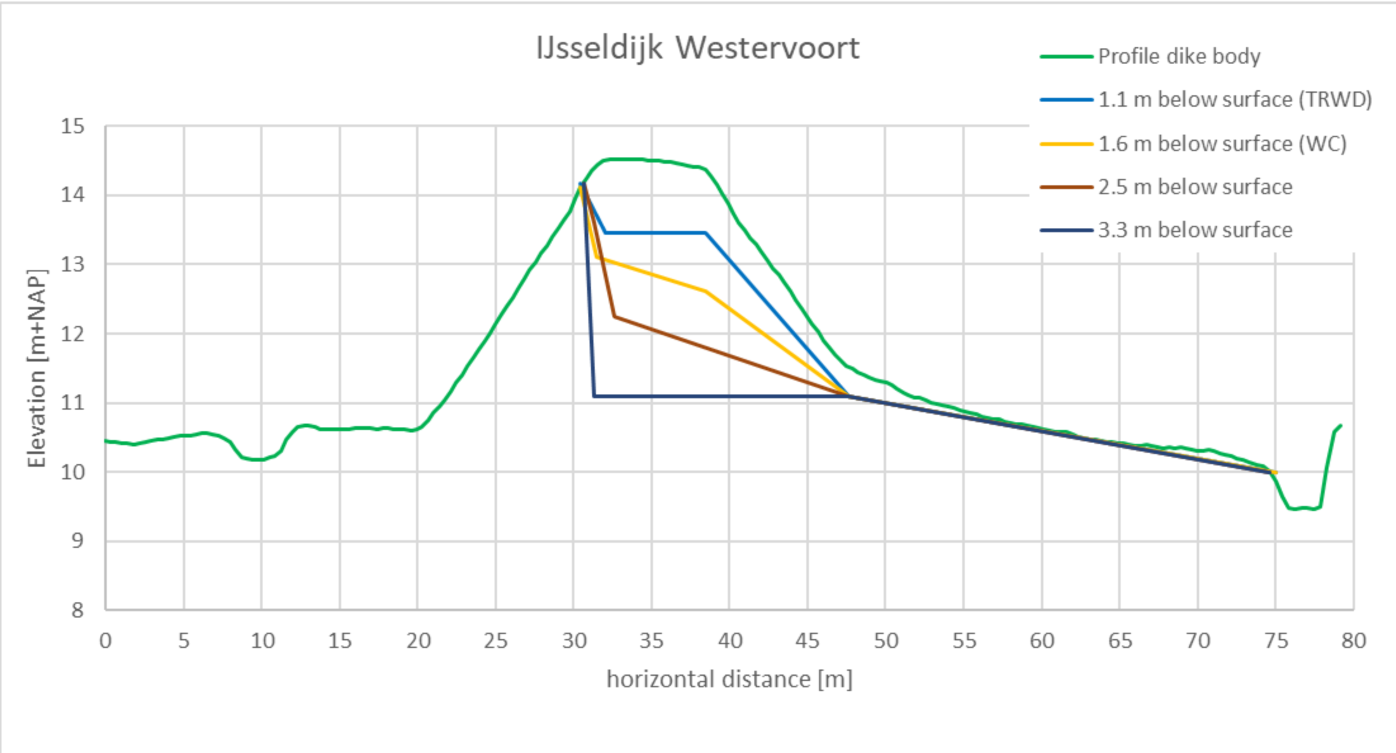

Figure 4-1: The location of the different phreatic surfaces within the dike body in Westervoort.

Table 4-1: The calculated factors of safety (FoS) and probability of failure (Pf) for each phreatic surface

Phreatic Surface [m below surface]	FoS
3.3	1.55
2.5	1.47
1.6	1.39
1.1	1.28

4.1.2 Influence of the Soil type

Above the phreatic surface, the soil type has an influence on the amount of suction stresses present in the soil, especially the SWRC of the soil. The bigger the zone between the phreatic surface and the top of the dike, the bigger the zone were effective suction stresses can be present. To determine the amount of effective suction stresses and the contribution to the safety factor of a dike body, a sensitivity analysis with different soil types and SWRCs is performed. The SWRCs are obtained from the subsoils in the Staring Serie (chapter 2.2.1). From the SWRC and the phreatic surface an effective suction profile is generated in Plaxis.
Since soil suction stresses only are generated between the groundwater level and the surface, the bigger the distance between the groundwater and the surface, the more possible generated suction stresses. Therefore the most effect of the soil suction can be expected with the phreatic surface 3.3 m below the surface of the dike. The river level outside the dike body is at WBN level. The suction profile is static, so only generated from the water table in the dike body. No evaporation or precipitation on top of the dike was used. During a very dry period higher suction stresses can be found in the soil, but since the high water events usually occur during the winter months, when the precipitation surplus is positive, high suction cannot be expected. More realistic is a situation where almost no effective suction is present in the top layer (the top 1.0 or 1.5 meter) (Lim, Rahardjo, CHang, & Fredlund, 1996).

Figure 4-2 shows the soil suction profiles and the effective degree of saturation over the depth for the different Staring Serie. The dike body and the topsoil every time get an different Staring Serie. The very heavy clay (Staring Serie O13) gives the biggest effective suction of 28 kPa, where the coarse sand (O5) give the lowest effective suction of maximum 1 kPa. The influence of the different Staring Serie on the FoS is shown in Figure 4-3. The coarse sand has the lowest safety factor (1.56), where the very heavy clay gives the highest safety factor (1.64). The difference between all sands are clearly visible, while the difference between all other soils (all non-sands) are very small (less than 0.01). For the further modelling the used Staring Serie for the dike body material and the topsoil is the very heavy clay (O13), since this clay gives the highest effective suction and therefore the biggest difference is expected in FoS compared to a model in which soil suction is ignored. Table 4-2 gives the calculated FoS for the very heavy clay (O13), the extremely loamy sand (O4) and the coarse sand (O5).

Table 4-2: The calculated FoS with and without taking into account static suctions form different soils.

Effect Suction	FoS
Ignore Suction	1.56
Static suction O13	1.64
Static Suction O4	1.63
Static Suction O5	1.56

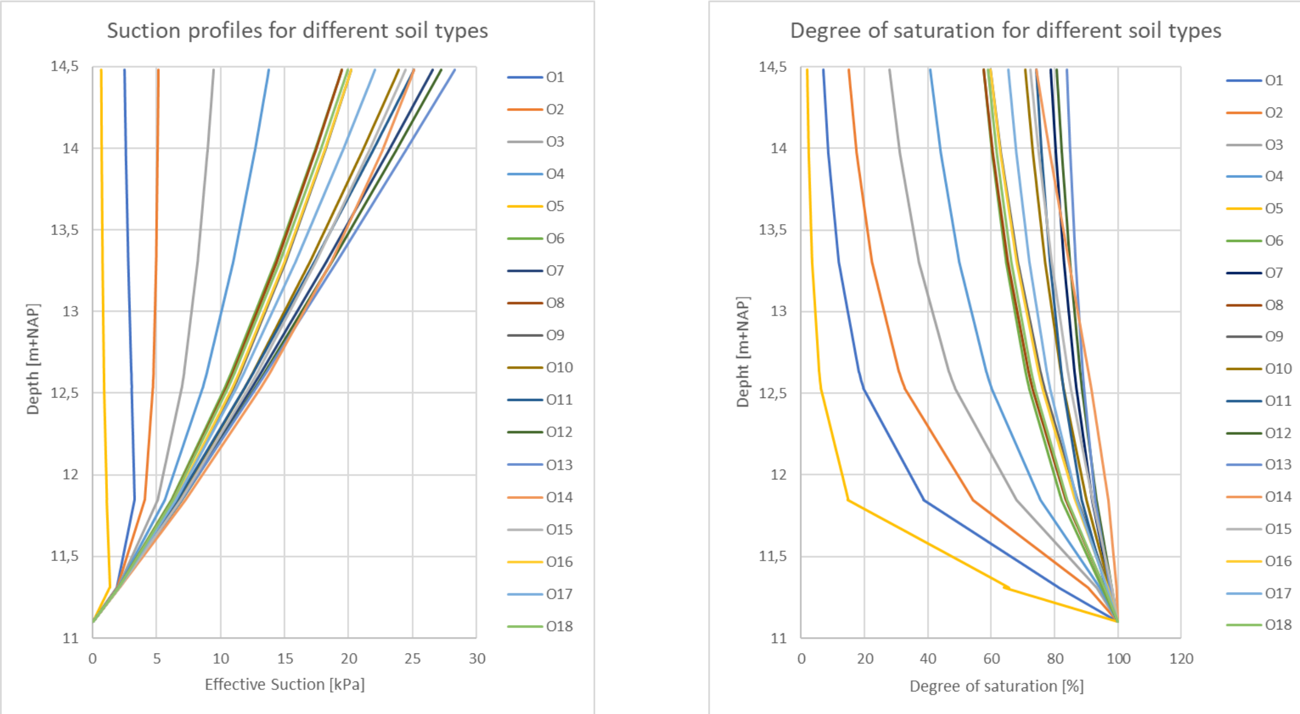

Figure 4-2: Left: The effective suction over de depth in the middle of the dike body. The suction is generated from the water table (3.3 m below surface) only, with the van Genuchten curves from the Staring Serie for each soil.
Right: The Degree of saturation over de depth in the middle of the dike body. The degree of saturation is generated form the water table (3.3 m below surface) only, with the van Genuchten curves from the Staring Serie of each soil.

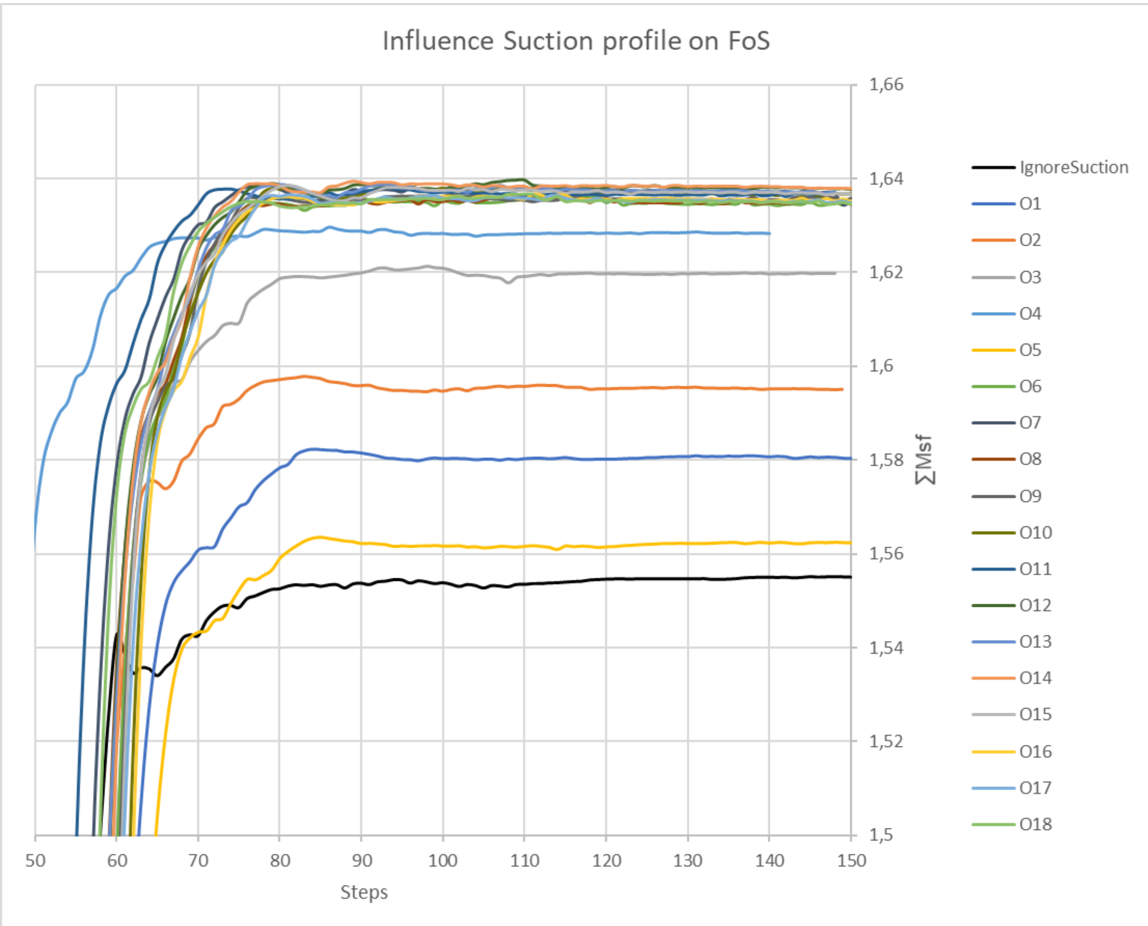

Figure 4-3: Influence of the different soils from the Staring Serie on the FoS. The Mohr-Coulomb soil model was used, with a phreatic surface 3.3 m below the surface. A fine meshing and a tolerated error of 0.01 was applied.

4.2 Field measurements

On two location Deltares is performing field measurements. On the IJsseldijk in Westervoort, the soil suction, VWC and the piezometric head is measured in the inner berm, inner toe and the outer toe of the dike. To install the water content reflectometers and the tensiometers a borehole was made (by hand), the measurement devices where placed and the first part of the borehole was filled with Bentonite. In the beginning of the measuring period the measurements may be affected by the installation procedure, furthermore it takes time for the sensor to equalize with the ground conditions. It is assumed these effects are negligible a month after installation. In Westervoort the devices where installed the 25th of October 2019, in Oijen in the end of September 2019.
Furthermore every two to four weeks a CPT is performed in the inner berm. In the Maasdijk in Oijen the soil suction and the VWC are measured in the crest of the dike. Every two to four weeks a CPT is performed in the crest of the dike. Besides the CPTs, FVTs are performed to measure the in-situ shear strength of the soils. The FVTs are performed several times on each location.

4.2.1 Field Measurements Westervoort

In Figure 4-4, Figure 4-5 and Figure 4-7 the results of the measurements performed by Deltares are shown, Figure 1-4 shows the location of sensors near the dike. As can be seen in the bottom figures of Figure 4-4, Figure 4-5 and Figure 4-7, the piezometric head of the sand layer, which begins around five meters below the surface below the toes and four meters below the surface in the berm, is more influenced by the river level, than the piezometric heads in the clay cover layer above.
The top figures gives the measured soil suction, the middle figure the measured VWC and the bottom figure the measured piezometric head. The graphs with the piezometric heads and the suction also show the precipitation surplus, which is the precipitation minus the evaporation measured at the weather station in Deelen about 10 km from the test location.

Outer toe

In the outer toe in Westervoort almost no soil suction stresses where measured (Figure 4-4). Only the tensiometer 2.0 meter below surface measured some soil suction stresses during May. Since the soil was almost fully saturated during the whole measuring period (according to the measured soil suction stresses), the VWC did not change significant.
In March and April there was a dry period in the Netherlands, the precipitation surplus was negative, which means there was net evaporation. In that period the tensiometers, at least in the top, where expected to measure some increasing soil suction. However this is not visible. While the piezometric head in the cover layer and the aquifer decreases during this period, the measured pore water pressure in the upper two tensiometers (1.0 and 1.5 m below surface) are staying around 0 kPa. The lower tensiometers (2.0 and 3.0 m below surface) do show a decrease in pore water pressure. The lowest tensiometer (3.0 m below surface, 7.60 m+NAP (Table 1-1) increases until 0 kPa.
The piezometric head in the same period is between the nine and ten m+NAP in the cover layer. Which means that the lower two tensiometers are below the phreatic surface and should measure negative soil suction stresses, the upper two tensiometers should measure soil suction during the end of May.
An explanation for the lack of measured soil suction in the outer toe in Westervoort can be cracks. To measure soil suction stresses the tensiometer should make contact with the surrounding soil. If a clayey soil dries, the volume of the soil will decrease, which will lead to cracks in the soil. If a crack is formed around the tensiometer, no capillary tensions will be formed and no soil suction will be measured. But since both upper tensiometers measures soil suction of 0 kPa, another option is that there is no suction in that area due to a high phreatic surface. In that case the measurements of the piezometric heads are not right, but they are actually higher. However the piezometric heads do follow the river level and precipitation surplus quite well, so they are looking to measure the right amount of piezometric head.
From the measured soil suction and the measured VWC, the SWRC from the soil around the tensiometer and water content reflectometer can be determined. However almost no positive soil suction stresses were measured and the VWC did not change significant. Therefore it is not possible the derive a SWRC from the measured data until the end of May.

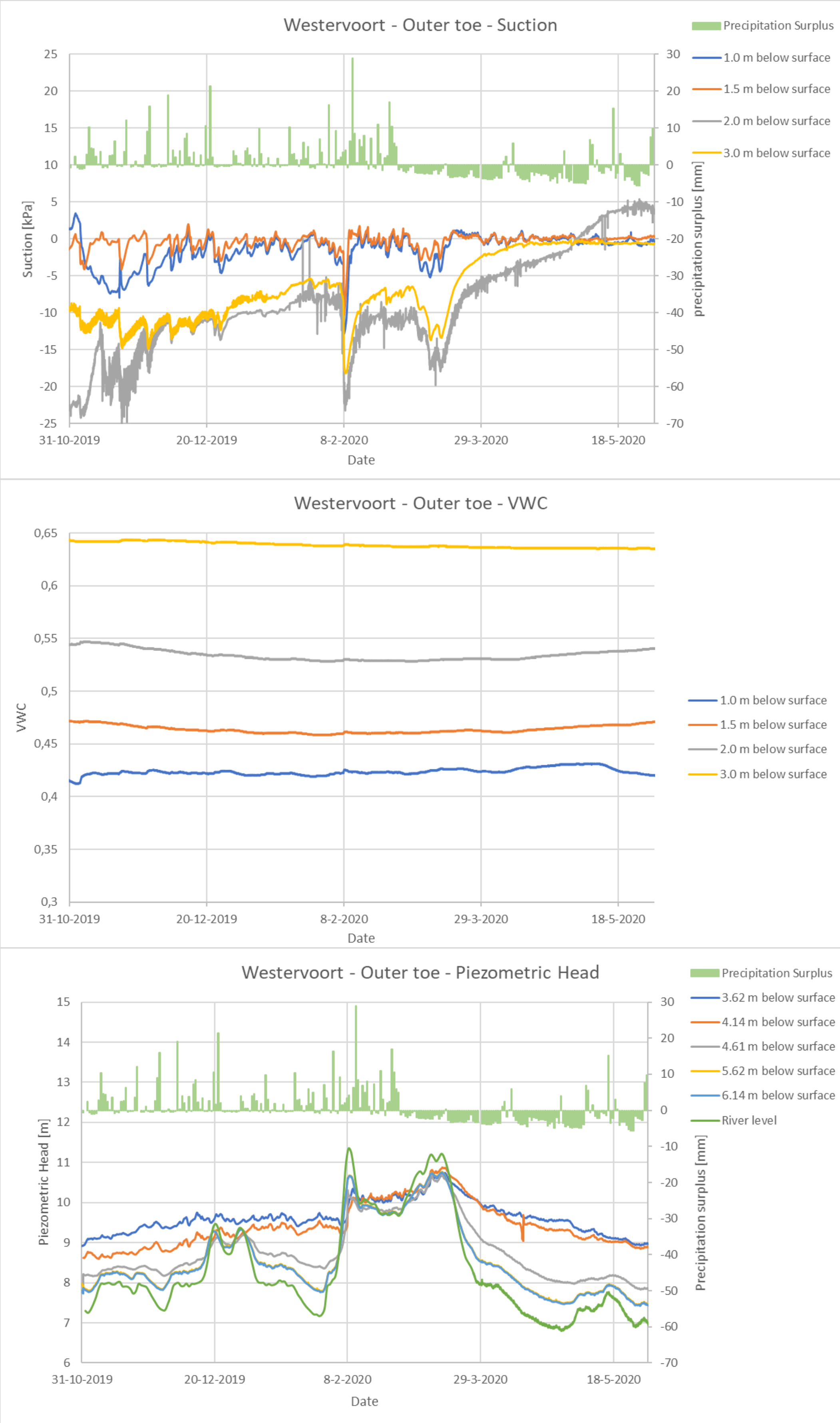

Figure 4-4: Field measurements from the outer toe in Westervoort. Top: suction and precipitation surplus, Middle: VWC, Bottom: piezometric head and precipitations surplus.

Inner toe

In the inner toe in Westervoort (Figure 4-5) soil suction stresses until 15 kPa are measured during the period from the end of March until the beginning of June. The tensiometers 1.5, 2.0 and 2.5 meter below surface only measured soil suction until 8 kPa or less. Since the degree of saturation with a soil suction of 8 kPa is about 100 %, there is not much change in the VWC. The VWC decreases a little bit during the winter months, but not significantly. Only the VWC from the upper water sensor (1.0 meter below surface) changes. The maximum VWC measured is about 0.41 and the lowest VWC measured, with a soil suction approximately 100 kPa was 0.37, which corresponds according to equation (2-6) with a degree of saturation of 90 %.
The piezometric head is mostly dependent of the river level. During the winter (December until March) the piezometric head in the cover is between the 9.5 and 11 m+NAP, during the dry period from March the piezometric head in the cover decreases from 11 m+NAP until 9 m+NAP. Since the highest tensiometer is on a depth of 10.21 m+NAP (Table 1-1), almost no soil suction should be measured during the winter months. Only the lowest sensor in the inner toe is below the 9 m+NAP (Table 1-1), therefore all sensors except the bottom one are expected to measure soil suction stresses during the spring. However, the upper Figure 4-5 shows all sensors measured soil suction during the spring. Therefore the phreatic surface is probably lower than the 8.81 m+NAP (depth of the lowest sensors). The soil suction measured with the tensiometers 1.0, 1.5 and 2.5 meter below surface are all increasing with about the same speed. The tensiometer 2.0 meter below surface stops increasing after it reached the 3 kPa. A possible explanation is the tensiometer loosed contact with the surrounding soil due to shrinkage of the clay cover.
During the winter the measured soil suction decreases after rainfall, but in the spring this effect is barely visible. This is possible due to the increasing temprature and therefore increasing evaporation during the spring.

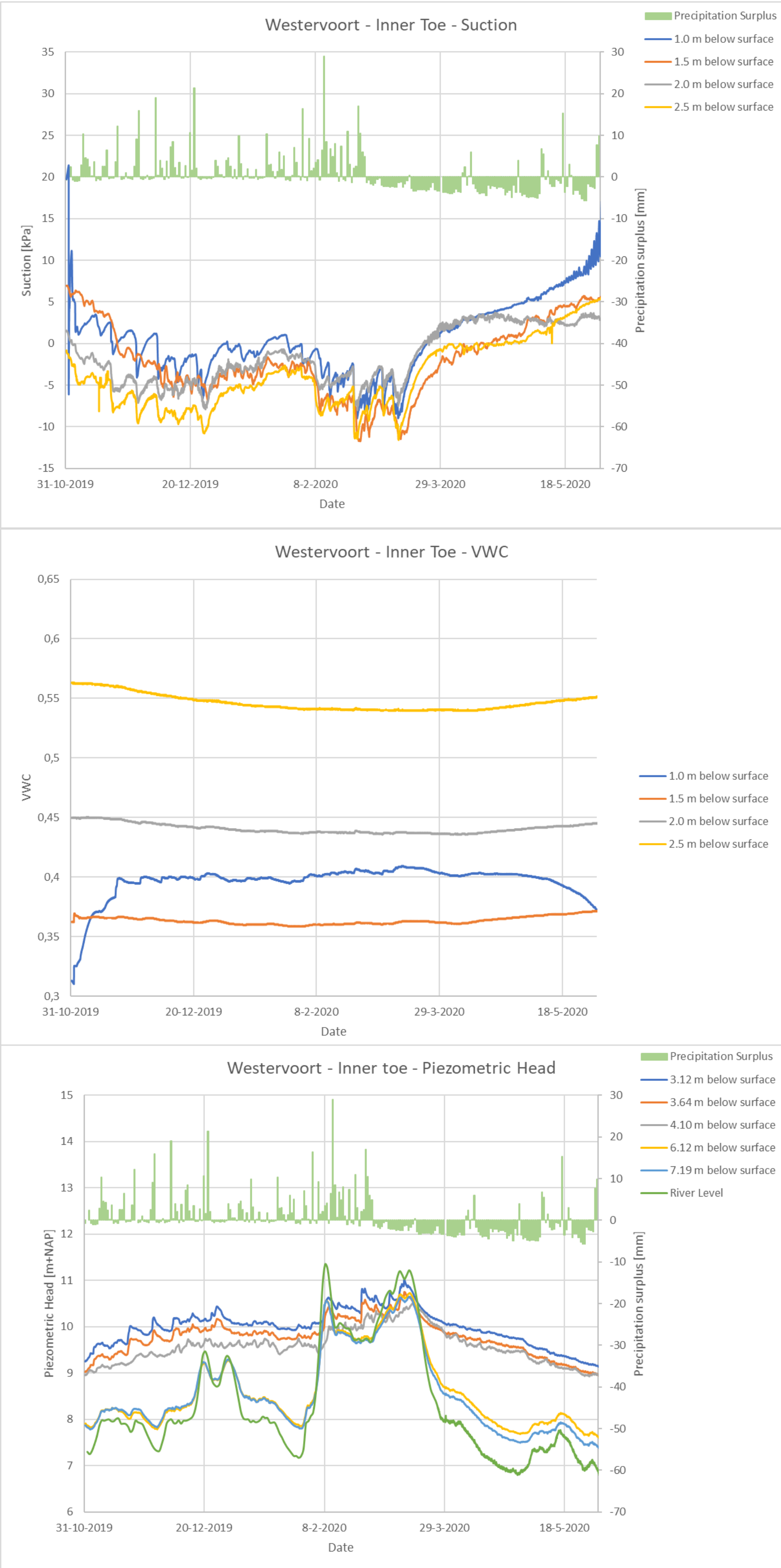

Figure 4-5: Field measurements from the inner toe in Westervoort. Top: suction and precipitation surplus, Middle: VWC, Bottom: piezometric head and precipitation surplus.

The tensiometer 1.0 m below surface have been measuring soil suction, from a state where the soil was fully saturated wihout any soil suction from 23 March. During the period from 23 March until the end of June[1], a soil suction of 97 kPa is measured. The measured VWC with this soil suction was 0.34. A SWRC was fitted to the data with the van Genuchten Equation (Equation (2-6)). The fitting parameters α and n gave values within the expected range (Figure 4-6) and the R^2 value of 0.86 shows the fit is good. With parameters outside of the expected range the R^2 values are most times below 0.8 (Chapter 4.2.2).
However the maximum measured soil suction was only 97 kPa, where a SWRC is normally calculated until a soil suction of 1500 kPa. The water content which is still left in the soil at 1500 kPa is called the residual water content (van Genuchten, 1980). For this case a residual VWC of 0.01 is assumed, based on the left water content in the clayey soils in the Staring Serie. Since only the behavior of the first 97 kPa suction is obtained, it is not sure if the found fitting parameters are the actually correct fitting parameters, but they are a best guess. With more data with higher measured soil suction stresses during the summer for example, a good approximation can be made for the fitting parameters.
The presented curve is the drying curve, it was not possible to derive a wetting curve. The only period where the tensiometers measured decreasing soil suction stresses for a longer period is right after the start. At this point it is assumed the tensiometer is still equalizing to his environment, which means it is not sure the measured data is correct.

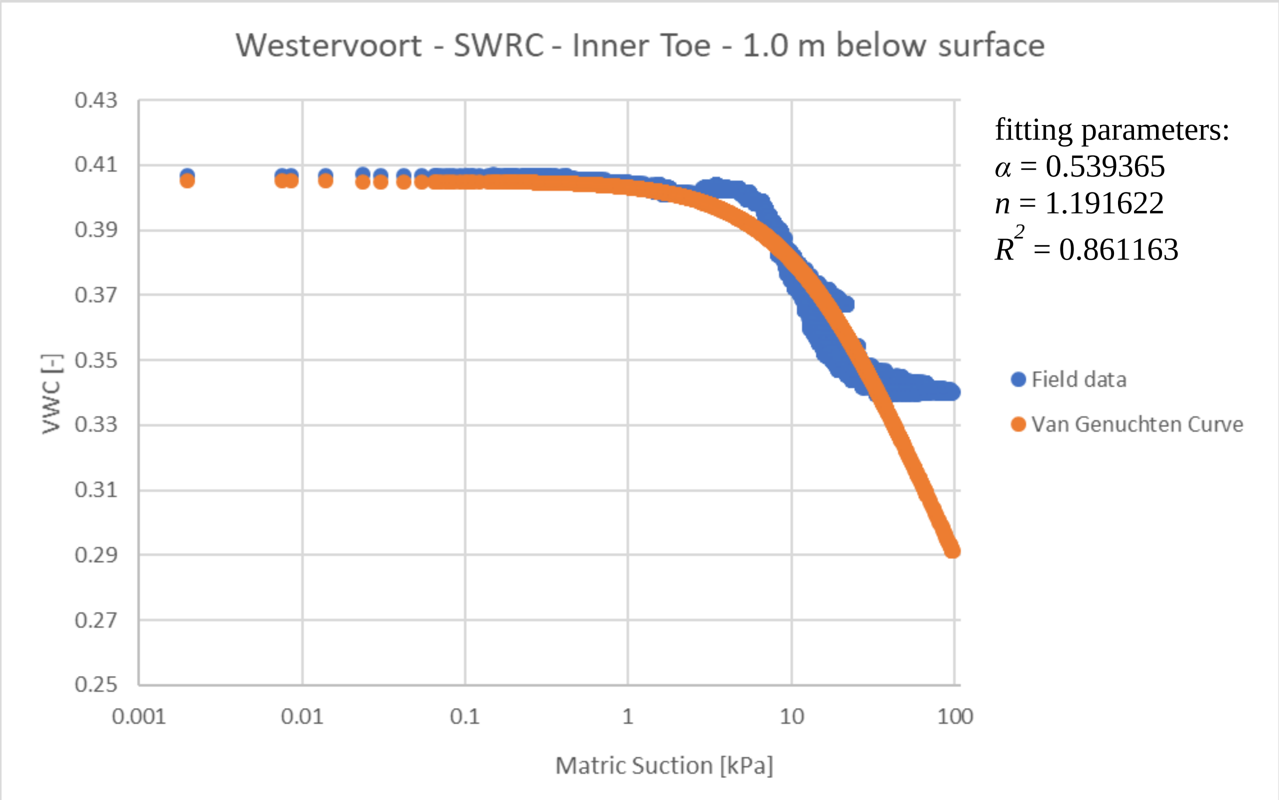

Figure 4-6: The SWRC (drying) fitted to the measured matric suction and volumetric water content 1.0 m below surface in the inner toe in Westervoort. The used data is from the period 23-03-2020 until 25-06-2020.

[1] The measurements results in Figure 4-5 are shown until the end of May, while there is data available until the end of June. Because of the work process it was not possible to implement the data of June in the Figures with the measured matric suction stresses, VWCs and the piezometric heads, but it was possible to determine part of the SWRC with the data, which is shown in Figure 4-6.

Inner berm

In the inner berm Figure 4-7 only the tensiometer 1.0 and 1.5 m below surface are measuring soil suction stresses. The measured soil suction one meter below surface goes until approximately 8 kPa, for the tensiometer 1.5 m below surface only small soil suction until 3 kPa are measured. The tensiometer two meter below surface shows a decreasing pore water pressure during the period with net evaporation from March.

The tensiometer 2.5 meter below surface did not measure any soil suction and only small pore water pressures. The piezometric head in the cover varies from eight until a little over ten m+NAP. From the end of March the piezometric head in the cover decreases until approximately eight m+NAP. The lowest tensiometer is on a depth of 7.88 m+NAP (Table 1-1), therefore the lowest tensiometer should always be below the piezometric head and therefore should not measure soil suction. However in that case it should measure negative soil suction (which is positive pore water pressure), like the tensiometer two meters below surface is measuring. Probably the tensiometer 2.5 m below surface is not measuring the correct values, since the measured soil suction does not change from the end of March. The tensiometer two meters below surface is only measuring negative soil suction stresses, but does follow the expected trend. Therefore it can be the tensiometer is not calibrated correct anymore. The two most shallow tensiometers show values as expected.

The VWC measured closest to the surface decreases from 0.47 until 0.43 when the measured soil suction is above the 5 kPa, which is as expected. The other measured VWC did not show a significant change, which is expected since no soil suction were measured above 3 kPa. With a soil suction of 3 kPa, most soils are still fully saturated.

Figure 4-7: Field measurements from the inner berm in Westervoort. Top: Suction and precipitation surplus, Middle: VWC, Bottom: piezometric head and precipitation surplus.

In the inner berm a SWRC can be fitted to the field data with the van Genuchten equation (equation (2-6)). The maximum measured soil suction in the end of June[2] was 15 kPa with a measured VWC of 0.41. The fitted curve is the drying curve with a R^2 value of 0.88, with α and n values of 0.41 and 2.29 (Figure 4-8). For this derivation the measured soil suction was even lower as for the one in the inner toe. Therefore also the fitting parameters for this SWRC are a best guess. By obtaining more data in summer, when higher measured soil suction and lower measured VWC are expected, a better guess can be made.
The wetting curve cannott be derived since there was not enough data.

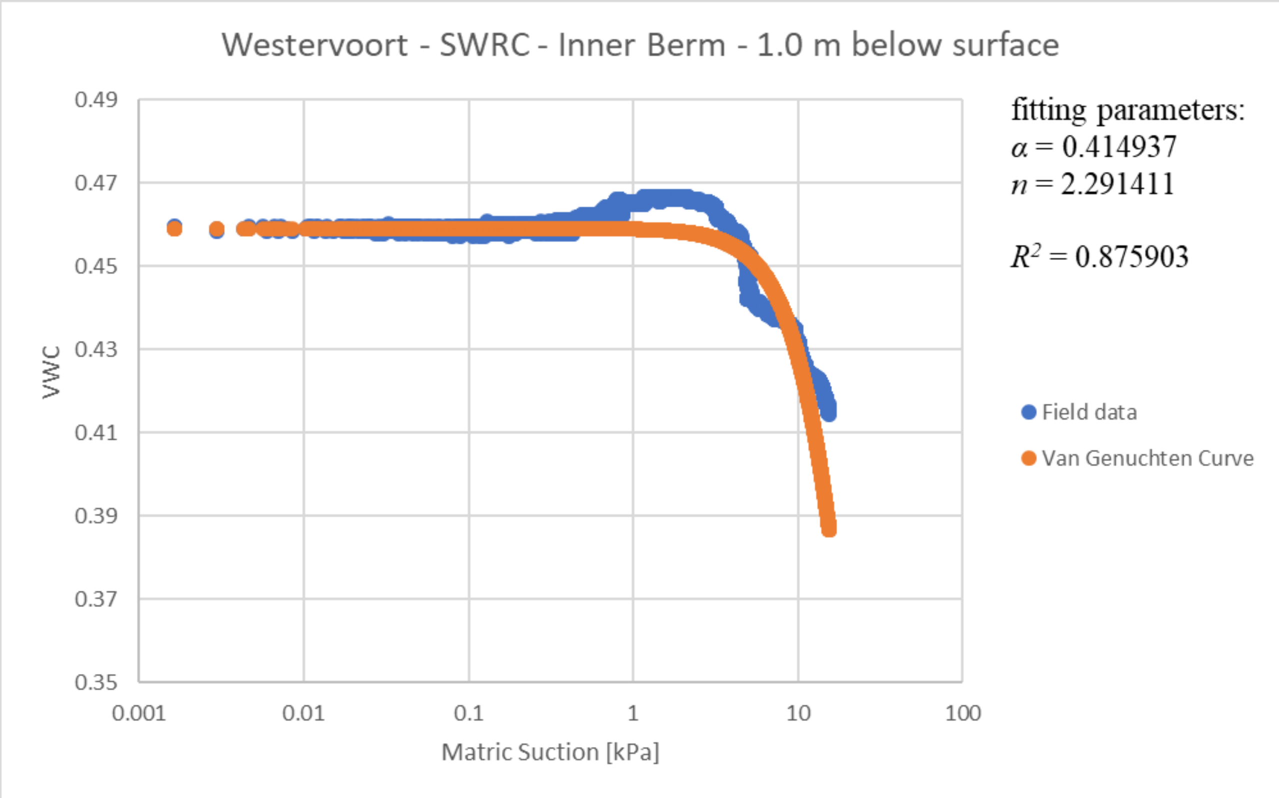

Figure 4-8: The SWRC (drying) fitted to the measured matric suction and volumetric water content 1.0 m below surface in the inner berm in Westervoort. The used data is from the period 30-03-2020 until 25-06-2020.

CPTs were performed in the berm in Westervoort ever two to four weeks, furthermore three FVTs were performed. The dates of this tests is are shown in Table 4-3.

Table 4-3: The dates on which the CPT's and FVT in the berm are performed during the winter of 2019/2020.

	October	**November**	**December**	**January**	**February**	**March**	**April**	**May**
CPT	31	15 28/29	19	13	04 10	10	06	11
FVT	31	29	-	-	-	-	06	-

[2] The measurements results in Figure 4-7 are shown until the end of May, while there is data available until the end of June. Because of the work process it was not possible to implement the data of June in the Figures with the measured matric suction stresses, VWCs and the piezometric heads, but it was possible to determine part of the SWRC with the data, which is shown in Figure 4-8.

From the CPT data the undrained shear strength is derived according to equation (2-31). The results of this derivation, combined for different months is shown in Figure 4-9. A N_{kt}-value of 12.5 is used, since that gave the best fit with the FVT data (van Duinen A. , 2020).
In Figure 4-9 is visible that the derived undrained shear strength in the lower part, below eight meters above NAP, did not change. The one meter top layer are showing a big range of measured shear strengths, from 180 until 430 kPa. During the winter season the derived shear strength lowers from 250 kPa in the beginning of November, until 150 kPa in February. During the dry period afterwards the derived undrained shear strength increases until more than 400 kPa.
In the graphs from November and April/May it can be seen that the N_{kt}-value of 12.5 gives a good fit with the FVT for all three situations. Therefore it is assumed that an empirical correlation factor of 12.5 gives a good representation for all the CPTs (van Duinen A. , 2020).
The yellow dashed line in the graphs give the expected shear strength according to equation (2-17), with a constant unit weight of 18 kN/m^3, cohesion of 0 kPa and a friction angle of 26.6 °. For this calculation the suction stress was not taken into account.

Note to this results are that the method used to derive the undrained shear strength from the CPT data normally only can be used below the phreatic surface. Therefore it is not sure if the derived shear strengths are correct for the upper part. According to the piezometers from Figure 4-7 the piezometric head varies during the measured period from a little over 8 until a little over 10 m+NAP. During February and March the piezometric head was the highest, between the 9.5 and 10 m+NAP. In that period the derived undrained shear strength should be most close to the reality. However there is no lab-data to compare this to and therefore this cannot be confirmed.
Furthermore one N_{kt}-value is used for the whole layer, where normally the N_{kt}-value changes with different layers. Since the soil according to the CPT-data until a depth of four meter is clay (Chapter 3.1), this does not have to be a problem, however the top 1.5 meter is probably influenced by the vegetation on top, which can be the reason that the probe resistance and therefore the derived undrained shear strength with equation (2-31) is much higher than expected.
Another thing to take into account is that the FVTs are performed in the end of October (fall), the end of November (fall) and in the beginning of April (spring). The piezometric heads during this period are both times around the same heights and also the measured soil suction stresses and VWCs are comparable. Therefore it is very logical the N_{kt}-value of 12.5 gave in both situations a good fit, but it is not sure if it also gave a good fit in a month with an increased river level and higher measured piezometric heads like in February and March.

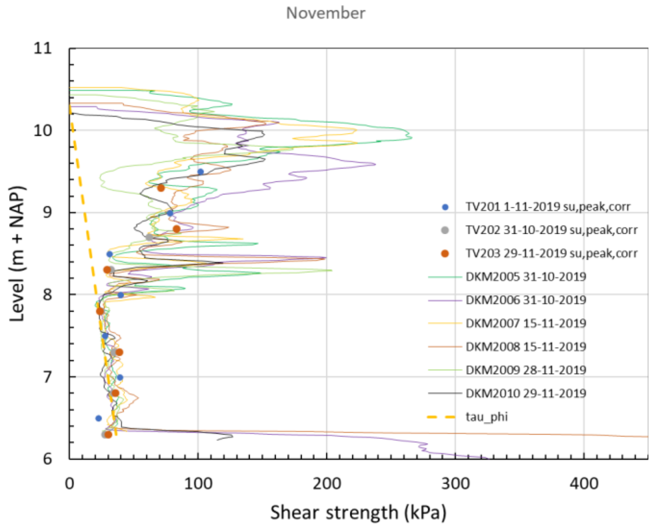

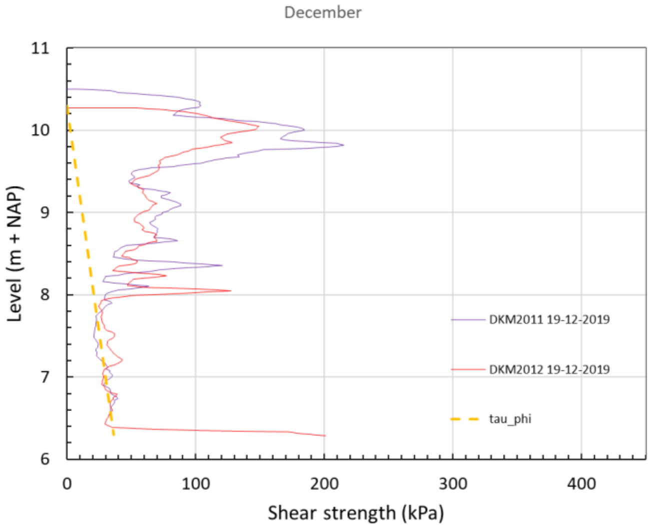

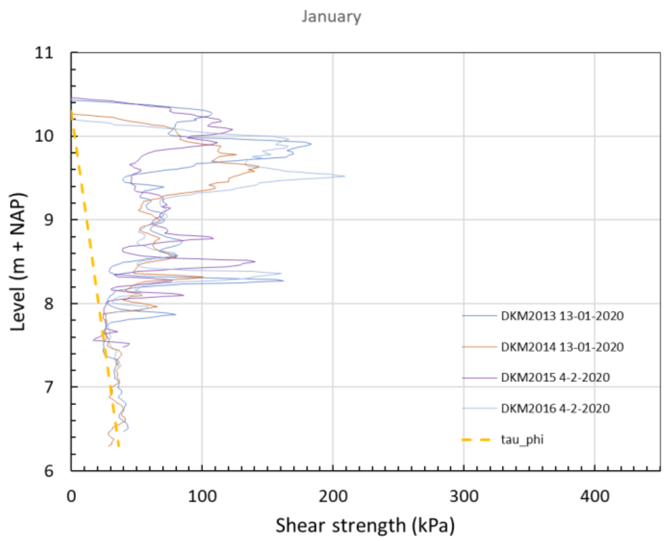

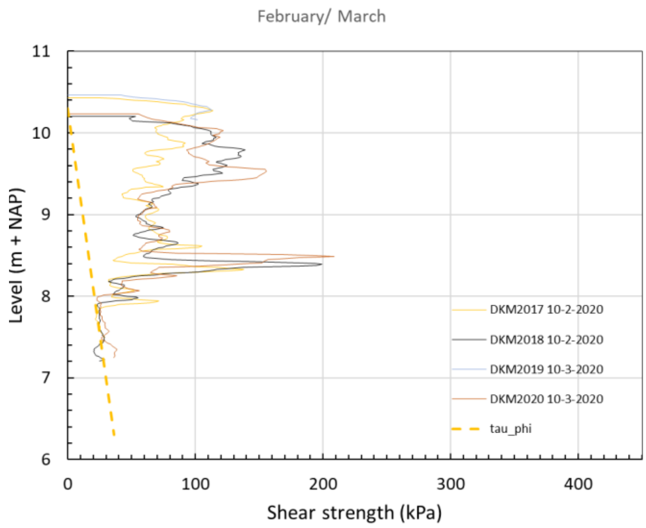

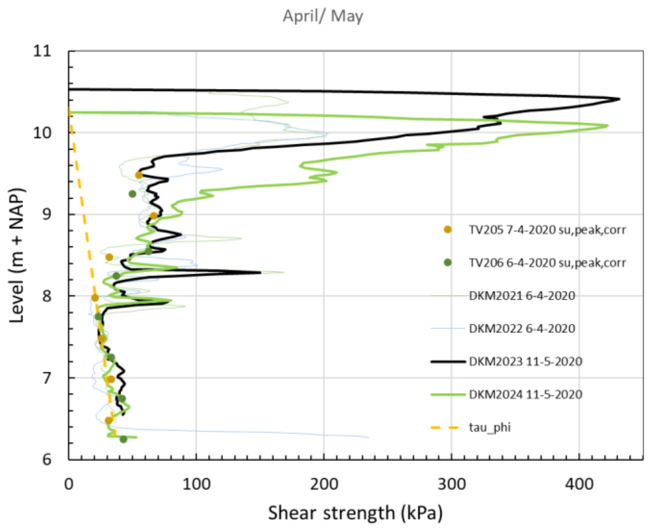

Figure 4-9: The undrained shear strength derived from the CPT data and the FVT-data over the period from November until May.

4.2.2 Field measurements Oijen

In Figure 4-11 the results of the measurements performed by Deltares are shown and in Figure 1-5 the location of the sensors in the dike in Oijen are shown. In Oijen only tensiometers and water content reflectometers are placed in the dike body.
The top figure of Figure 4-11 gives the measured soil suction and the precipitation surplus. The precipitation surplus is calculated with data from the weather station in Herwijnen 20 km North-East of the test location. There was no increased (Figure 4-10) river level recorded during the winter months. Therefore all the change in soil suction stresses and VWCs are assumed to be caused by the change in precipitation and evaporation. During the whole season soil suction is only measured in the dike body.

The highest soil suction stress is measured in the end of May. Before that period the precipitation surplus was negative for a longer period which have led to increased measured soil suction stresses. During the period with a negative precipitation surplus all tensiometers measured increasing soil suction stresses. The tensiometer one meter below surface measured soil suction until 100 kPa in the end of May, the measured VWC decreased as expected from 0.38 (degree of saturation is 100%) until 0.34 (degree of saturation is 89%). Unexpected for this tensiometer is the later reaction to the period with only evaporation from the beginning of March. The first measured positive soil suction is after 18 May. Before that period the pore water pressure decrease slightly, but not as fast as expected.
A possible explanation can be water which is still infiltrating through the soil. The period before there was quite some precipitation, the dike is very wide in that area, which means all the water has to infiltrate or evaporate. This can mean water was stills infiltrating through the dike during the period with a negative precipitation surplus. However in that case, the deeper tensiometers should show a decrease in measured soil suction in the end of May, since the water was still infiltrating. Another explanation can be the bentonite on top of the tensiometers. It can be possible the bentonite prevents the water from escaping and therefore negative soil suction stresses will continuously will be measured, but in that case the same behavior should be seen with other tensiometers. Also the measured VWC does not change much during the period from March until half May, therefore it seems the tensiometer is measuring the correct value.

The measured VWC 1.7 and 2.4 m below surface were decreasing when the measured soil suction was increasing. The change is small, but since the measured soil suction are maximum 5 or 10 kPa this is as expected.
8 February the tensiometer 3.1 m below surface, measured a fast decrease in soil suction from almost 10 kPa until approximately 3 kPa, after that the soil suction decreases more slowly. In the same period the VWC is starting to increase. The measured VWC 3.1 m below surface increases fast from 0.32 until 0.41 in February and from the beginning of May it decreases again. In the same period the measured suction 3.1 m below surface becomes negative, which most likely means the phreatic surface in the dike body increases until above the 3.1 m below surface. The river level during that period was not higher than usual (Figure 4-10), therefore that cannot be the reason. It is possible the water board AA en Maas increased the groundwater level in the hinterland. Therefore, the weather was the dominating source in the change of measured soil suction and VWC, except for the tensiometer 3.1 m below surface.
The difference in measured VWC 3.1 m below surface is quite big, since the measured soil suction stresses is maximum 10 kPa. The difference in measured VWC is from 0.41 (assumed to be 100% saturated) until 0.32 (according to equation (2-3) 77.5 % saturated). This behavior is more expected from sandy soil, than from a (silty) clay. More information about this behavior can be found in Chapter 2.2.

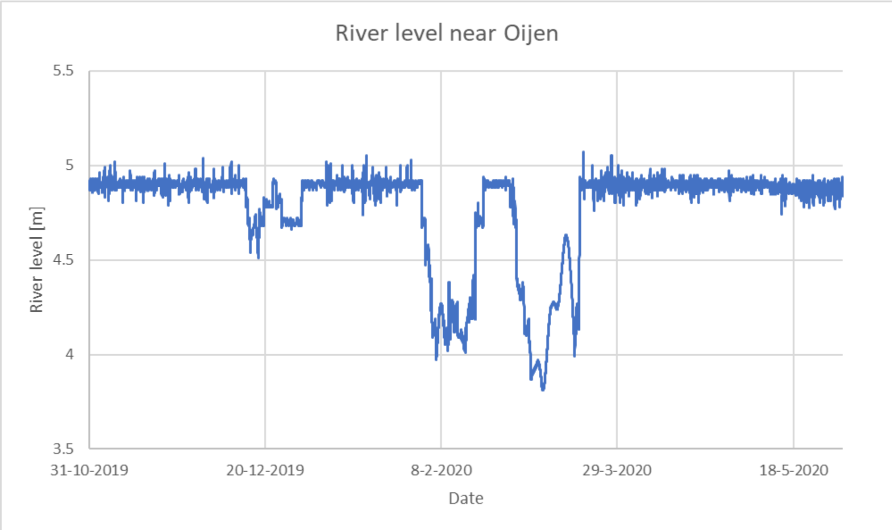

Figure 4-10: River level in in Lith, 1.2 km downstream from Oijen.

Figure 4-11: The measured suction stress (upper) and volumetric water content (lower) in the crest of the Maasdijk in Oijen. The suction stress 1.0 m below surfaces increased until 104 kPa on 31 May.

From the measurements of soil suction and VWC the drying and wetting SWRCs are obtained. The wetting curve is obtained from November until half March and the drying curve is obtained from data from half March (except for the most shallow tensiometer) until the end of May. The obtained SWRC can be found in Figure 4-12 and the exact dates the data is obtained from can be found in Table 4-4. Also for this obtained SWRC only small variations in soil suction and VWC were measured. Therefore more information from summer is needed to make a better guess.

Usual the value for α are between the 0 and 1.5 and the values for n between one and four. For the drying curves 1.7 and 3.1 m below surface the α-values are higher than 1.5. Also the R^2 values for that cases are lower than 0.8, which shows that the fit is worse than the other drying curves fitted.

Probably the wetting curves measured below are more scanning curves. Normally the wetting curve is obtained from a soil suction from 1500 kPa and the residual VWC, until a fully saturated state with no soil suction. In the field this stage is not reached, therefore the "wetting" curve we obtained is probably a scanning curve from the drying curve to the real wetting curve. To obtain the wetting curve, lab tests are probably needed, since soil suction of 1500 kPa probably will not be reached in the field.

The drying curve obtained for the soil around the tensiometer 1.7 m below surface, is probably also a scanning curve. The lowest soil suction the tensiometer measured on that depth, was -0.26 kPa on the 23 of February. Later on 12 March also some small negative soil suction where measured. Since this measurements were always for a short time (less than 24 hours) that low, the soil probably was not completely wetted. Therefore the obtained drying curve is probably not the real drying curve, but more a scanning curve, hence the high value for the α fitting parameter.

Table 4-4: The measured soil suction and VWC between the dates in the table are used to obtain the fitting parameters for the van Genuchten Equation, to obtain the SWRC for each depth.

Depth [m below surface]	**Wetting Curve**	**Drying Curve**
1.0	12-11-2019 until 28-11-2019	19-05-2020 until 31-05-2020
1.7	30-11-2019 until 13-01-2020	14-03-2020 until 31-05-2020
2.4	29-11-2019 until 12-03-2020	16-03-2020 until 31-05-2020
3.1	09-01-2020 until 28-02-2020	14-04-2020 until 31-05-2020

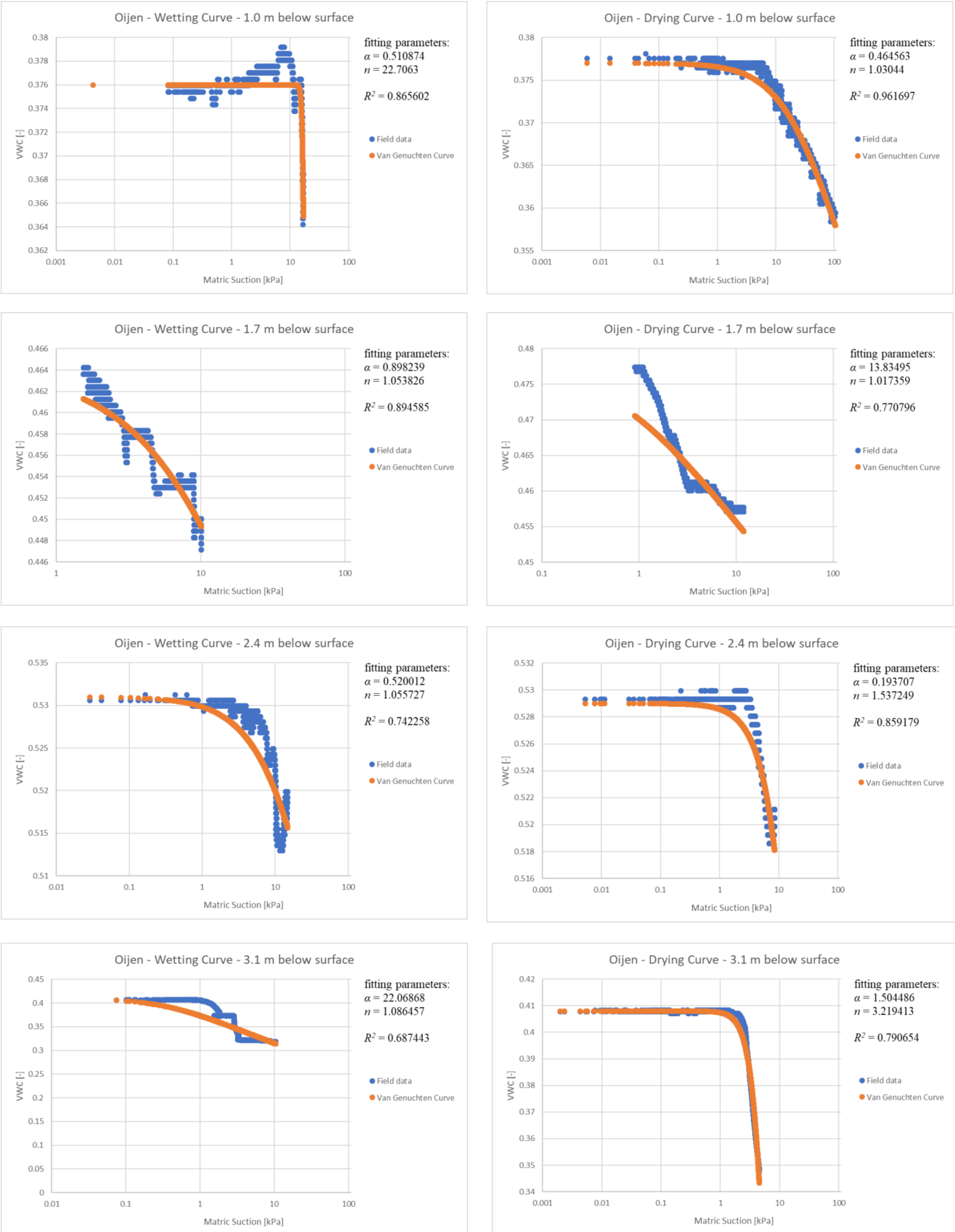

Figure 4-12: the drying and wetting SWRC obtained from the field data measured in Oijen.

CPTs were performed in the crest in Oijen ever two to four weeks, furthermore five FVTs were performed. The dates of this tests is are shown in Table 4-5.

Table 4-5: The dates on which the CPT's and FVT in the crest are performed during the winter of 2019/2020.

	October	**November**	**December**	**January**	**February**	**March**	**April**	**May**
CPT	24	14 26	19	13	04	09	08	11
FVT	23 24	27	-	-	-	-	09 10	-

Figure 4-13 shows the undrained shear strength derived from the CPT and FVT data. The undrained shear strength is derived with equation (2-30), with a N_{kt} value of 15 (van Duinen A. , 2020). This empirical correlation factor gives the best fit with the FVT-data.

During the winter months a decrease of the undrained shear strength is shown in the upper layer. Where it gave peaks until 150 kPa in November, it only is around 50 kPa during the wet months after. During the dry period in April and May the undrained shear strength increases until approximately 270 kPa. The shear strength in the rest of the clay body is more or less constant.

The yellow dashed line in the graphs give the expected shear strength according to equation (2-17), with a constant unit weight of 18.7 kN/m^3, cohesion of 0 kPa and a friction angle of 26.6 °. For this calculation the soil suction stress was not taken into account.

To this results the same notes should be considered as described with the CPT and FVT in Westervoort (Chapter 4.2.1).

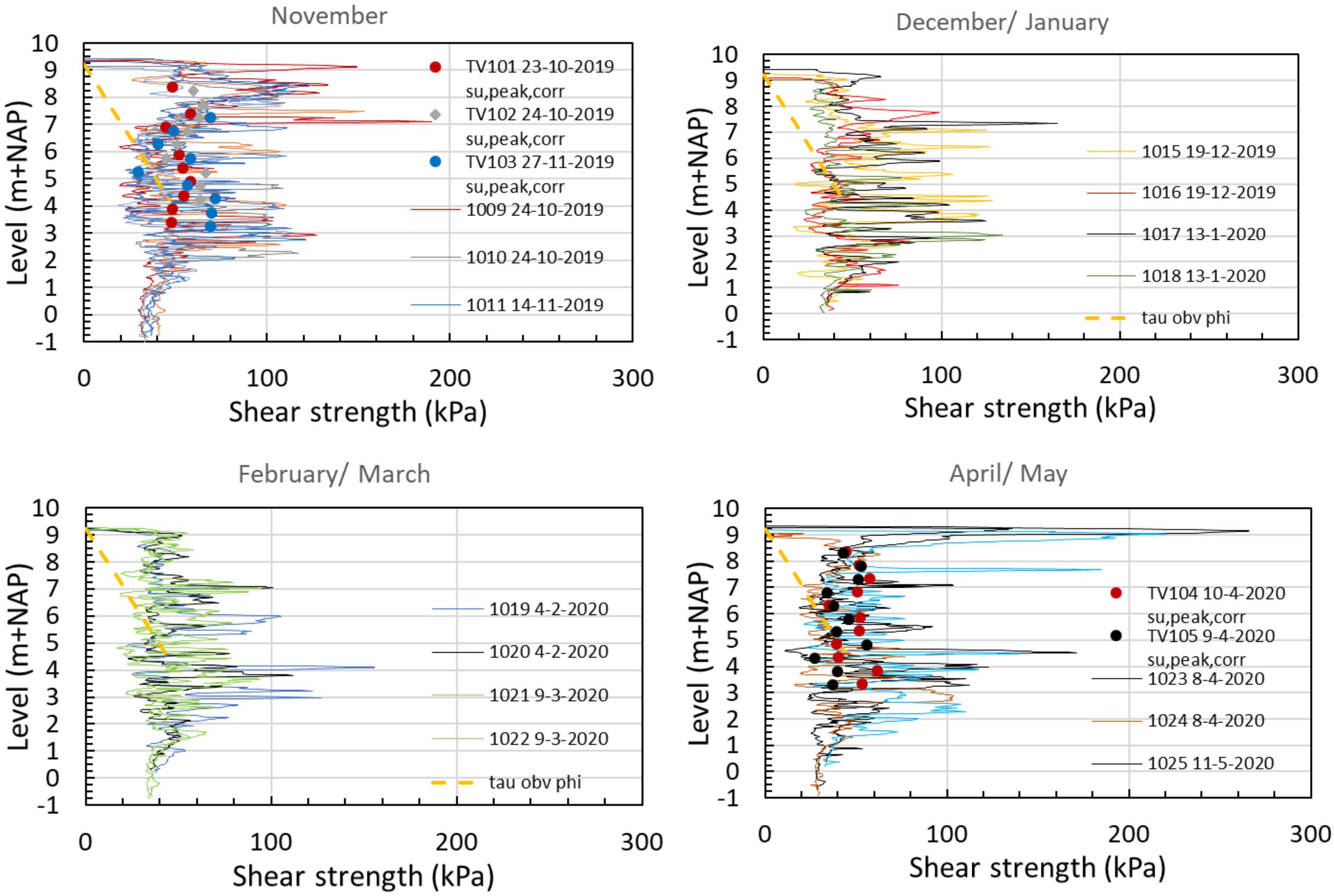

Figure 4-13: The undrained shear strength derived from the CPT data and the FVT-data over the period from November until May.

4.3 Model fit

In the WBI different soil models are used to model soil behavior. Normally if soils have a low permeability and are below the water table, it is assumed to behave undrained and above the water table the soil is assumed to behave drained. Since at least one tensiometer in the dike body in Oijen was always measuring soil suction, it can be assumed somewhere in the dike body there was drained behavior. However, on 12 March the highest measured soil suction in the dike body is less than 2 kPa. This was measured at a depth of 1.7 m below surface and all the other tensiometers were measuring negative soil suction stresses. Therefore only a small part of the dike behaves drained.
Therefore two methods are tried to fit the model to the measured data. Modelling with the SHANSEP concept and with the HS model. The suction is taken into account how they are measured. Since in the berm in Westervoort no soil suction stresses were measured until the end of March, no suction is taken into account until that moment. In the crest in Oijen suction was measured during the whole winter, so with the calculated SWRC with the van Genuchten equation, the actual suction in that moment was implemented in the model, by giving the concerned soil layer in Plaxis a specific degree of saturation.

4.3.1 Fit with the SHANSEP concept

In the SHANSEP concept in Plaxis the undrained shear strength is calculated with equation (2-30). But instead of using the OCR, the apparent OCR (OCR*) is used. The apparent OCR is used to fit the shear strength computed by the model, to the shear strength derived from the CPT data. To do this the soil layers in the berm, from surface until two meters below surface, are divided in soil layers of 0.2 until 0.5 meter. Deeper than two meters below surface the modelled shear strength according the used soil models was almost the same as expected according equation (2-19), therefore no changes where necessary over here. In the dike body the soil layers are divided in layers of about 0.7 until 1.1 meter, dependent of the sensor depths.
The apparent OCR, which is used to fit the shear strength calculated by the model to the shear strength calculated from the CPT data, does not have to be the OCR which would be found in a consolidation test. The apparent OCR is the OCR* with which the model generates the same shear strengths as derived from the CPT data. Figure 4-14 and Table 4-6 shows the results from the berm from the IJsseldike in Westervoort and Figure 4-15 and Table 4-7 show the results from the Crest in Oijen.

Table 4-6 shows the used apparent OCRs for the berm in Westervoort. The apparent OCR from 8 until 9.5 m+NAP increases during the months with the higher piezometric heads and decreases when the piezometric head decreases in April. In December the apparent OCRs until one meter below surface increased and they decreased again in January. This is probably due to higher piezometric head in the aquifer (sand layer below the cover). Therefore the effective vertical stress decreases which means a higher OCR is needed to maintain the shear strength.
The apparent OCRs are very high, since the shear strength determined from the CPT data was higher than expected. However no soil suction stresses where measured in the berm in Westervoort between November and April, so the higher shear stress cannot be caused by the soil suction, since there was not any.
Especially in the top layer the shear strengths are much higher than expected from the model behavior without the apparent OCRs. This was probably caused by the vegetation on top of the berm.
Furthermore during the summer the soil suction stresses can increase until over 100 kPa, one meter below surface. In that case the effective stress in that period will be higher, which can be the cause of the high apparent OCR.
The highest pore pressures where measured during February/March, which should lead the lower shear strength, however this was not visible in the shear strength from the CPT-data. Therefore the apparent OCRs in February/March are higher than for January.

Table 4-6: The used apparent OCR values to fit the model shear strength to the shear strength obtained from the CPT-data for the berm in Westervoort.

Depth [m+NAP]	November OCR*	December OCR*	January OCR*	February/March OCR*	April/May OCR*
10-10.5	22	40	35	50	50
9.8-10	30	60	45	50	80
9.5-9.8	22	30	30	50	20
9-9.5	12	15	15	20	10
8.5-9	9	11	10	20	9
8-8.5	5	7	7	10	5

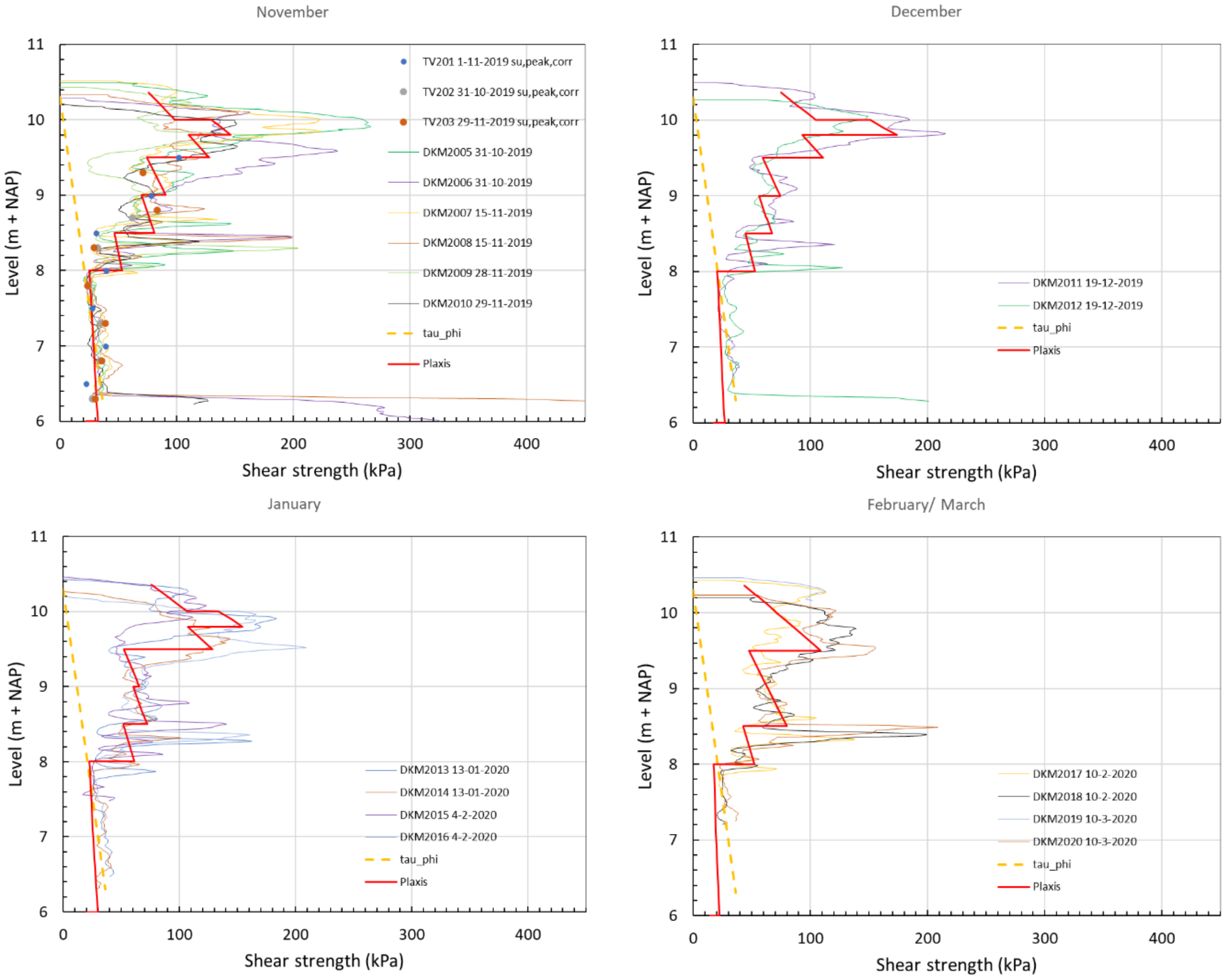

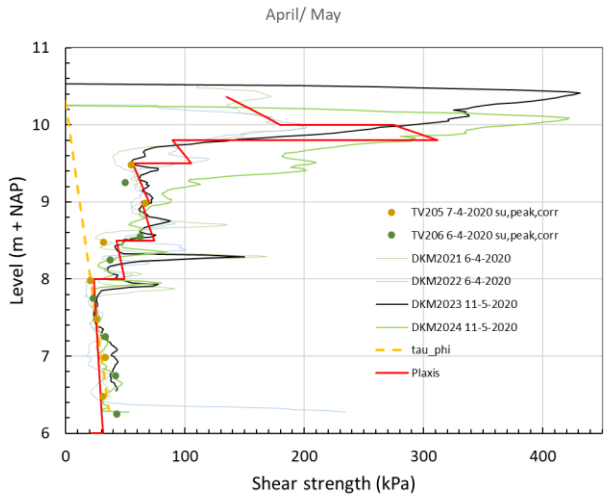

Figure 4-14: The fit from the model with the shear strength obtained from the CPT-data. The SHANSEP concept was used to fit the model. The fit is made for in the berm in Westervoort.

Table 4-7 shows the used apparent OCRs for the crest in Oijen. Also in Oijen the shear strength in the upper part decreased during the winter and increased in the spring. The apparent OCR in the upper part (8 until 9 m+NAP) decreased until 2.5 after which it increases again to 3. For the lower part the apparent OCR decreases from December until April/May.

The shear strengths in Oijen were also a higher than expected, but not as much as in the berm in Westervoort. The tensiometer one meter below surface did not measure soil suction from November until half May. The other tensiometers did measure a decrease in soil suction until half March, after which the measured soil suction stresses increases again.
Therefore it is expected the apparent OCR for the layer between eight and nine m+NAP will not change during December until April/May, since the measured soil suction did not change. However a decrease is visible in the apparent OCR in January, but this is caused by the decrease of shear strength obtained from the CPT data.
The layer from 7.3 until eight m+NAP shows a decrease of apparent OCR from beginning December until April/May. The shear strength in the same period decreases. Therefore the decrease in apparent OCR is coming from the decrease in shear strength, even when the soil suction was increasing in the period from half March until the end of May.
The layers from 5.3 until 7.3 m+NAP are showing an increase in apparent OCR in February, while in this month the lowest soil suction is measured. However the shear strength obtained from the CPT data did not change significant, which explains the increase in apparent OCR. After that the apparent OCR is decreasing again, since the measured soil suction increases.
Furthermore these apparent OCRs are mostly below the 3, which can mean the apparent OCR is the real OCR. In that case the OCR from February/March is the real OCR, since in that moment there were almost no soil suction measured in the dike body (only 2 kPa 1.7 m below surface). The increase of OCR can in that case be the results of increasing or decreasing soil suction or pore water pressure.

Table 4-7: The used apparent OCR values to fit the model shear strength to the shear strength obtained from the CPT-data for the crest in Oijen

Depth [m+NAP]	November OCR*	December OCR*	January OCR*	February/March OCR*	April/May OCR*
8.0-9.0	6	3	2.5	3	3
7.3-8	3	3	2.5	2.5	2
6.6-7.3	2.5	3	2.5	3	2
5.3-6.6	2	2.25	2.25	2.5	2
<5.3	1.5	2	2	2	1.5

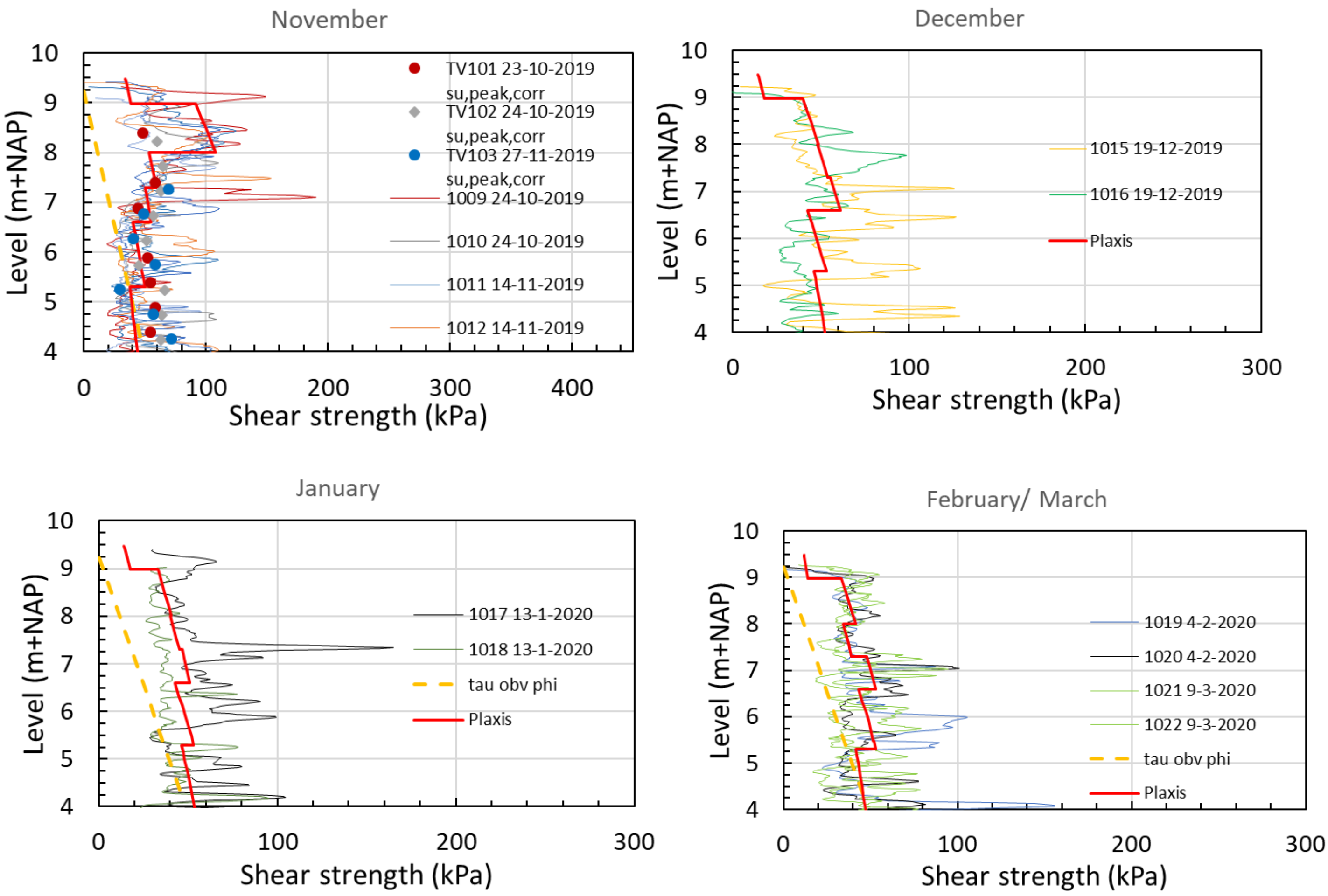

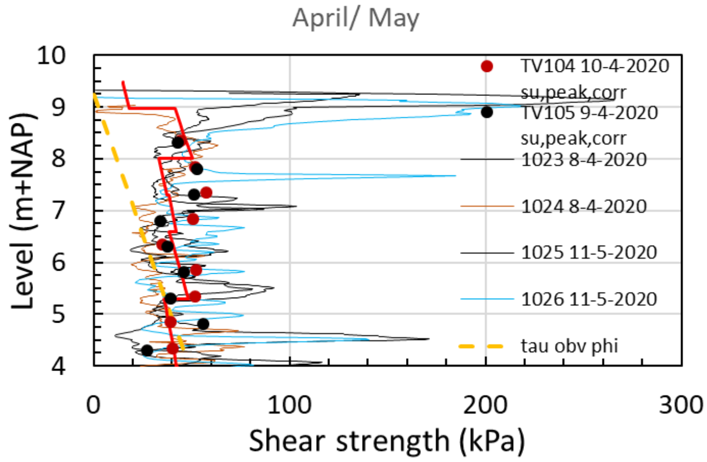

Figure 4-15: The fit from the model with the shear strength obtained from the CPT-data. The SHANSEP concept was used to fit the model. The fit is made for in the crest in Oijen.

4.3.2 Fit with the Hardening Soil model

In the Hardening soil model the shear strength is calculated with equation (2-19). The calculated shear strength in Plaxis is fitted to shear strength obtained from the CPT data by changing the cohesion. Therefore the cohesion changes in the apparent cohesion (cohesion*), which is not the real cohesion, but just a fitting parameter to fit the calculated shear strength from the model to the shear strength calculated with the CPT data. The soil layers are divided as described in the beginning of Chapter 4.3.1.
Figure 4-16 and Table 4-8 show the results from the berm from the IJsseldike in Westervoort and Figure 4-15 and Table 4-7 show the results from the Crest in Oijen.

Table 4-8 shows the apparent cohesion for the berm in Westervoort. The apparent cohesion which fit the model shear strength to the shear strength obtained from the CPT data, decreased during the months with a higher piezometric head and decreases during the spring. Only during the spring soil suction were measured. The most shallow tensiometer measured the highest soil suction, which can explain the increase in apparent cohesion in April/May. The tensiometers in Westervoort were installed in the end of October, which means the measured data from November can be used (Chapter 4.2). Therefore it is not sure the measured soil suction in November is the same is the measured soil suction measured in April/May.
Until March no soil suction stresses where measured in the field, therefore the apparent cohesion, which is too high to be the actual cohesion of the soil, cannot be caused by suction stress. The actual cohesion cannot be 100 kPa, but a normal cohesion will be around the 30 kPa maximum (Normcommissie 351006 'Geotechniek', 2019). The high cohesion in the top are most likely caused by the vegetation on top, which influences the soil until a depth of approximately one until 1.5 meter below surface. Deeper in the soil the high cohesion can be the results of high soil suction which are possibly measured during the summer period.

Table 4-8: The used apparent cohesions to fit the model shear strength to the shear strength obtained from the CPT-data for the berm in Westervoort.

Depth [m+NAP]	**November Cohesion***	**December Cohesion***	**January Cohesion***	**February/March Cohesion***	**April/May Cohesion***
10-10.5	100	95	105	100	100
9.8-10	175	170	140	100	175
9.5-9.8	115	100	100	100	115
9-9.5	80	70	70	70	80
8.5-9	65	70	70	70	65
8-8.5	40	45	50	45	40

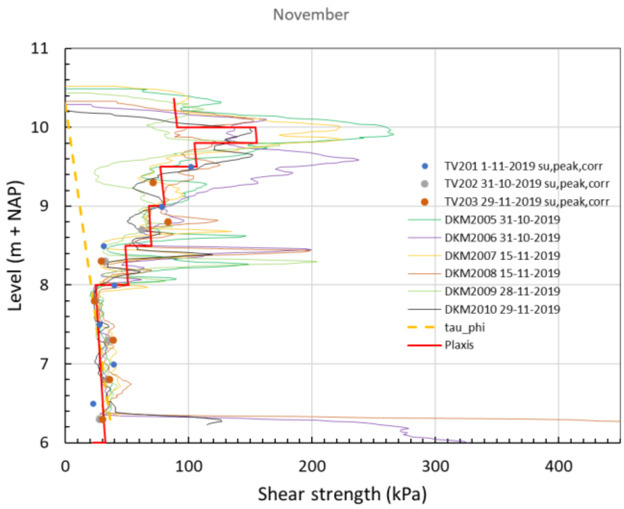

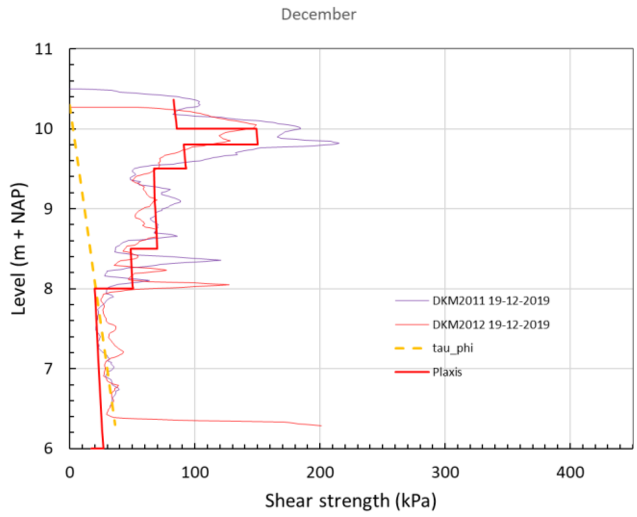

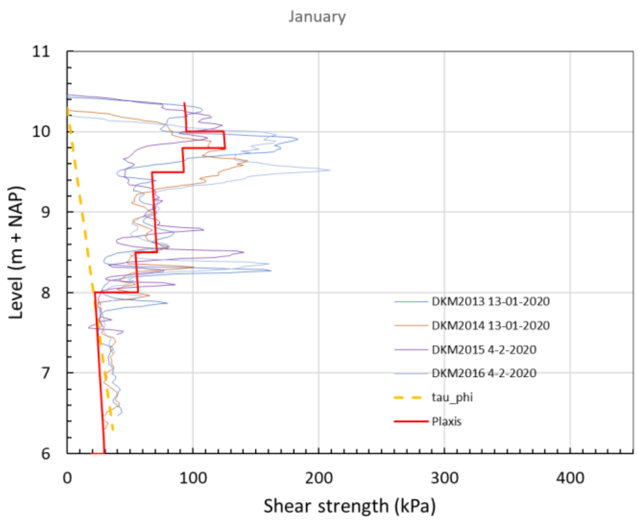

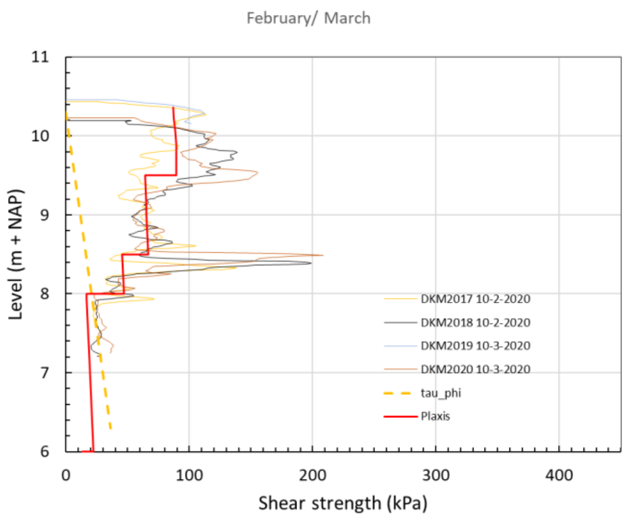

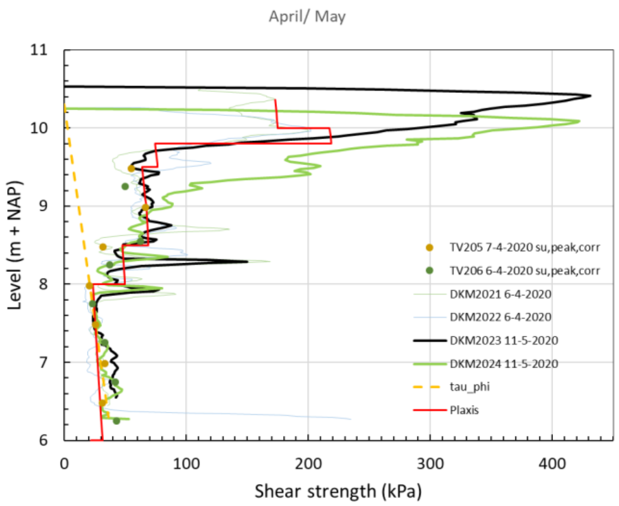

Figure 4-16: The fit from the model with the shear strength obtained from the CPT-data. The Hardening Soil model was used to fit the model. The fit is made for in the berm in Westervoort.

Table 4-9 shows the apparent cohesions needed to fit the shear strength of the model, to the shear strength calculated from the CPT data in Oijen.
For the top layer until a depth of eight m+NAP, the apparent cohesion decreases during the winter months where no soil suction stresses where measured and is increasing again when soil suction stresses are measured again. However the decrease in apparent cohesion happens from November until January and the increase happens from January until the end of May, but the measured (negative) soil suction is more or less constant during the whole period from December until half May. So the decrease and increase of apparent cohesion cannot be explained from the measured soil suction.
The deeper layers (below 8 m+NAP) show a decrease in apparent cohesion from December until the end of May, while the measured suction stresses were increasing again from half March. So also here the change in apparent cohesion cannot be explained by the change in measured soil suction.

Table 4-9: The used apparent cohesions to fit the model shear strength to the shear strength obtained from the CPT-data for the crest in Oijen.

Depth [m+NAP]	**November Cohesion***	**December Cohesion***	**January Cohesion***	**February/March Cohesion***	**April/May Cohesion***
>9	40	35	20	45	120
8-9	90	35	15	35	50
7.3-8	55	35	20	25	25
6.6-7.3	20	40	20	30	20
5.5-6.6	15	30	25	25	15
<5.5	5	10	20	20	5

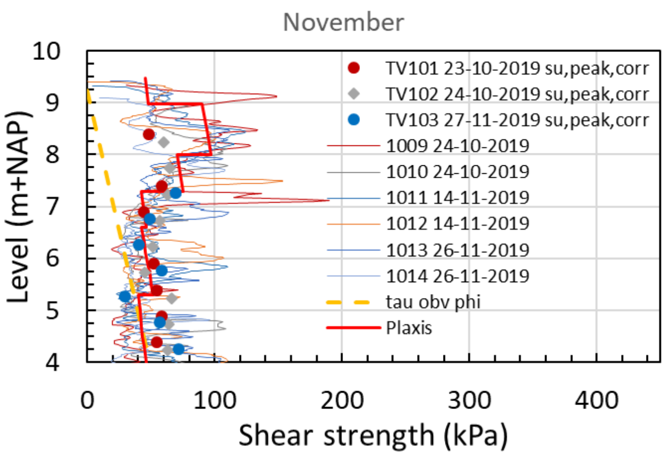

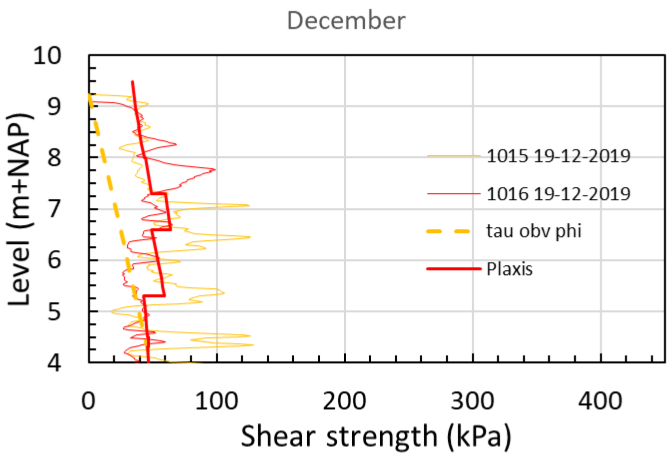

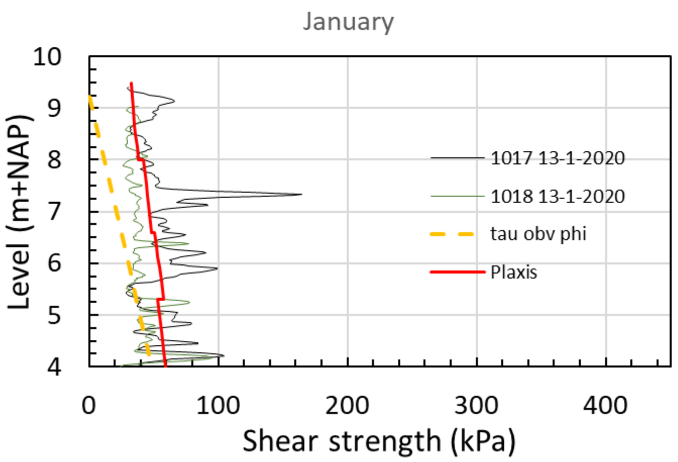

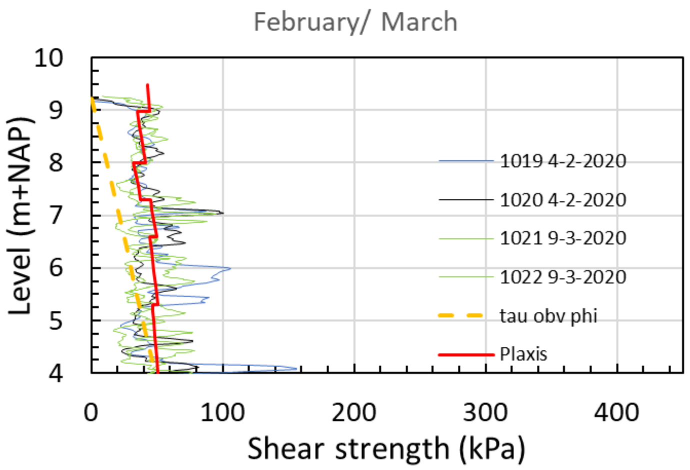

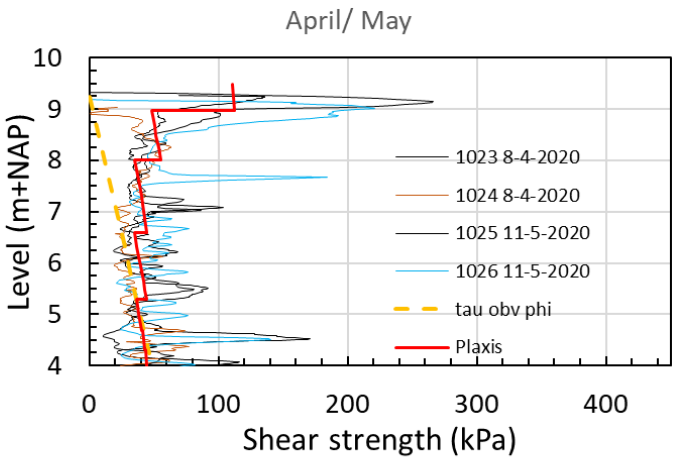

Figure 4-17: The fit from the model with the shear strength obtained from the CPT-data. The tau-phi method was used to fit the model. The fit is made for in crest in Oijen.

4.3.3 Extrapolation to WBN situation

The results from the model fit with the Hardening Soil model (apparent cohesion) will be used to compare the FoS in a WBN-situation where the extra strength is taken into account, to the FoS in a WBN-situation where the suction stress is ignored, so no apparent cohesion is used. This will be done separately for the inner berm and for the crest, since the information for both parts come from different test locations. For the SHANSEP concept this will not be done, since the pore pressure influences the effective stress, which influences the shear stress directly and indirect by the apparent OCR. Therefore it is difficult to predict the apparent OCR in case of WBN situation.

The suction stress is taken into account by implementing an apparent cohesion on the soils in the dike body, inner toe and the berm. Furthermore a fine mesh is used, with a tolerated error of 0.005 and a phreatic surface in the dike body according to the WC, since this is the most realistic phreatic surface. For the soil models a mixture of the HS and SS model is used. The soils which gave values for the shear strength according to the equation (2-19) are modelled with the SS model, the soils with apparent cohesions and the more sandy soils are modelled with the HS model.

From the results from the berm in Westervoort it can be derived which apparent cohesion predicts the measured shear strength the best in different situation during the winter. In February/March the piezometric head in the cover is around the 10 m+NAP, which is just below surface. Therefore this apparent cohesion should be there during a WBN event. For the inner toe, which consists of a sandy clay to clayey sand, the apparent cohesion of the strongest layers from the berm is assumed to be present.
From the results from the crest in Oijen, the lowest soil suction where measured during March, but the lowest apparent cohesions to fit the model where found in January. Since the most normative situation is needed to perform the assessment of the dike body, the apparent cohesions of January are used in this final assessment of the WBN situation. Since in January there was no high river level in the Maas near Oijen, the apparent cohesions during a WBN event will be probably lower for the part of the dike which is below the phreatic surface during a WBN event. Since the most conservative estimate of the phreatic surface during a WBN event is 2.2 m below surface. The apparent cohesion of the layers lower will only change in that case. Since a couple of layers will have a lower apparent cohesion, the shear strength will be lower too. Therefore the FoS in a real WBN event will be lower than the FoS which is calculated in this situation.

The results in terms of FoS are shown in Table 4-10. When all cohesion are zero, except for the top layer (cohesion is 5 kPa, to prevent micro instability), the FoS is 1.54. This is higher than in the FoS calculated in chapter 3.2.3 Influence Soil Models, but this is caused by the different phreatic surface in the dike body.
If apparent cohesions are added in the dike body, the FoS increases until 1.94. This is an increase of 0.4, which is quite a lot. The slip surface did not change significant compared to the situation without apparent suction stresses.
If apparent cohesions are added in the berm and inner toe, the FoS increases until 2.12. This is an increase of 0.58, which is a big increase. The slip surface did change also compared to the situation without apparent cohesions (Figure 4-18). This is a results of the apparent cohesions in the berm. If the cohesion increases the shear strength increases and therefore shearing will not happen until the shear stress is higher than the shear strength.

Table 4-10: Results with and without apparent cohesion applied in different soil layers during a safety assessment of WBN level in terms of FoS.

Situation	**FoS**
With apparent cohesions berm	2.12
With apparent cohesions in the dike body	1.94
Without apparent cohesions	1.54

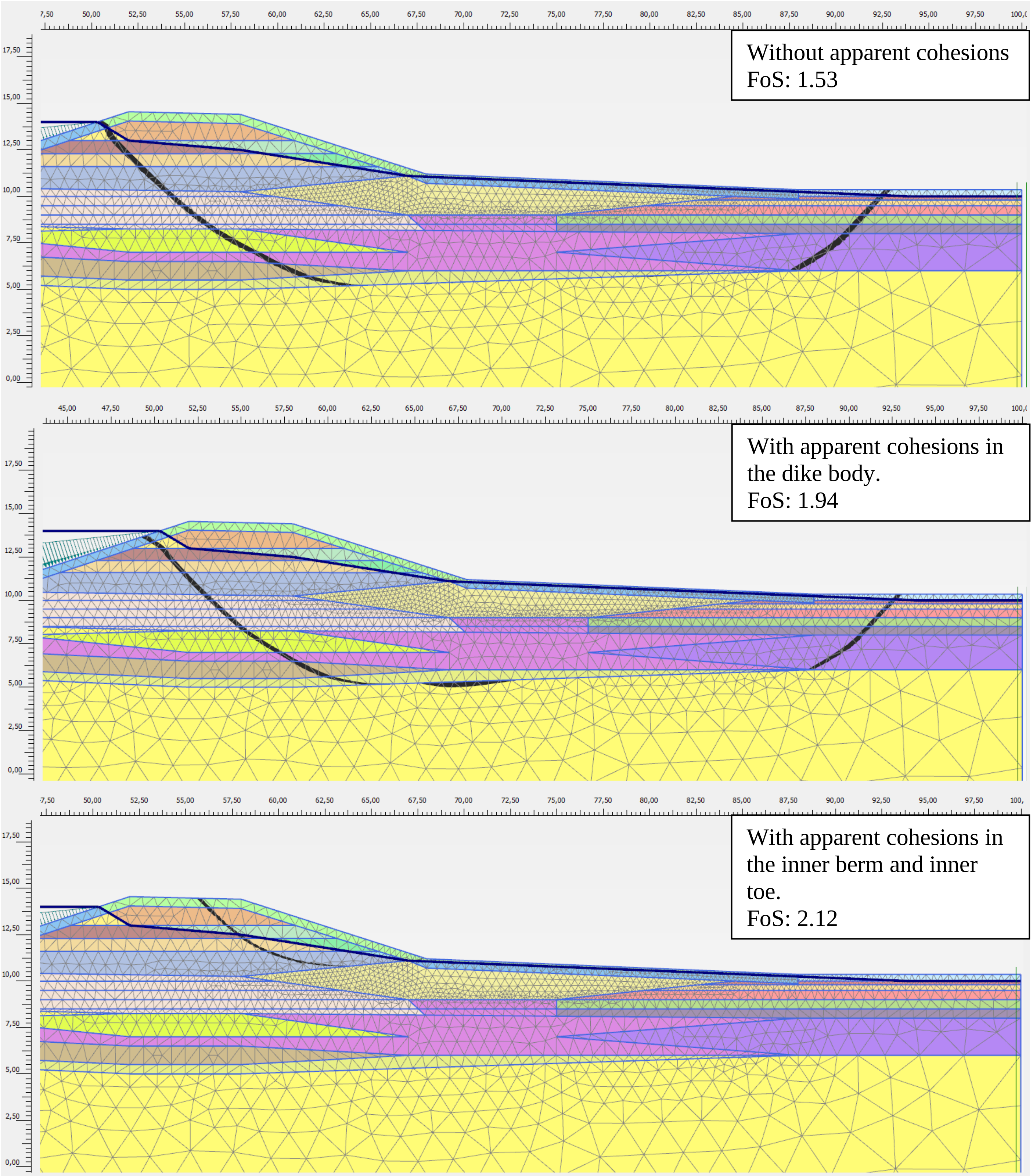

Figure 4-18: Slip surfaces for the modelled dike with and without apparent cohesions according to the field data.

5 Interpretation

Chapter 4 gave an overview of the results of the sensitivity analysis, the field measurements and the model fit. In this chapter the results are interpreted, starting with the interpretation of the sensitivity analysis, after that the interpretation of the field data and last the interpretation of the model fit.

5.1 Sensitivity analysis

In the sensitivity analysis the effects of the depth of the phreatic surface and the effect of the different soils in the Staring Serie are evaluated. As stated in literature there are different ways to model the phreatic surface in the dike body during a WBN event. A conservative way to do this is the method from the TRWD (TAW, 2004), where the phreatic surface in this case is 1.1 m below the top of the dike. A less conservative and more realistic method is the WC (Deltares, 2017), where the phreatic surface in this case is 1.6 m below the top of the dike. Two more phreatic surfaces were tested, 2.5 meter and 3.3 meter below the surface of the dike.
With this sensitivity analysis, the suction was ignored. However, the lower the phreatic surface, the bigger the zone where suction can be present and the bigger the influence of the suction on the shear strength. Even without taking the suction into account, the influence of the phreatic surface is significant. The lower the phreatic surface, the higher the FoS. This is caused by the lower water pressure in the dike body, which means a higher effective vertical stress, resulting in a higher shear strength (equation ((2-17) and (2-18)), which can lead to a higher FoS. However a higher effective stress also lead to higher load on the dike body which can result in a lower FoS. But since the FoS according to the sensitivity analysis increases with a lower phreatic surface, it seems the net effect of a lower phreatic surface in the dike body is a higher FoS.
If suction is taken into account this effect is stronger, since the effective suction increases further above the phreatic surface, as can be seen in Figure 4-2. Especially the finer soils O6 until O15 from the Staring Serie show an increase in effective suction with height above the phreatic surface. However in reality the effect will be less than visible in chapter 4.1.2, since the phreatic surface likely is higher than 3.3 m below surface. Furthermore the top of the dike body (1 until 1.5 m below surface) is highly influenced by the weather. Therefore, suction cannot be expected in the upper area of the dike body (Chapter 4.2.2). To model the influence of the suction on the FoS, the location of the phreatic surface in the dike body has to be known. The used prediction methods (TRWD and WC) are both expected to be conservative. Therefore, the real phreatic surface is probably lower than the location the TRWD and WC are calculating.

Furthermore a static state analysis of the groundwater flow is advised in the WBI (Ministerie van Infrastructuur en Milieu, 2019), but it is not known how long it takes to reach the static state situation or if it is reached at all. Also, the generation of pore pressures within the dike body during the WBN event is not known. A time dependent analysis about the generation of pore pressures (and soil suction stresses) within a dike body, is advised to generate more knowledge and insight in the location of the phreatic surface in a dike body during a WBN event.

5.2 Field Measurements

From November until the end of May the field data of the sensors in Westervoort and Oijen are shown in chapter 4.2. From the suction and the VWC measurements, the SWRC wetting and/or drying curve was obtained if possible. This was possible for all the sensors in the crest in Oijen and for the upper sensors (one meter below surface) in the berm and inner toe in Westervoort. For the deeper layers this was not possible since there was not enough data with a (high enough) positive soil suction or enough variation in VWC. In Figure 5-1 the SWRCs obtained from the field data (Chapter 4.2) are shown in the same figure with the SWRCs from soils from the Staring Serie.
In chapter 4.2 it is already mentioned that the wetting curves obtained from the field data in Oijen are probably more scanning curves, since the 1500 kPa soil suction, which is needed to obtain the wetting curve, is not reached in the field.
The obtained SWRC for the tensiometer 1.7 m below surface has relatively high values for the fitting parameters α and n, which is likely caused by the fact that this obtained drying curve is a scanning curve since the lowest measured soil suction was only -0.26 kPa for a short time.

The soils in the dike body in Oijen and inner berm in Westervoort consist of clayey soils. Based on this, the obtained SWRCs are expected to be comparable to the clayey soils of the Staring Serie. However, the SWRC in Oijen 1.7 and 3.1 m below surface and in the inner toe in Westervoort are more comparable to the SWRCs from the sandy soils in the Staring Serie. From the inner toe in Westervoort it is known the soil was sandier than in the berm. From the drilling in Oijen (Appendix III, Figure III-1) it is known there are small sand layers 3 until 3.8 meter below surface. The tensiometer only measures a couple of cm^3, but the water content reflectometer measures a couple of dm^3. In this couple of dm^3 it couls have taken into account part of a sand layer, in which the VWC decreases faster in case of small soil suction stresses, which explains the obtained SWRC from the field data.
However, most tensiometers only measure soil suction stresses until approximately 10 kPa, where normally the SWRC is obtained for higher suction stresses. These higher suction stresses are likely measured during summer and after a whole year of measuring it is possible to obtain a SWRC from the field data with higher measured suction stresses. Furthermore, the SWRC obtained from the field data has to be compared to the SWRC obtained in the lab from a soil, to compare the in-situ behavior with the behavior in the lab.

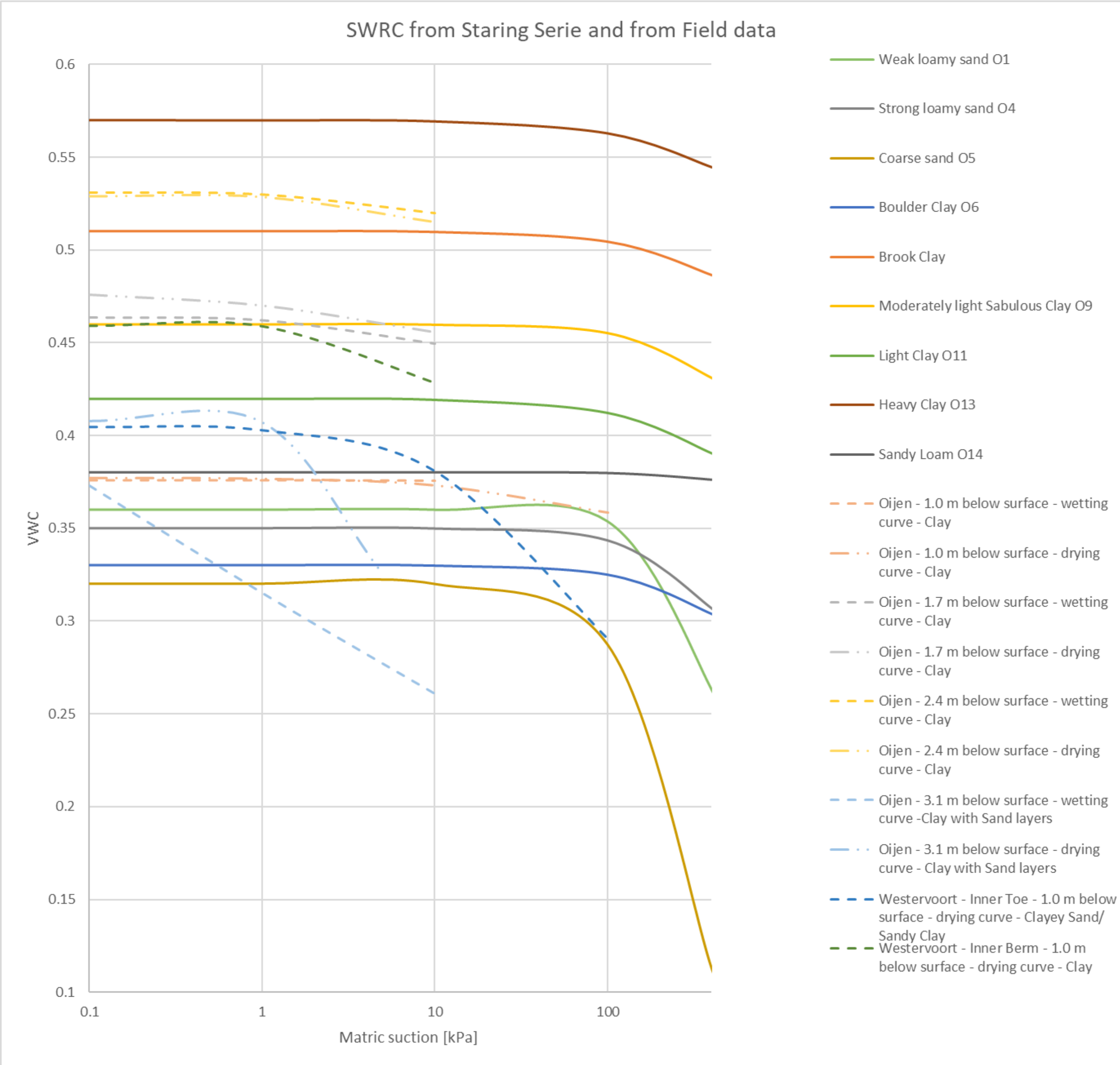

Figure 5-1: Comparison from the SWRC from the Staring Serie and the SWRC obtained from the field data.

From the sensitivity analysis about the soil type (Chapter 4.1.2) it is known the FoS does not change significant between the clayey soils. Therefore the exact SWRC of the soil does not have to been known as long as it is known if the soil is a sandier soil, since the increase in FoS is significantly lower in that case.

Figure 5-2 shows the shear strength obtained from the CPT data and from the FVT on the left axis. On the right axis the measured soil suction is displayed. The Figures are only made for Oijen, since in Westervoort not enough suction stresses are measured. In the graphs a trend is visible between the shear strength and the measured soil suction. If the measured soil suction decreases, the shear strength decreases and if the measured soil suction increases the shear stress increases. However, the amount of decrease and increase of the shear strength cannot be explained by the change in measured suction only. According to equation (2-19) effective suction multiplied by the tangent of the friction angle, is the contribution of the suction to the shear strength. The effective suction can be calculated by multiplying the measured suction with the degree of saturation (equation (2-19)).
At a depth of 1.7 meter below surface a soil suction increase of 5 kPa was measured from 10 March until 11 May. If the degree of saturation was 100 %, the maximum effect of the suction on the shear strength according to equation (2-19) was: $5 \cdot 1 \cdot \tan(32) = 3.12$ kPa. The average increase which is visible is larger than expected from the increase in suction based on equation (2-19). 2.4 meter below surface with an increase in measured suction, an increase in measured shear strength is not visible.

Overall the shear stress is higher than expected compared to equation (2-19), especially in the periods with high measured suction. This can have different causes.

1. The shear strength obtained from the CPT data is not accurate.
   The N_{kt} value for the shear strength is determined with a comparison with the FVT. These FVTs were performed in the end of October, November and April. For example in Oijen, one meter below surface, the FVTs performed in November and April are both performed during a measured soil suction of approximately 2 kPa. However, looking at the fit in November the FVT was in the middle of the CPT-data and in April the FVT was on the lower side of the CPT data.1.7 meter below surface the measured FVTs in April are 20 kPa higher than the calculated shear strength from the CPT data. The soil suction measured during these times are approximately 10 kPa in November and 3 kPa in April. 2.4 meter below surface the shear strength from FVTs in November are in the middle of the shear strengths from the CPT data, likewise in November. A lot of differences are measured, but overall there are quite in the middle.
   However FVTs are not performed in the months with the lowest measured effective suction and the highest piezometric heads, February and March. Next to that, during the end of May when the measured soil suction is increasing to values of 100 kPa one meter below surface, FVTs are not performed to fit the CPT data and evaluate the N_{kt}. Therefore, it is possible the N_{kt} value of 12.5 is not a sufficient fit in the situation soil suction is not measured or when high soil suction is measured. Since the N_{kt} value influences the shear strength calculated from the CPT data, it can be the shear strength obtained from the CPT data is not accurate.

2. The suction and VWC measurements are not accurate.
   The suction and VWC measurement devices are placed in the soil, with on top a couple of cm bentonite. Bentonite is a soil which absorbs a lot of water and has the capability the hold the water for a long time, even in a dry surrounding. This can result in a higher measured VWC and a wrong measured suction stress. This can be tested by take some samples, from which the suction and VWC are measured in-situ in the field and later in the lab and compare them.
   Another option is the response time of the sensors. The used tensiometers have a response time of only 5 seconds for a pressure change between 0 and 85 kPa. So in between these values the measured soil suction stresses should be in time. Only the tensiometer one meter below surface in Oijen measured suction stresses above the 85 kPa, therefore the measurements above 85 kPa can be inaccurate.

Figure 5-2: Shear strengths obtained from the CPT-data, the Field Vane Test (FVT) and the measured matric suction in the crest in Oijen.

5.3 Model Fit

From the CPT-data the undrained shear strength is determined with equation (2-31). In Chapter 4.3 the model is fitted to the data with the apparent OCR in the SHANSEP concept and the apparent cohesion for the HS model. In the results it is visible that the shear strength lowers in the top layer during the winter months and increases again in the spring. Therefore, the apparent OCRs and apparent cohesions do change during the seasons to. A very specific trend is not visible when comparing the apparent cohesion or OCR with the measured soil suction stresses in the field.

The lowest soil suction stresses in the dike body in Oijen were measured in March, however the lowest apparent cohesions and lowest apparent OCRs are needed in January. A possible explanation for this is that the shear strength obtained from the CPT data decreased between January and February/March.

In the inner berm in Westervoort, soil suction stresses were only measured during spring. For the other periods negative soil suction stresses were measured. The piezometric head was the highest during February/March, which was the same period the apparent cohesions where the lowest. However, the apparent OCRs during February/March were higher than the apparent OCRs in January. This can possibly be caused by the vertical effective stress, since the vertical effective stress does not only influence the undrained shear strength directly, but also indirectly via the OCR (equation ((2-28)).

The results from the model fit with the HS model are extrapolated to the WBN-situation. For this extrapolation the situation with the lowest cohesion was chosen from the model fit. The result shows a big increase in FoS from 1.54 until 1.94 for the apparent cohesions in the dike body and an increase from 1.54 until 2.12 for the apparent cohesions in the berm.

Note to this calculation is that the average apparent cohesions are used, likewise other default parameters. However normally in the assessment of a dike body, the characteristic values are used. The characteristic values are the values with a 5% probability to be lower in the reality. If these values would be used the apparent cohesions probably will be lower and likewise the increase in FoS will be lower. Therefore this evaluation of the FoS increase is only to show that there is an increase in FoS, but nothing can be said about the amount of increase in stability which will happen in reality.

6 Conclusion and recommendations

The main question of this report is: What is the influence of the soil suction on the slope stability of the dike and how can it be modelled? To answer this question six sub questions are formed and answered in this report. Below a short summary of the answers to all the sub questions is given, followed by some recommendations for the waterboard and further research.

6.1 Conclusion

What is the most progressive and conservative hydraulic state of the dike in the initial state (before the start of the WBN event) and during the WBN event in steady state?
The hydraulic state before the WBN event can be calculated with the formula of Dupuit or with the TRWD. Dupuit gives a more realistic height of the phreatic surface where the TRWD gives a more conservative state. During the WBN event there are two ways to determine the hydraulic state of the dike. The more conservative method is with the TRWD while the less conservative method is the method used in the WC. A more elaborate answer is found in Chapter 2.3.
From the sensitivity analysis it is known that the influence of the phreatic surface in a dike body is of great influence on the FoS of the dike body. A lower phreatic surface lead to lower pore water pressures in the dike body, which leads to a higher effective vertical stress, a higher shear strength and probably to a higher FoS. This effect is enhanced since more effective suction stresses can be present, the bigger space between the phreatic surface and the top of the dike (zone 2 + 3 from Figure 1-2). Therefore more research to the location of the phreatic surface in a dike body is recommended (Recommendation 1).
From the field measurements (Chapter 4.2) it is known, suction is present in the dike body during the whole measured period. However, in the top layer no soil suction was measured and therefore it is assumed in the top one meter of a dike body no suction stresses will be present during a high water event. 1.7 meter below the top of the dike body, suction was measured for almost the whole duration of winter. Consequently, it can be assumed that with a phreatic surface lower than 1.7 m below the top of the dike, suction stresses are present in the dike body.

What is the effect of the soil suction on the shear strength of clay and the slope stability of the dike?
From the literature study the influence of the suction stress on the shear strength and therefore the stability of the dike body are explained. In case there is suction in a pore, the vertical effective stress of a soil increases. If the vertical effective stress increases, the shear strength increases (according to equation (2-19)) which results in an increase of dike body stability. Especially in clayey soils the capillary zone, the unsaturated zone above the phreatic surface where suction stresses are present, can be several meter high. A more elaborate answer can be found in Chapter 2.4.
However, the measured shear strengths where significantly higher than expected based on the soil unit weight, friction angles and measured suction in the soils. More research is needed to find a reason for the high measured shear strengths in the soils. A possibility is that these high shear strengths are caused by the higher soil suction stresses in the past. Therefore it is maybe possible that clay has some memory or aging effects. (Recommendation 2).

What is the maximum influence of the soil suction in the dike body on the factor of safety in case of a clay dike in the most positive and negative case?
In the most positive case, the phreatic surface in the dike body is as low as the initial condition, for example according to Dupuit (around 3.3 meter below surface for the modelled dike) and there is suction through the whole dike body above the phreatic surface (static suction, the suction is only influenced from the water table). In the worst case, the phreatic surface is according the TRWD (1.1 meter below surface for the modelled dike). In the worst case, the FoS was 1.28 in the best case 1.64. The difference between these two is mainly caused by the difference in phreatic surface. If only the contribution of the soil suction is taken into account, with a phreatic surface 3.3 meter below surface, the FoS increases from 1.55 to 1.64, which is considered a significant increase.

Remarks for this calculation are that expectation values from the Manual Macro Stability are used instead of the parameters for the soil itself. Beside that a phreatic surface 3.3 meter below surface in case of a WBN event and suction through the whole dike body is not realistic probably. Furthermore, a probability of failure is a better way than the FoS to compare the situation with or without taken suction into account. In that case a probabilistic analysis is needed (Recommendation 3).

Is it worthwhile to perform a time dependent analysis of the initial situation, the development of the phreatic surface and the influence of the factor of safety of slope stability of the dike?
Since the phreatic surface has a big influence on the FoS of the dike, a time dependent analysis with this development is worthwhile. In that case also the generation of pore water pressures and soil suctions are modelled to a more realistic situation, which calculates the time needed to achieve steady state conditions. From this evaluation can be concluded if steady state is reached at all during a WBN event. If not a different, probably lower, phreatic surface can be assumed during a WBN event.
Furthermore, from the measurements in Oijen it is known that the top one meter below surface is influenced by precipitation and evaporation. The tensiometer at a depth of 1.7 m below surface is not influenced by precipitation and evaporation, meaning the weather influences the soil suction in the soil for a depth between the 1.0 and 1.7 m depth. A time dependent analysis, gives a better determination for which depth the weather influences the soil suction in the dike body (Recommendation 1).

How can the stability modelling of the unsaturated zone be improved by using the field data obtained by Westervoort and Oijen.
From the measured soil suction and the VWC the increase of the effective stress from the suction is calculated. From the data it is known that in the dike body from 1.7 meter below surface to 2.4 meter below surface there are generally some soil suction stresses present. However, the measured soil suction during the winter months where low, with values between 0 and 10 kPa. Hence, the contribution to the shear stress during that period is minimal, according to equation (2-19), with a maximum of 6.2 kPa and an effective suction of 10 kPa. The measurements from one meter below surface in the dike body are always below 0 kPa. This means water pressure is present instead of suction, which is assumed to be the result of the precipitation surplus.
The modelling of the unsaturated zone is improved by taking into account the static suction for the part of the dike body above the phreatic surface until 1.5 m below surface (further research recommended, Recommendation 1). This is done by measuring the in-situ suction and the VWC, or by implementing a SWRC from a comparable soil from the Staring Serie or a SWRC obtained from lab tests. Since only one dike body was measured and the results from soil suction and VWC measurements are not yet compared to lab SWRC, more test location are recommended to verify this data (Recommendation 4).

Should the WBI be improved according to the results of this research?
According to the results of this research suction stresses of approximately 0 to 10 kPa are measured in a very wide dike body, without an increased river level, until 1.7 meters below surface and above the phreatic surface. Therefore, it can be assumed that in case of WBN event suctions are present in a dike body, if the phreatic surface in the dike body is lower than 1.7 meter below surface. The influence of the suction will not be very large in most cases, since the measured suctions are low. In most cases the assumed phreatic surface in the dike body is higher than 1.5 meter below surface. However, in some cases the zone from the phreatic surface in WBN event until the top of the dike can be 1.7 m or even larger. For example in storm dominated areas. The duration of the WBN is only a couple of days in a storm dominated area, whereas it is a couple of weeks in discharge dominated areas.
From the results of this research alone the WBI cannot be improved, but it is worthwhile to perform more research for special cases where the zone from the WBN event until the top of the dike is at least 1.5 meter or more and on some dike bodies with a more conventional geometry than the dike body in Oijen (Recommendation 5).

In total the suction contributes to shear strength through the effective vertical stress. Possibly even more, since the measured shear strengths were higher than expected. Other possibilities for the higher shear strengths are memory or aging effects of the clay or influences from other strength effects. The contribution of the suction is modelled by taking the effective suction into account from the phreatic surface in the dike body until 1.7 meter below the top of dike. Less than one meter below the top of the dike the pore water pressure will be influenced by the precipitation and evaporation, which means that after precipitation no suction will be present. It is unsure how deep the precipitation and evaporation influences the soil exactly, but at least until 1 meter below surface and maximum until 1.7 meter below surface.

To model the suction a SWRC obtained from the soil would be the best option. Since the difference in influence of the SWRCs form the Staring Serie was minimal, a SWRC from the Staring Serie or obtained from lab data can also be an option.

6.2 Recommendation for the Water Boards

The WBI has a “comply or explain” approach, which means the assessment of the dike should meet the requirements. If the dike does not meet the requirements, the dike has to be reinforced, or the water board should explain why the dike does not meet the initial requirements, while still being safe enough. For these dikes an “expert test” (In Dutch, toets op maat), can be performed. In this case the influence of the suction can be considered. In some cases, this can help to motivate why a dike does meet the requirements.

As stated in Chapter 6.1 the precipitation and evaporation influence the dike body until a depth of at least one meter below surface. 1.7 meter below surface the influence of the precipitation and evaporation was not visible anymore. Furthermore, the tensiometer 1.7 meter below surface measured soil suction during almost the whole winter. Only on two separate days negative soil suctions where measured. Therefore, it can be expected there are always some (small) soil suctions present in the soil between the phreatic surface and 1.7 meter below surface.

The recommendation for the water boards is to take the suction into account in the following situation. If the dike body does have a phreatic surface deeper than 1.5 meter below surface the suction can be taken into account. According to this study he precipitation and evaporation influence the soil until at least 1 meter below surface, so 1.5 meter below surface is an assumption, for the exact location more research is needed. The suction can only considered to be present in the zone between the phreatic level and 1.5 meter below surface (Figure 6-1). To do this, a SWRC is needed from the soil or a comparable soil. The SWRC can be obtained from soil suction and VWC measurements in the soil, from a SWRC from lab tests, or from the Staring Serie. The SWRC can be entered in Plaxis or another modelling program which is used. It is advised to use static suction, since only the upper 1.5 meter of the dike is assumed to be influenced by the precipitation and evaporation. The upper 1.5 meter of dike should be modelled to be dry, as is done in the current assessment.

To determine the location of the phreatic surface in a dike body during a WBN-event a groundwater flow analysis in Plaxis (PlaxFlow) can be performed. Since the TRWD and the WC give both a conservative prediction of the phreatic surface, a PlaxFlow analysis will probably give a more realistic location of the phreatic surface. This phreatic surface is expected to be lower than the phreatic surface obtained with the TRWD or the WC, which lead to a bigger unsaturated zone were soil suction stresses can be present.

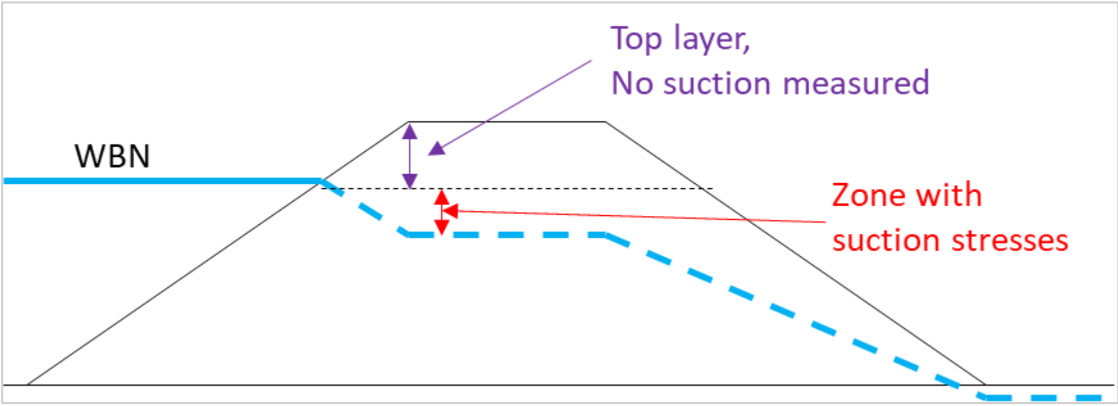

Figure 6-1: The dike body with phreatic level in a WBN event. If the phreatic surface is more than 1.5 m below surface, the suction can be taken into account for the part of the dike body which is above the phreatic surface, but below the 1.5 m from surface.

6.3 Recommendation for further research

Recommendations for further research can be found below.

1. Since the phreatic surface within the dike body during a WBN event is of great influence on the FoS of the dike, it is important to know how far the phreatic surface of a dike body is increasing during a WBN event. The lower the phreatic surface in the dike, the higher the FoS. Besides that, the amount of suction in a dike body is dependent on the height of phreatic surface.
   In the upper one meter the pore water pressure is highly influenced by the precipitation and evaporation. The suction in that region is not constantly there. 1.7 meter below surface this influence was not visible anymore. With further research a better idea of the zone which is influenced by the weather can be found.
   The lower the phreatic surface, the bigger the region where suctions can be present. Now steady state groundwater conditions are assumed during a WBN event for the rivers in eastern Netherlands, but the groundwater flow is not steady state during a WBN event. More knowledge about the development of phreatic surface and the pore pressure during an increasing river level will improve the understanding of the generation of pore water pressures and to the influence of the soil suction on the FoS. Therefore, research to the development of the phreatic surface and the pore pressure within a dike body during a WBN event should be performed. This can be a combination of field research and a time dependent analysis in a modelling program.

2. It is recommended to research which parameters are influenced by the suction. In the literature only the effective stress is found as an influenced parameter, but since the calculated shear strengths from the CPT data where higher than expected other parameters may be influenced too, for example the cohesion or OCR. Especially the influence of high suctions during the summer on the shear strength of soil during period without suction should be researched, since this can be the cause of the high measured shear strengths in the berm in Westervoort and the crest in Oijen.

3. It is recommended to perform a probabilistic analysis on one whole dike body. This since the results of the assessments are normally given as a Probability of Failure, which is easier to compare than the FoS.

4. It is recommended to compare the SWRCs obtained from the sensor data to the SWRCs obtained in the lab. Also, compare in-situ measured soil suction and VWC to the obtained SWRC in the lab. This since the behavior of soil in the field can be different than in the lab. This is done to create more insight in the behavior of suction in soils in a dike body.

5. Recommended is to measure more dikes, to make sure the suction is also there in different types of dikes. In this case it is recommended to at least place sensors in the inner toe, crest and outer to of the dike. If this is compared with enough soil test the probabilistic analysis from recommendation 3 can be performed on the same dike body.
   Also, the dike body in Oijen is quite wide, which can lead to lower suction stresses, since less water from precipitation will run off and more water will infiltrate in the dike body. Therefore, a more conventional dike body should be chosen as the next test location.

7 References

Arends, M. (2018). *Consequentieanalyse initieel niet verzadigde zone.* Zwolle: Arcadis.

de Bakker, H., & Schelling, J. (1989). *Systeem van bodemclassificatie voor Nederland, De hogere niveaus.* Wageningen: Winand Staring Centre.

Deltares. (2017, 09 29). Software voor de beoordeling van primaire waterkeringen. *BM - Macrostabiliteit*. Delft, Zuid-Holland, Nederland: Deltares.

Deltares. (2019, November). D-stability. *Slope stability software for soft soil engineering - user manual, D-stability 20.1*.

den Haan, E., H.M., v. e., Visschedijk, M., & J., M. (2013, 12 01). Isotachenmodellen: Help, hoe kom ik aan de parameters. *Geotechniek*, 62-69.

Fredlund, D., Rahardjo, H., & Fredlund, M. D. (2012). *Unsaturated Soil mechanics in Engineering Practice.* Hoboken, New Jersey: John Wiley & Sons.

Heidemij - adviesbureau. (1986, juli). *Polderdistrict Rijn en IJssel.* Heidemij Adviesbureau (internal report).

Kumar, S., & Malik, R. S. (1990). Verification of quick capillary rise approach for determining pore geometrical characteristics in soils of varying texture. *Soil Science*, 883-888.

Li, Y., Zhang, C., Chen, C., & Chen, H. (2018). Calculation of Capillary Rise Height of Soils by SWCC Model. *Advances in Civil Engineering*, 2-12.

Lim, T., Rahardjo, H., CHang, M., & Fredlund, D. (1996). Effect on rainfall on matric suctions in residual soil slope. *Canadian Geotechnical Journal, volume 33*, 618-628.

Lu, N., & Likos, W. J. (2004). *Unsaturated soil mechanics.* Wiley.

Meij, R. v., Bruijn, H. d., Blinde, J., Schweckendiek, T., & Zwan, I. v. (2011, 03 11). Schematisering waterspanningen in WTI 2017 (Ringtoets). Delft, Zuid-Holland, Nederland.

Ministerie van Infrastructuur en Milieu. (2019). Schematiseringshandleiding macrostabiliteit.

Normcommissie 351006 'Geotechniek'. (2019, Juli). NEN-EN 1997-1+C1+A1/NB. *Eurocode 7*. Delft, Zuid Holland, Nederland: Koninklijk Nederlands Normalisatie-instituut.

Peck, R. B., Hanson, W. E., & Thornburn, T. H. (1994). *Foundation Engineering.* Wiley.

Plaxis. (2019, October 11). Workshop Modelling Groundwater in Plaxis. Delft: Plaxis B.V.

Plaxis. (2020, June 01). Material Model Manual CONNECT Edition V20.03. Delft: Plaxis B.V.

Plaxis. (2020, June 02). Plaxis 2D-Reference Manual CONNECT Edition v20.03. Delft: Plaxis B.V.

Rivieren Nederland. (2020, 07 29). *Grote rivieren Nederlad*. Retrieved from Rivieren Nederland: http://www.rivierennederland.nl/grote-rivieren-nederland/

Rowe, K. R. (2011). *Geotechnical Engineering Handbook.* New York: Springer Science.

Rozing, A. (2012, mei 9). Richtlijn/ aanbeveling stationair en niet-stationair rekenen (grondwaterstroming) bij Dijkversterking volgens HWBP. Nederland: Deltares.

Schweckendief, T., Krogt, M. v., Rijneveld, B., & Teixeira, A. M. (2017, Oktober 3). Handreiking Faalkansanalyse Macrostabiliteit. Delft, Zuid-Holland: Deltares.

TAW. (1995). *Druk op de Dijken, De toestand van de rivierdijken tijdens het hoogwater van januari-februari 1995.* Delft: Technische Adviescommissie voor de Waterkeringen.

TAW. (2001). *Technisch Rapport Waterkerende Grondconstructies.* Technische Adviescommissie voor de Waterkeringen.

TAW. (2004). *Technisch Rapport Waterspanningen bij Dijken.* Delft: Technische Adviescommissie voor de Waterkeringen.

van Duinen, A. (2020). *Shear Strength of Initially Unsaturated Soil.* Delft: Deltares (internal report).

van Duinen, A., van Hoven, A., Visschedijk, M., & Wichman, B. (2018). *Shear Strength of Initially Unsaturated Soil.* Delft: Deltares (internal report).

van Genuchten, M. (1980). A closed-form equation for predicting the hydraulic conductivity of unsaturated soils. *Journal of Soil Science Society of America*(44), 892-898.

van Heerebeek, F. (2017). *Grondonderzoek voor de 4e toetsronde - Resultaten geotechnisch onderzoek.* Inpijn-Blokpoel Ingenieursbureau. Son en Breugel: Inpijn-Blokpoel Ingenieursbureau.

Visschedijk, M., Vork, J., & Zwanenburg, C. (2020, maart). POVM Eindige elementmethode. Tiel: POV Macrostabiliteit.

Wösten, J., Veerman, G., de groot, W., & Stolte, J. (2001). *Waterretentie- en doorlatendheidskarakteristieken van boven-en ondergronden in Nederland: de Staringreeks.* Wageningen: Alterra.

Zwanenburg, C. (2017, december). Bijlage C Modellering Dijksmateriaal. *POVM Rekentechnieken - Basisrapport Eindige-elementenmethode (onderdeel 6.2.6A)*.

Appendix I. Figures Safety Factors

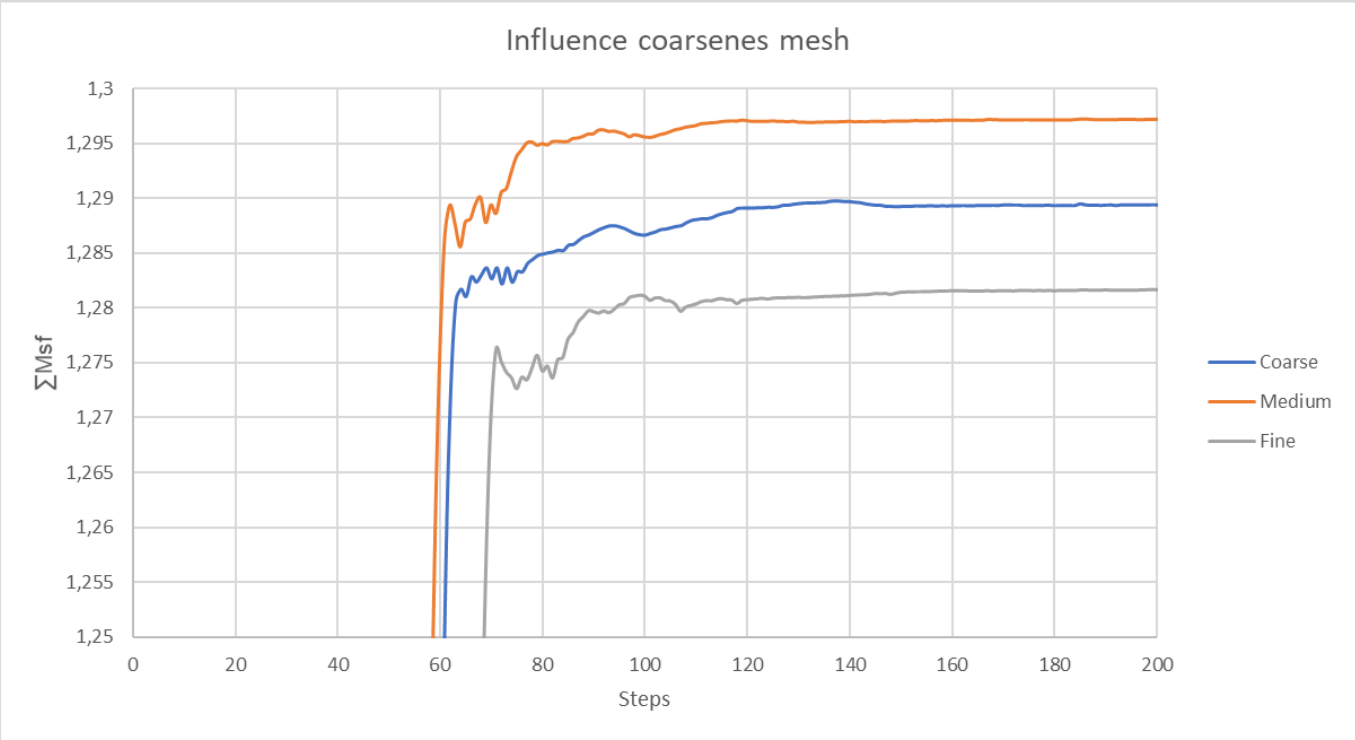

Figure I-1: Influence of the mesh on the safety factor. The tested model has a phreatic surface according to the TRWD, suction is not taken into account, the Mohr-Coulomb soil model is used and the tolerated error was set at 1%.

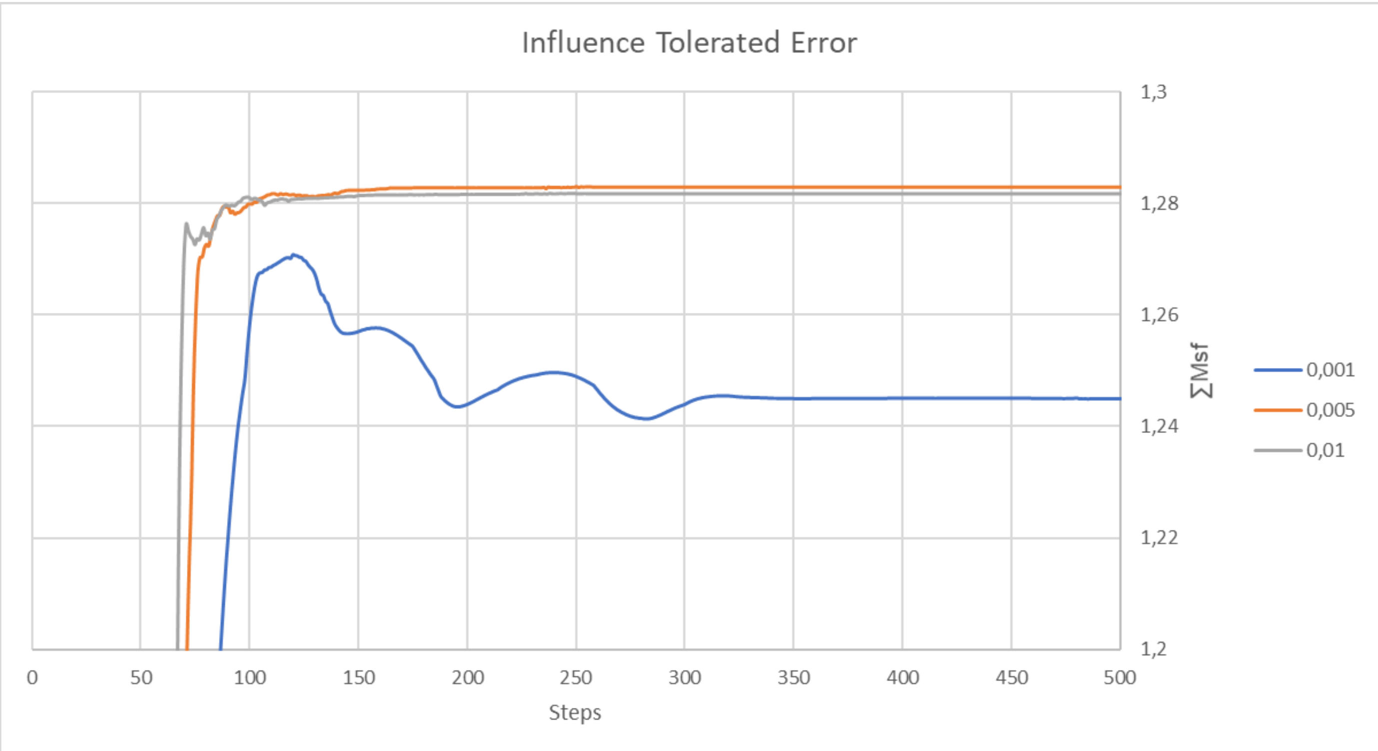

Figure I-2: Influence of the tolerated error on the safety factor. The tested model has a phreatic surface according to the TRWD, suction is not taken into account and the Mohr-Coulomb soil model with a fine meshing is used.

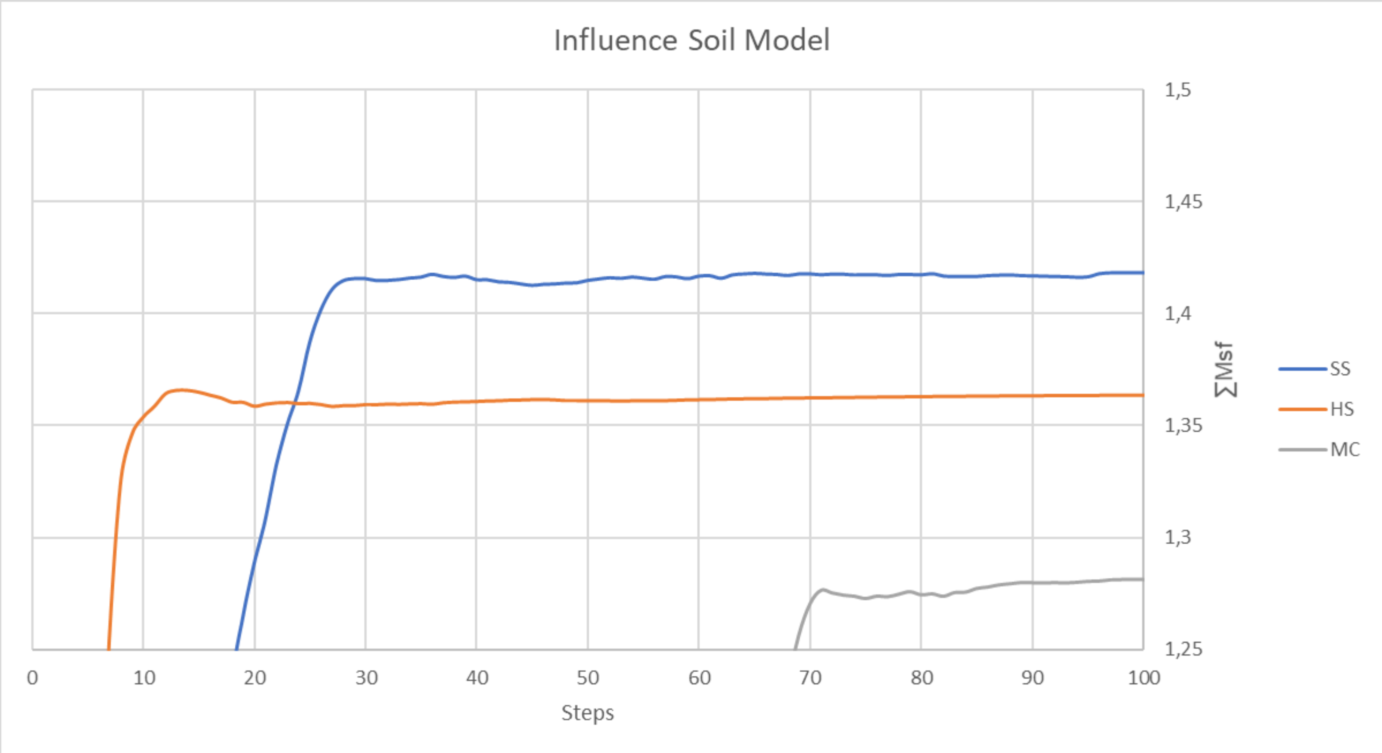

Figure I-3: Influence of the soil model on the safety factor. The tested model has an tolerated error of 0.01, suction is not taken into account, the phreatic surface according to the TRWD was used and the mesh is fine.

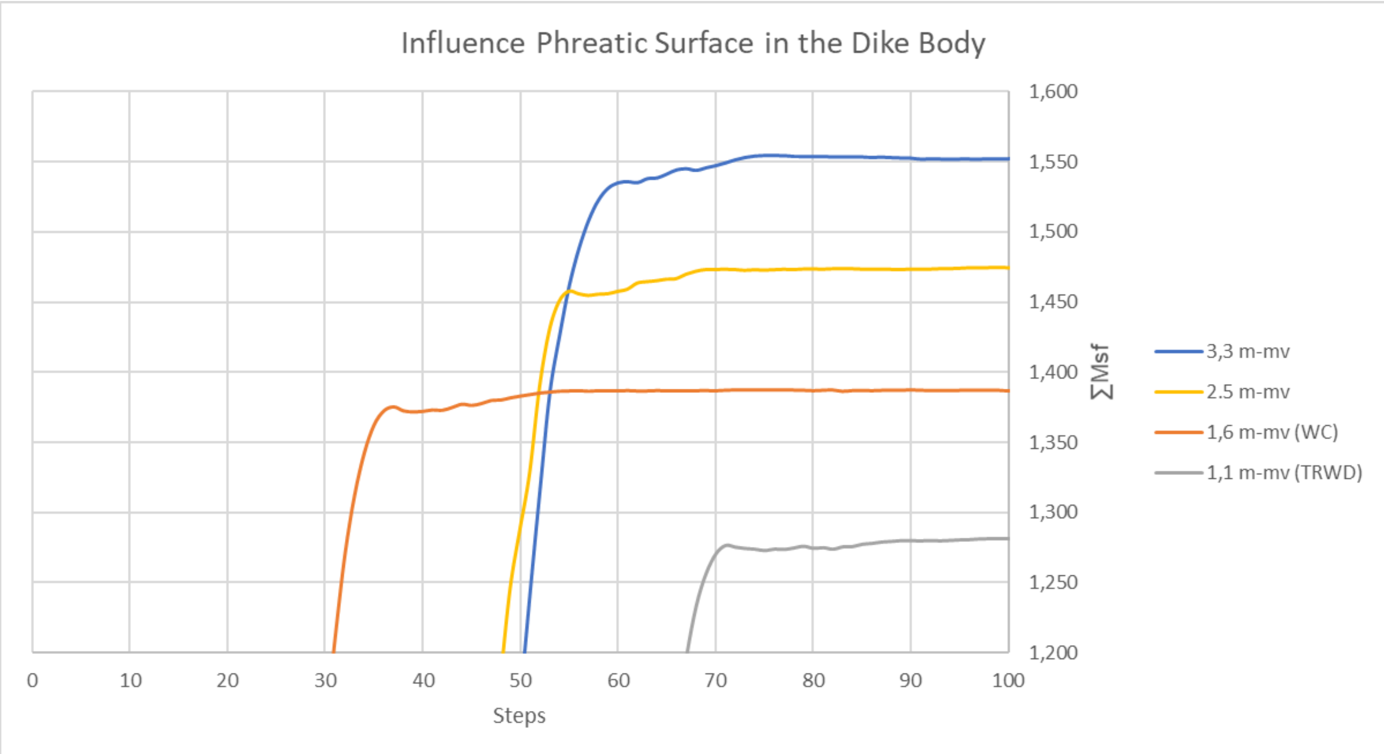

Figure I-4: Influence of the phreatic surface of the dike body on the safety factor. The tested model has an tolerated error of 0.01, suction is not taken into account and the Mohr-Coulomb soil model with a fine meshing is used.

Appendix II. Slip Surfaces

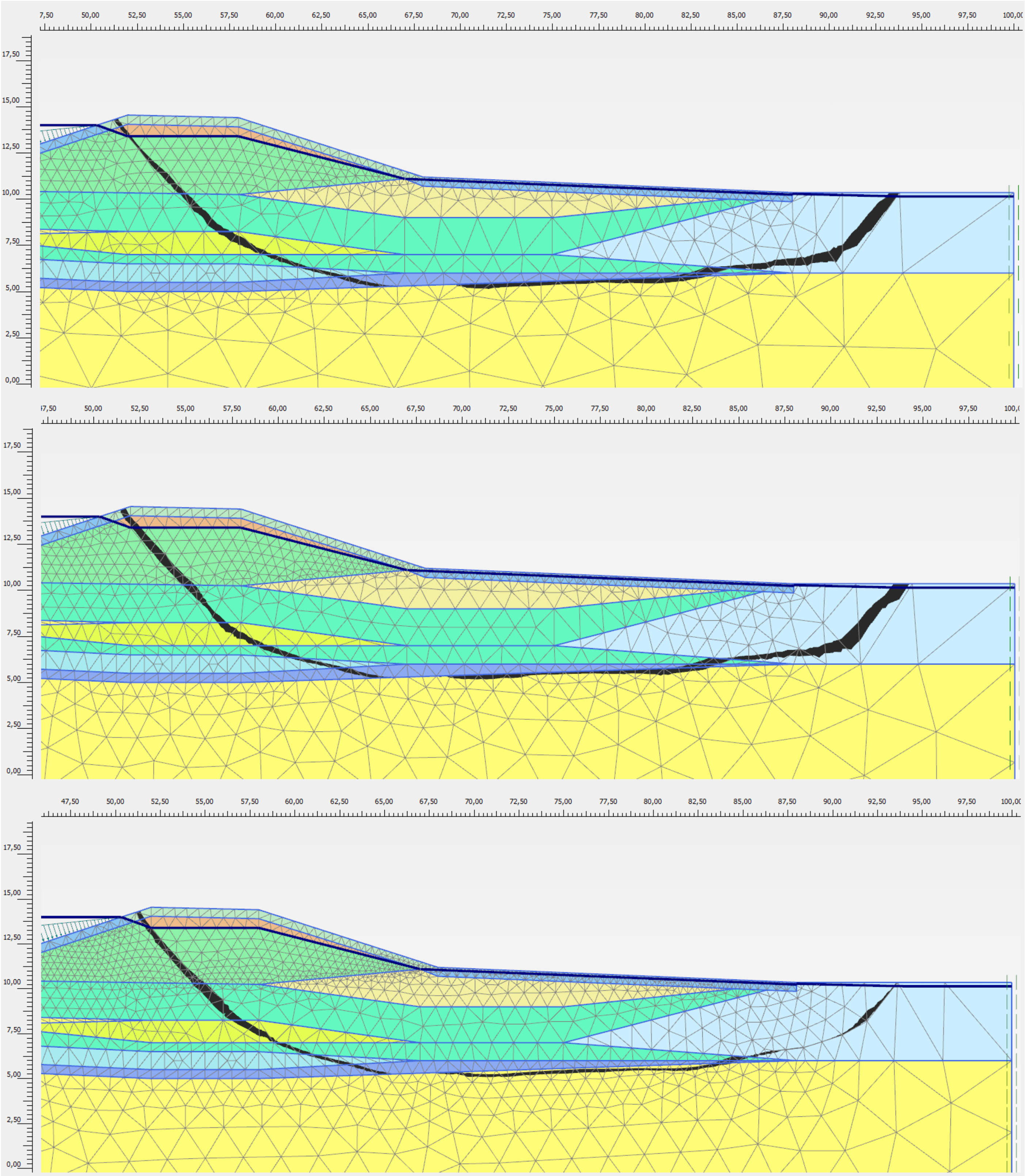

Figure II-1: Failure surfaces from a calculation with different meshes in Plaxis. A coarse mesh is used for the upper graph, a medium mesh for the middle graph and a finer mesh for the lower graph.

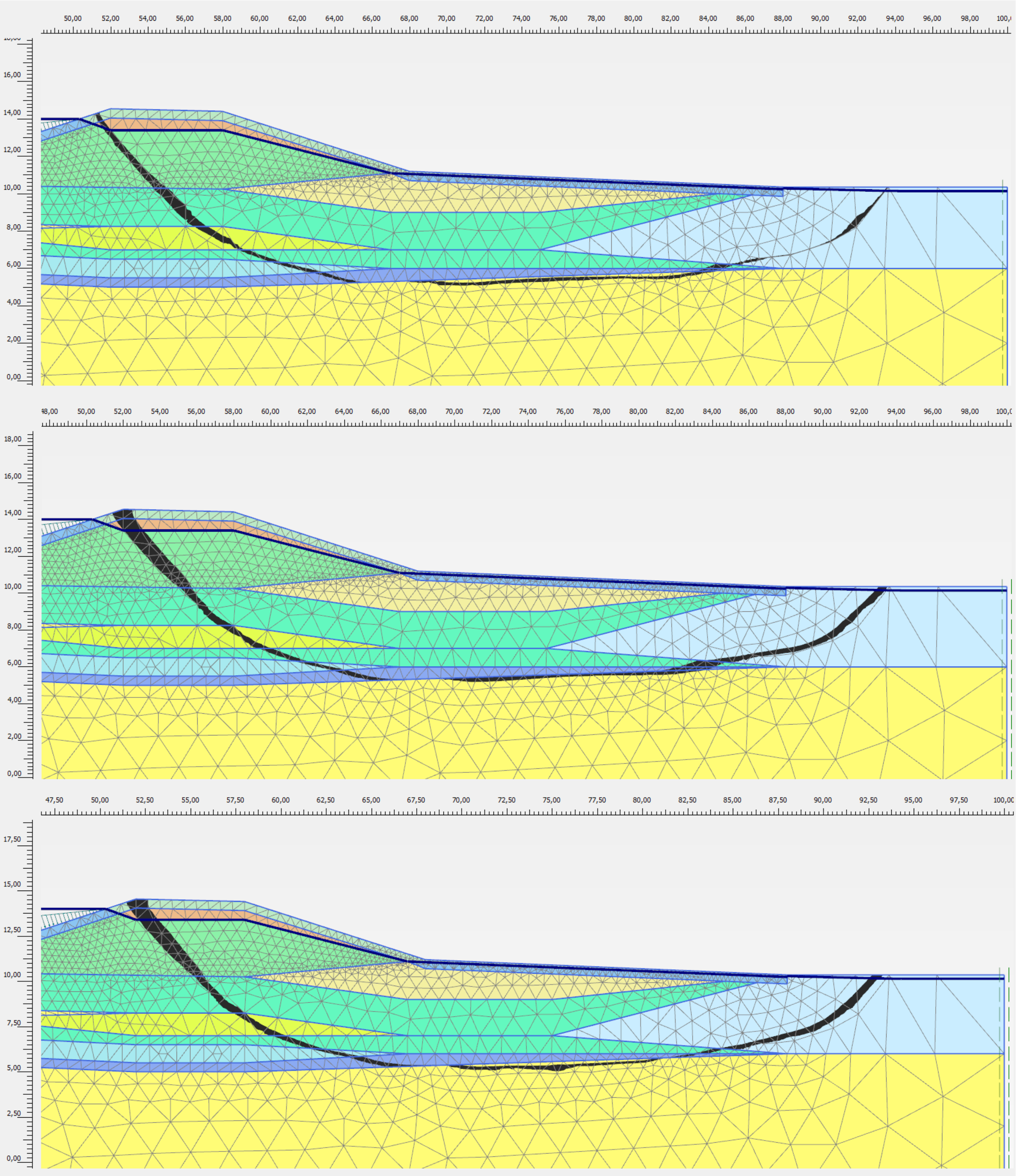

Figure II-2: Failure surfaces from a calculation with tolerated errors in Plaxis. A tolerated error of 0.01 is used for the upper graph, a tolerated error of 0.005 for the middle graph and a tolerated error of 0.001 for the lower graph.

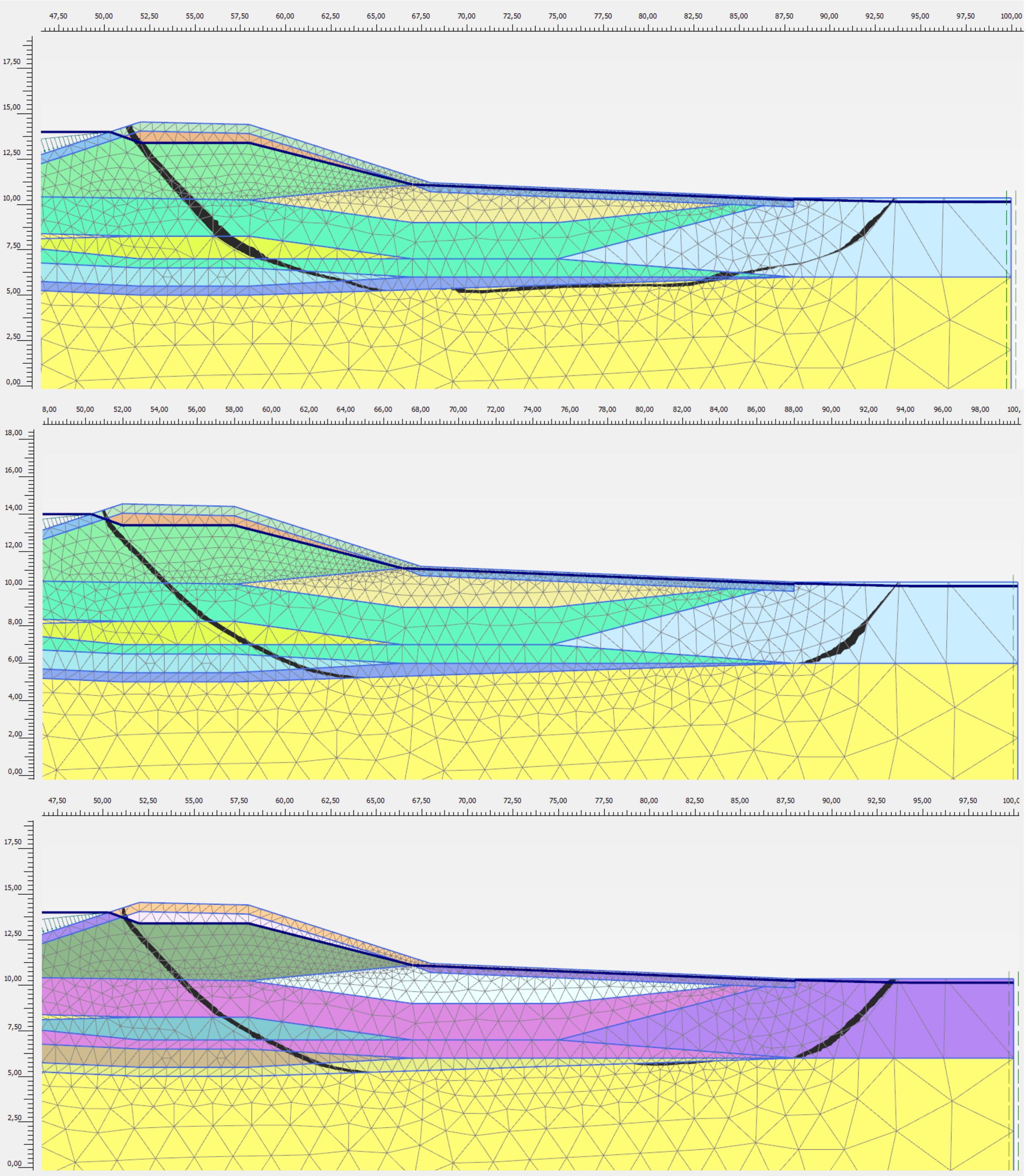

Figure II-3: Failure surfaces from a calculation with different soil models in Plaxis. The Mohr-Coulomb soil model is used for the upper graph, the Hardening Soil model for the middle graph and the Soft Soil with the Hardening Soil model for the lower graph.

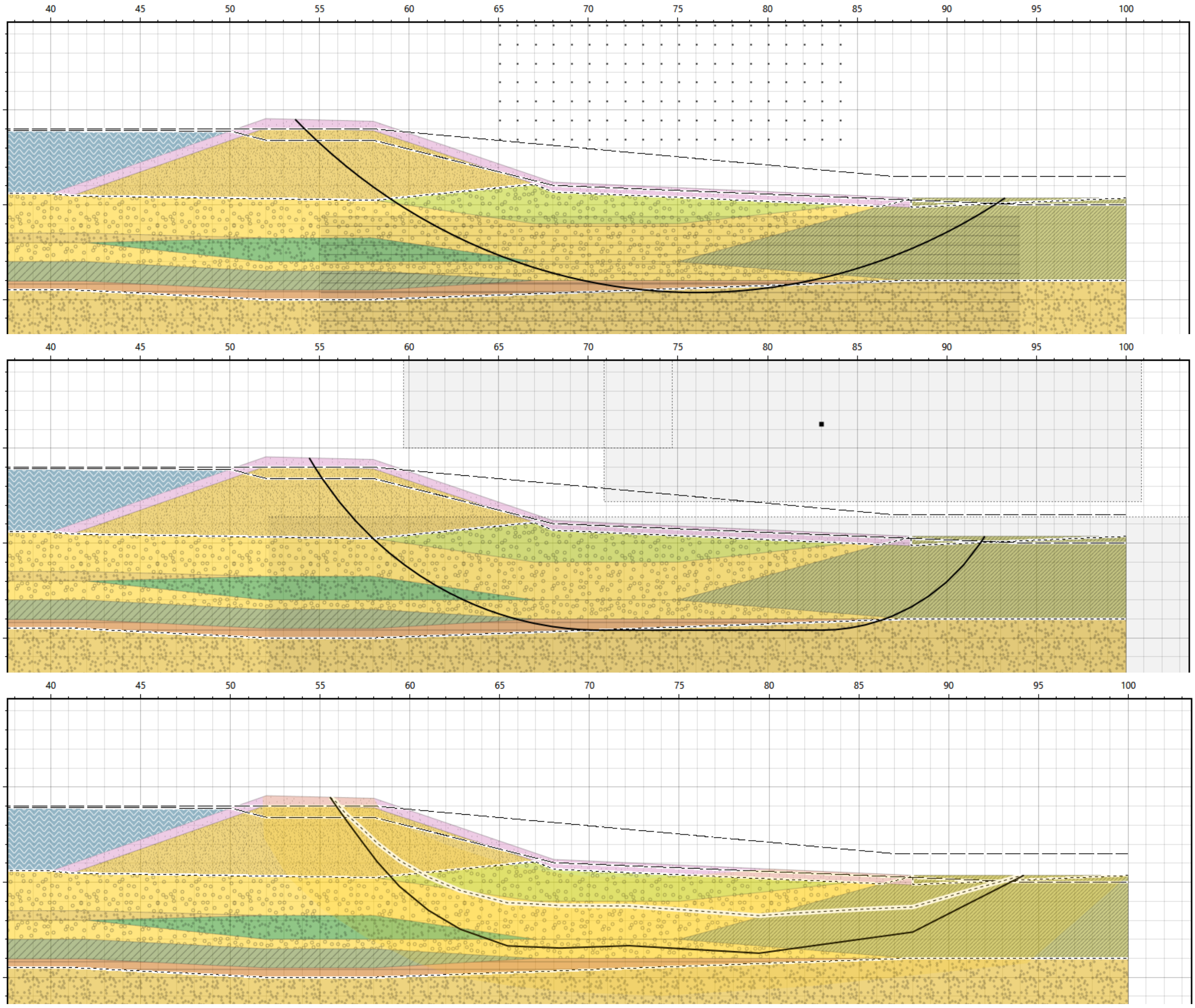

Figure II-4: Failure surfaces from a calculation with D-stability. The Bishop method is used for the upper graph, the Uplift Van for the middle graph and the Spencer for the lower graph..

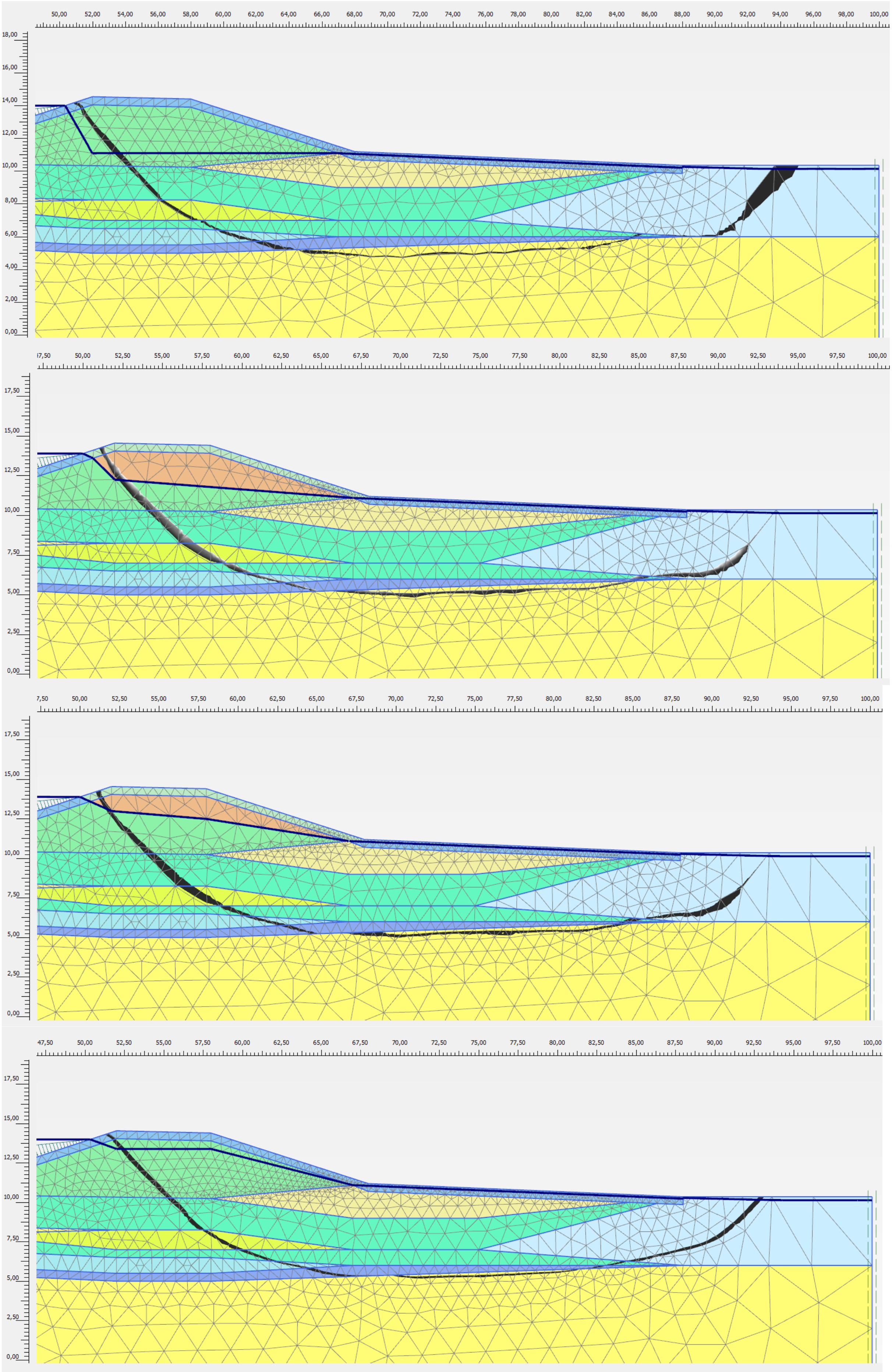

Figure II-5: Failure surfaces from a calculation with different phreatic surfaces in Plaxis. A phreatic surface 3.3 m below surface is used for the upper graph, 2.5 m below surface for the second graph, 1.6 m below surface for the third graph and 1.1 m below surface for the bottom graph.

Appendix III. Soil Test Results

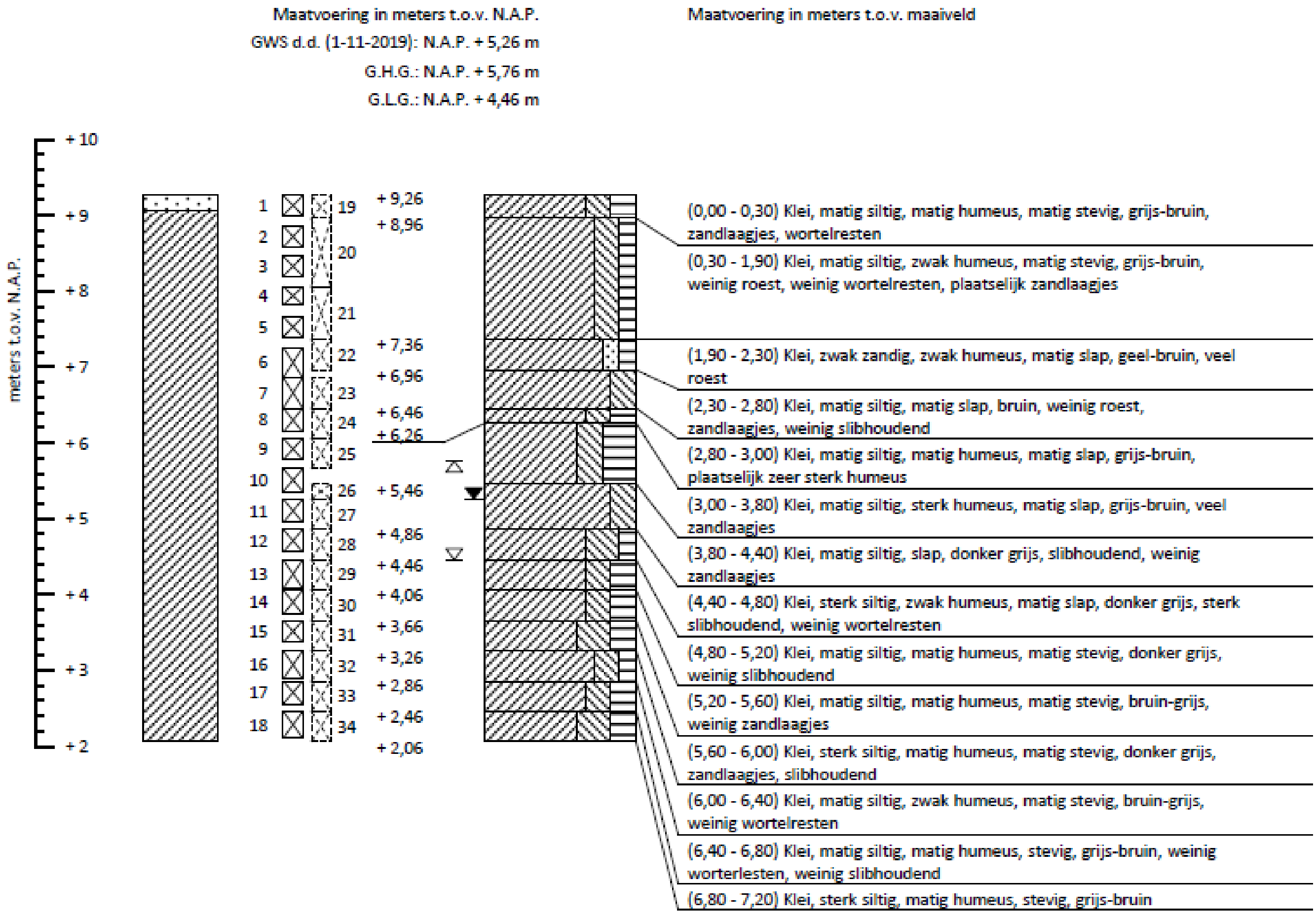

Boorstaat o.b.v. grondidentificatie in het veld (NEN 5104)

Boring conform NEN-EN-ISO 22475-1

Meetlocaties Maasdijk te Oijen	RD coördinatensysteem	Oijen	
Deltares	X = 161 715,20	Pulsboring (mechanisch)	
Wiertsema & Partners RAADGEVEND INGENIEURS	Y = 425 395,65	Boormeester: Liekel Mellema	
	Uitgevoerd: 31-10-2019 t/m 1-11-2019	Opdrachtnr.: 74499	AKKOORD UITV
	Blad 1 van 1	Boornummer: B002	

Figure III-1: Borehole diagram from the Crest in Oijen

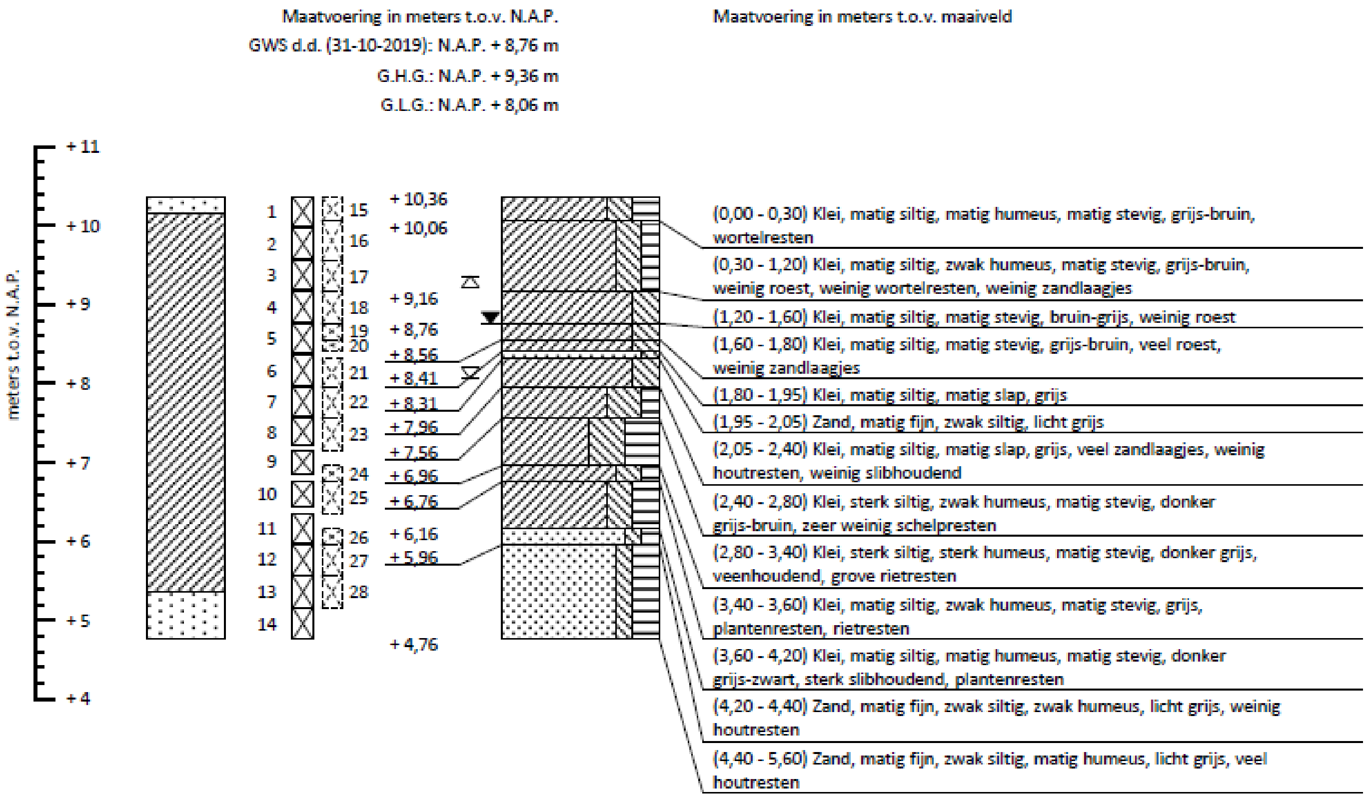

Boorstaat o.b.v. grondidentificatie in het veld (NEN 5104) — Boring conform NEN-EN-ISO 22475-1

Meetlocaties IJsseldijk te Westervoort	RD coördinatensysteem	Westervoort	
Deltares	X = 194 453,07	Pulsboring (mechanisch)	
Wiertsema & Partners RAADGEVEND INGENIEURS	Y = 442 126,92	Boormeester: Liekel Mellema	
	Uitgevoerd: 31-10-2019	Opdrachtnr.: 74499	AKKOORD UITV
	Blad 1 van 1	Boornummer: B201	

Figure III-2: Borehole diagram from the inner berm in Westervoort

Boring	Monster nummer	Monsterdiepte (m - mv)	Niveau monster t.o.v. N.A.P.	Vol. gewicht 100% verz. (indicatief)	Nat volumegewicht	Droog volumegewicht	Watergehalte in gewichts %	Gehanteerde soortelijke massa ***	Poriën getal	Poriën volume	Watergehalte	Verzadigingsgraad
				γ_{sat}	γ_n	γ_{dr}	W_g	r	e	n	W_v	S_r
		[m]	[m]	[kN/m³]	[kN/m³]	[kN/m³]	[%]	[kg/m³]	[-]	[%]	[%]	[%]
B 201	2_a	0,45	9,91	19,7	19,1	16,0	19,0	2629,8**	0,61	37,94	31,08	81,91
B 201	3_a	0,85	9,51	19,2	18,2	15,0	21,3	2646**	0,73	42,04	32,64	77,64
B 201	4_a	1,25	9,11	19,2	18,6	15,1	23,5	2645,7**	0,72	41,88	36,20	86,43
B 201	5_a	1,65	8,71	18,8	18,4	14,3	28,4	2659,4**	0,82	45,06	41,52	92,15
B 201	5_b	1,90	8,46	18,3	18,3	13,8	32,5	2602 *	0,85	45,80	45,80	99,99
B 201	6_a	2,05	8,31	17,9	17,8	13,1	35,7	2635,4**	0,97	49,29	47,68	96,73
B 201	7_a	2,45	7,91	16,9	16,8	11,5	46,9	2598,2**	1,22	55,00	54,80	99,64
B 201	8_a	2,90	7,46	14,6	14,6	8,0	81,3	2513,9**	2,07	67,41	66,56	98,73
B 201	8_b	3,05	7,31	13,4	13,2	6,2	112,1	2331 *	2,67	72,73	71,28	98,01
B 201	9_a	3,30	7,06	14,3	14,2	7,6	87,5	2427,4**	2,14	68,13	67,72	99,40
B 201	10_a	3,70	6,66	12,2	11,8	4,5	164,8	2142,6**	3,71	78,77	74,96	95,16
B 201	10_b	3,85	6,51	13,2	13,0	5,9	119,4	2301 *	2,80	73,70	72,28	98,07
B 201	11_a	4,02	6,34	12,9	12,8	5,7	126,1	2179,4**	2,77	73,50	72,84	99,11
B 201	11_b	4,25	6,11	18,5	17,9	14,2	26,6	2605 *	0,80	44,54	38,44	86,30

Figure III-3: CLA of the berm in Westervoort

Boornummer	Monster	Referentie niveau: NAP	Beschrijving volgens NEN 5104	Gebruikte zeven [mm] met cumulatieve gewichtspercentages d>																		Zandfractie			
				4	2	1,4	1	0,71	0,500	0,355	0,250	0,180	0,125	0,09	0,063	0,045	0,038	0,020	0,016	0,002	0,000	Mz [mm]	fijnheids getal Fm [-]	D_{60} / D_{10} [-]	D_{15} [mm]
B201	M002	+9,96 tot +9,86 m.	Ks4g1	0,8	0,9	1,0	1,3	1,6	2,3	3,4	5,4	8,6	15,1	22,9	33,2	37,1	40,3	56,1	60,7	79,2	100,0	0,115	0,258	1,907	0,075
B201	M003	+9,56 tot +9,46 m.	Ks4	-		0,1	0,2	0,4	0,8	1,2	2,3	3,7	8,2	14,6	24,5	28,9	32,7	51,0	56,6	77,7	100,0	0,102	0,115	1,675	0,072
B201	M004	+9,16 tot +9,06 m.	Ks3	-			0,2	0,3	0,5	0,8	1,8	2,9	4,2	5,8	9,7	12,1	14,4	31,4	38,1	70,1	100,0	0,109	0,067	1,974	0,072
B201	M005	+8,76 tot +8,66 m.	Ks3	-		0,4	1,0	1,4	2,0	2,7	3,6	4,9	7,4	10,3	15,3	17,6	19,6	32,2	36,9	67,2	100,0	0,122	0,140	2,157	0,074
B201	M006	+8,36 tot +8,26 m.	Ks4	-		0,1	0,2	0,5	1,0	3,0	9,7	18,4	25,4	30,1	35,5	37,5	39,3	50,1	53,6	76,2	100,0	0,184	0,363	2,648	0,089
B201	M007	+7,96 tot +7,86 m.	Ks3	-			0,1	0,3	0,9	2,8	6,9	10,5	12,9	14,5	17,1	18,4	19,6	30,0	35,2	69,0	100,0	0,215	0,208	3,130	0,091
B201	M008	+7,56 tot +7,46 m.	Ks1	-		0,2	0,4	0,7	1,5	2,6	4,4	5,9	6,7	7,3	8,0	8,5	8,9	13,9	16,9	48,0	100,0	0,269	0,130	3,232	0,119
B201	M009	+7,16 tot +7,06 m.	Ks1	-					0,3	0,6	1,3	1,9	2,4	2,8	3,2	3,5	3,7	5,8	7,1	38,1	100,0	0,214	0,040	3,073	0,096
B201	M010	+6,76 tot +6,66 m.	Ks1, plantenresten	-		0,3	1,3	2,2	3,5	4,9	6,7	8,4	9,7	10,7	11,6	11,7	12,3	14,0	15,0	36,5	100,0	0,297	0,212	3,845	0,117
B201	M011	+6,36 tot +6,31 m.	Ks1, plantenresten	-		0,3	1,0	1,9	3,2	6,0	12,2	17,4	19,9	21,0	22,1	22,6	22,9	25,4	26,5	40,1	100,0	0,267	0,363	2,413	0,147

Figure III-4: Grain size distribution in the berm in Westervoort

Boring	Monster nummer	Monsterdiepte (m - mv)	Niveau monster t.o.v. N.A.P.	Vol. gewicht 100% verz. (indicatief)	Nat volumegewicht	Droog volumegewicht	Watergehalte in gewichts %	Gehanteerde soortelijke massa ***	Poriën getal	Poriën volume	Watergehalte	Verzadigingsgraad
				γ_{sat}	γ_n	γ_{dr}	W_g	r	e	n	W_v	S_r
		[m]	[m]	[kN/m³]	[kN/m³]	[kN/m³]	[%]	[kg/m³]	[-]	[%]	[%]	[%]
B 001	2_a	0,60	8,63	18,8	15,9	14,6	8,8	2616,1**	0,76	43,09	13,04	30,26
B 001	3_a	0,90	8,33	19,2	17,6	15,1	16,1	2621**	0,70	41,18	24,84	60,32
B 001	5_a	1,75	7,48	19,0	18,5	15,0	23,8	2599,5**	0,70	41,28	36,36	88,08
B 001	6_a	2,10	7,13	18,7	18,3	14,4	27,1	2605,9**	0,78	43,68	39,76	91,02
B 001	7_a	2,50	6,73	18,4	17,7	13,8	28,3	2628,9**	0,87	46,47	39,80	85,64
B 001	8_a	2,95	6,28	18,6	18,3	14,2	28,7	2620,5**	0,81	44,61	41,60	93,26
B 001	10_a	3,75	5,48	18,8	18,6	14,5	27,8	2628,5**	0,77	43,62	41,20	94,46
B 001	11_a	4,10	5,13	17,6	17,1	12,6	36,0	2622,1**	1,04	51,00	46,28	90,74
B 001	12_a	4,50	4,73	19,6	19,3	15,7	22,6	2649,5**	0,65	39,41	36,28	92,05
B 001	13_a	4,85	4,38	18,4	18,1	13,9	30,6	2640,9**	0,87	46,47	43,24	93,04
B 001	13_b	4,95	4,28	19,2	18,7	15,2	23,3	2607 *	0,69	40,67	36,08	88,72
B 001	14_a	5,25	3,98	19,2	19,0	15,2	24,8	2605 *	0,68	40,43	38,48	95,18
B 001	14_b	5,45	3,78	19,1	18,7	14,9	25,2	2664,6**	0,75	42,94	38,28	89,15
B 001	16_a	6,15	3,08	18,5	18,3	14,0	30,4	2624,1**	0,84	45,57	43,40	95,25
B 001	17_a	6,65	2,58	17,0	16,2	11,7	38,4	2622,2**	1,20	54,53	45,80	84,00
B 001	18_a	6,90	2,33	18,7	18,4	14,3	29,1	2634,7**	0,81	44,75	42,36	94,65

Figure III-5: CLA from the crest in Oijen

Boornummer	Monster	Referentie niveau: NAP	Beschrijving volgens NEN 5104	Gebruikte zeven [mm] met cumulatieve gewichtspercentages d>																Zandfractie			
				1,4	1	0,71	0,500	0,355	0,250	0,180	0,125	0,09	0,063	0,045	0,038	0,020	0,016	0,002	0,000	Mz [mm]	fijnheids getal Fm [-]	D_{60} / D_{10} [-]	D_{15} [mm]
B001	M002-a	+8,83 tot +8,47 m.	Ks3	0,1	0,1	0,3	0,6	1,0	1,6	3,8	12,6	18,6	22,5	23,9	25,4	37,4	42,1	65,3	100,0	0,132	0,149	1,872	0,086
B001	M003-a	+8,43 tot +8,16 m.	Ks2			0,2	0,2	0,5	1,0	1,7	5,8	10,6	14,3	15,8	17,6	30,9	36,0	61,8	100,0	0,114	0,070	1,742	0,077
B001	M005-a	+7,63 tot +7,37 m.	Ks2		0,0	0,0	0,1	0,1	0,4	0,9	2,3	3,6	5,2	6,3	7,6	21,9	28,2	58,5	100,0	0,115	0,028	1,862	0,075
B001	M006-a	+7,23 tot +6,90 m.	Ks2			0,1	0,1	0,4	1,1	2,4	4,4	6,2	8,1	9,6	11,3	26,6	32,8	61,6	100,0	0,132	0,056	2,098	0,078
B001	M007-a	+6,83 tot +6,68 m.	Ks3	0,2	0,3	0,6	1,1	2,5	6,9	10,9	13,4	14,6	16,9	19,1	21,3	35,6	40,8	65,3	100,0	0,220	0,217	3,087	0,096
B001	M008-a	+6,43 tot +6,16 m.	Ks3	0,2	0,4	0,7	1,1	1,5	2,3	4,3	9,1	12,7	15,9	17,6	20,0	35,3	40,7	66,3	100,0	0,137	0,129	2,046	0,083
B001	M010-a	+5,63 tot +5,31 m.	Ks2		0,3	0,6	0,9	1,3	1,9	3,3	5,3	7,2	9,8	11,6	13,8	29,7	35,8	64,0	100,0	0,135	0,084	2,235	0,077
B001	M011-a	+5,23 tot +4,97 m.	Ks3		0,3	0,7	1,1	1,7	2,4	3,4	5,1	6,9	9,9	11,4	13,8	32,5	39,1	66,2	100,0	0,128	0,089	2,240	0,075
B001	M012-a	+4,83 tot +4,49 m.	Ks4				0,2	0,4	2,1	11,5	26,4	33,5	38,4	41,3	43,9	57,7	61,8	77,5	100,0	0,149	0,287	1,968	0,093
B001	M013-a	+4,43 tot +4,34 m.	Ks3			0,3	0,7	1,9	6,7	20,5	31,8	34,6	36,0	36,9	38,1	45,9	49,0	70,0	100,0	0,191	0,392	1,786	0,130
B001	M014-a	+4,03 tot +3,88 m.	Kz3		0,1	0,5	1,7	4,0	14,8	46,4	69,4	73,6	75,3	76,5	77,3	81,8	83,2	89,7	100,0	0,197	0,860	1,662	0,136
B001	M014-b	+3,88 tot +3,70 m.	Ks4			0,1	0,5	1,7	6,2	14,9	27,4	34,4	39,6	43,3	46,0	59,7	63,9	78,8	100,0	0,156	0,341	2,120	0,093
B001	M016-a	+3,23 tot +2,92 m.	Ks2		0,1	0,3	0,5	0,7	1,1	1,4	2,2	2,8	3,7	4,7	6,1	18,9	24,7	58,4	100,0	0,145	0,039	2,391	0,078
B001	M017-a	+2,83 tot +2,48 m.	Ks2		0,2	0,5	0,6	0,9	1,6	4,3	9,0	11,5	13,8	15,3	16,8	29,8	35,2	64,3	100,0	0,147	0,114	2,102	0,087
B001	M018-a	+2,43 tot +2,23 m.	Ks2					0,2	0,3	0,5	1,0	1,3	1,6	2,1	2,9	12,3	17,8	55,4	100,0	0,145	0,013	2,202	0,081

Figure III-6: Grain Size distribution from the crest in Oijen

Appendix IV. Influence Weather on the Suction and Piezometric Head

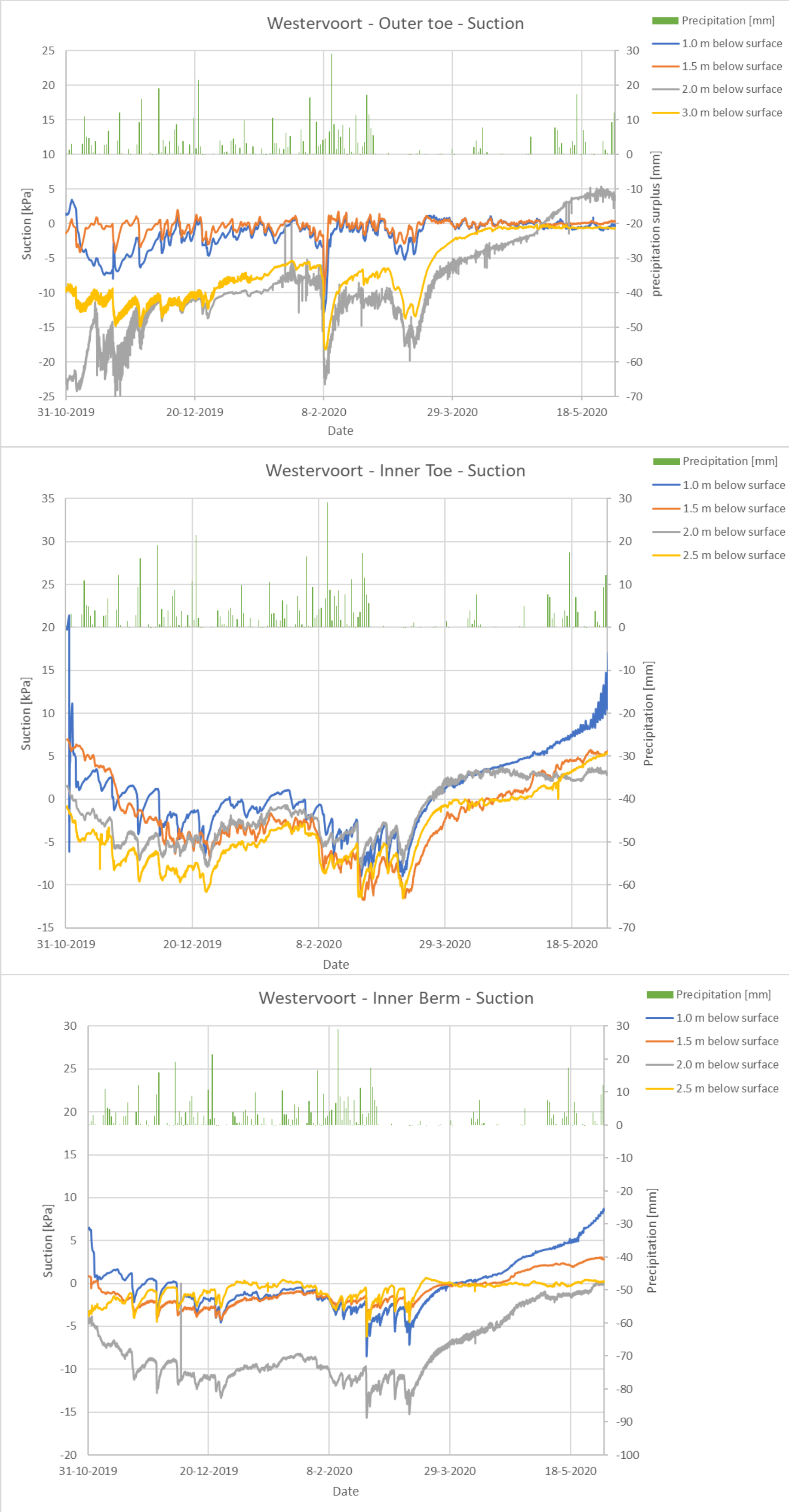

Figure IV-1: The soil suction stresses measured in Westervoort in the outer toe, inner toe and berm with the precipitation.

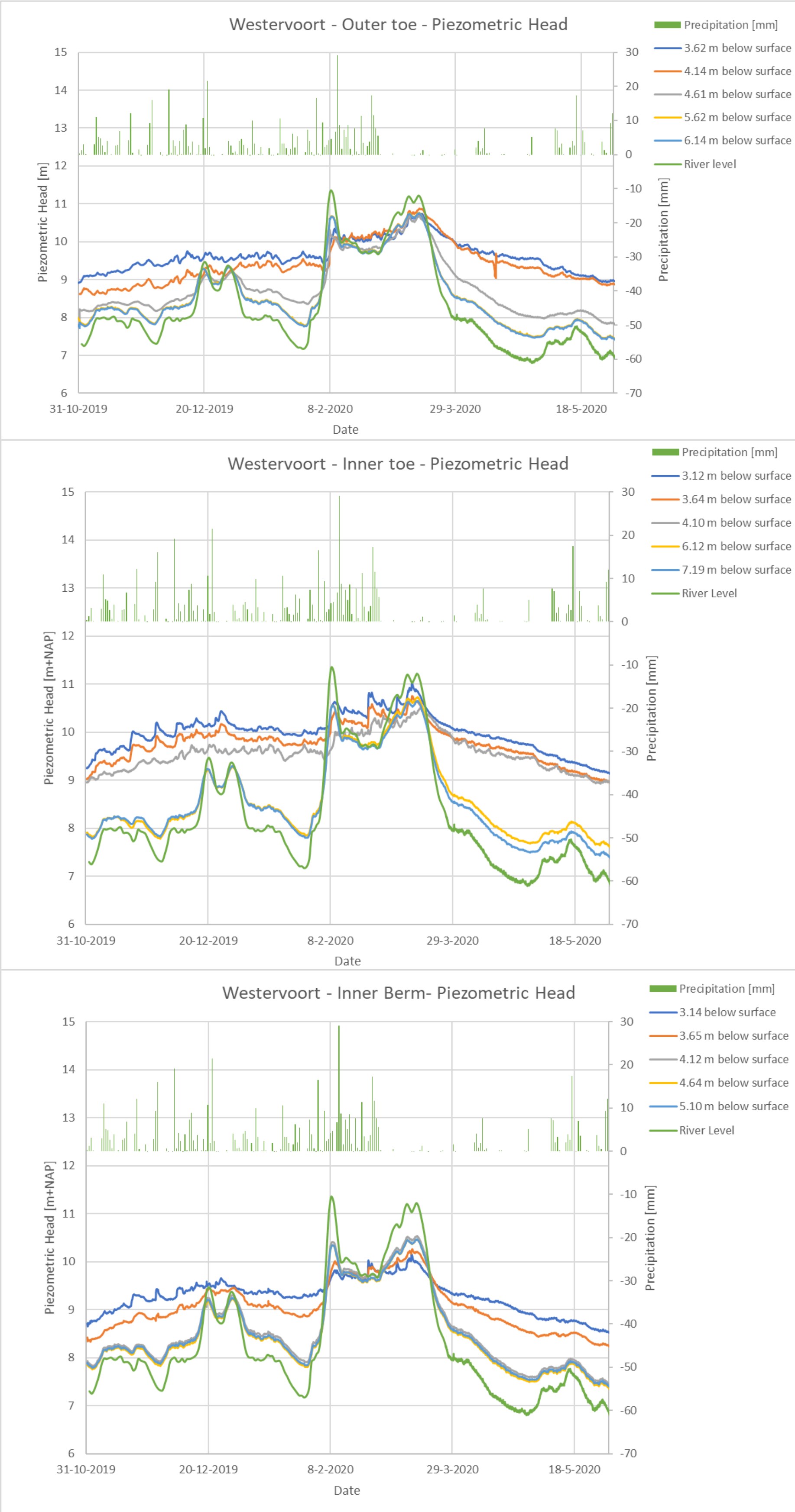

Figure IV-2: The piezometric head measured in Westervoort in the outer toe, inner toe and berm with the precipitation.

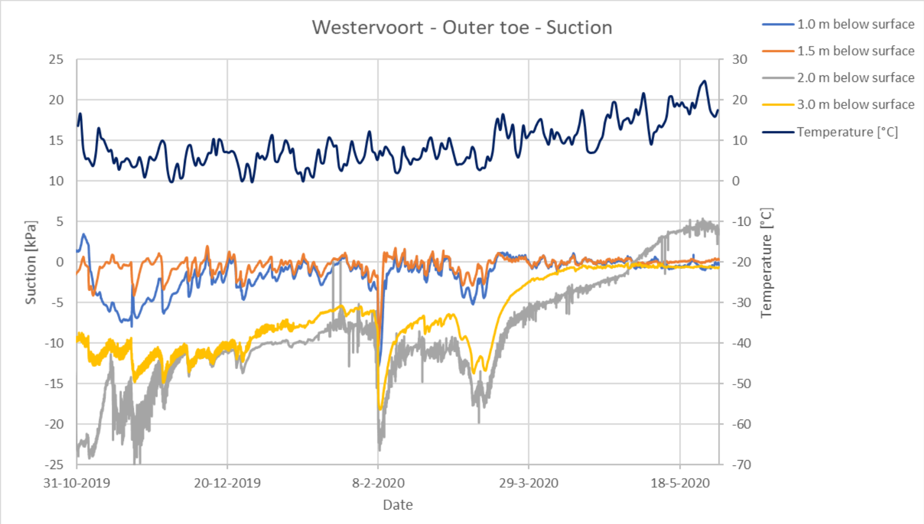

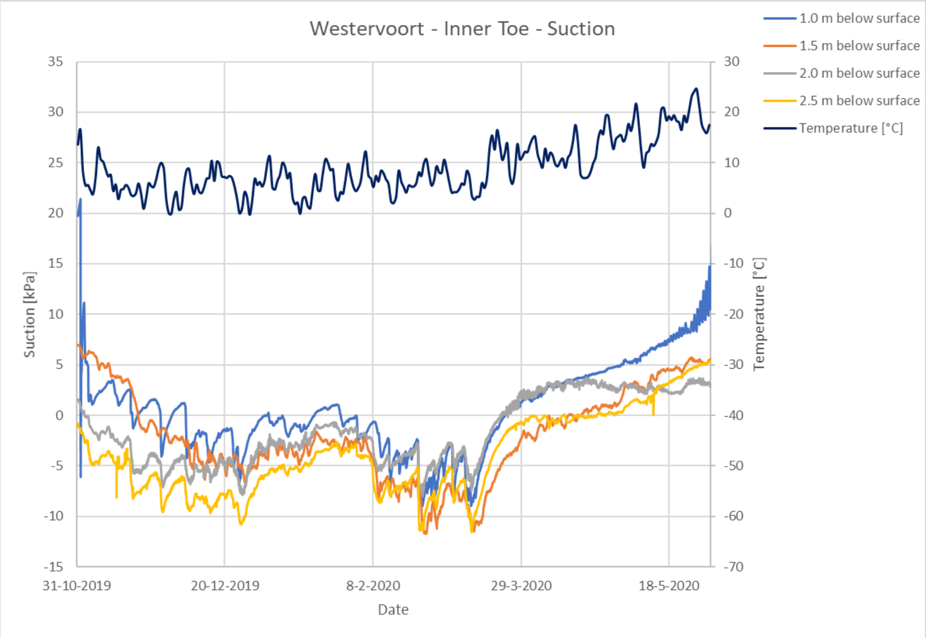

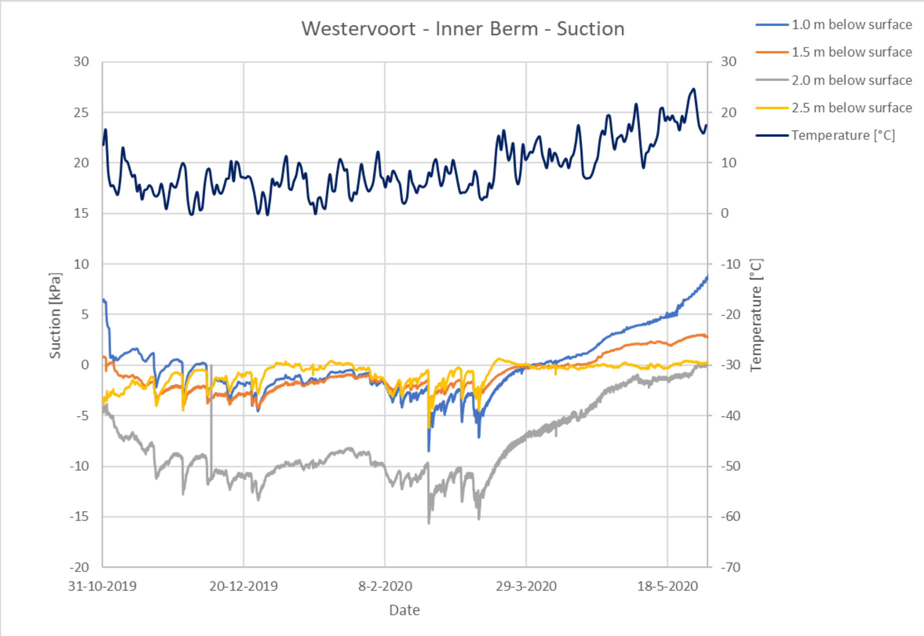

Figure IV-3: The soil suction measured in Westervoort in the outer toe, inner toe and berm with the Temperature.

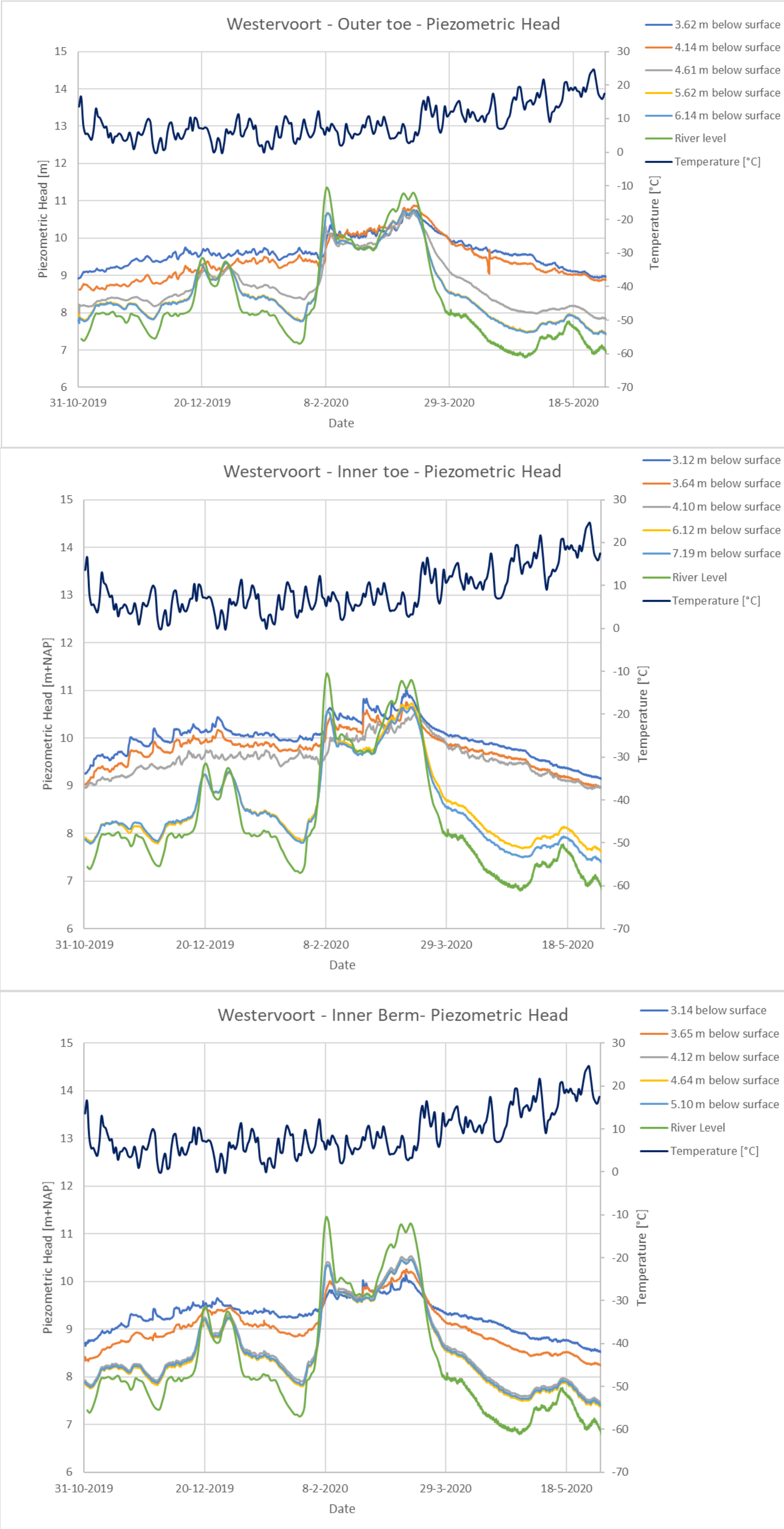

Figure IV-4: The piezometric head measured in Westervoort in the outer toe, inner toe and berm with the Temperature.

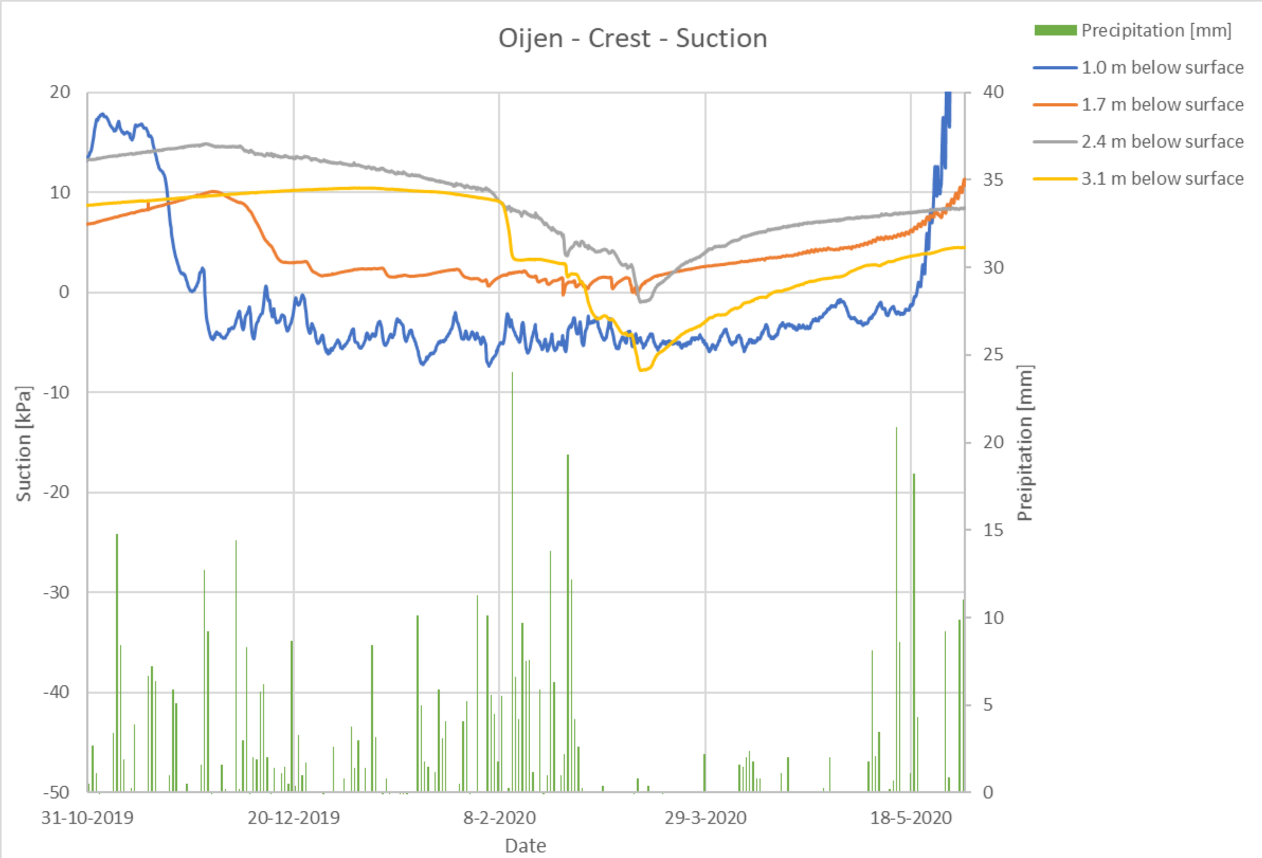

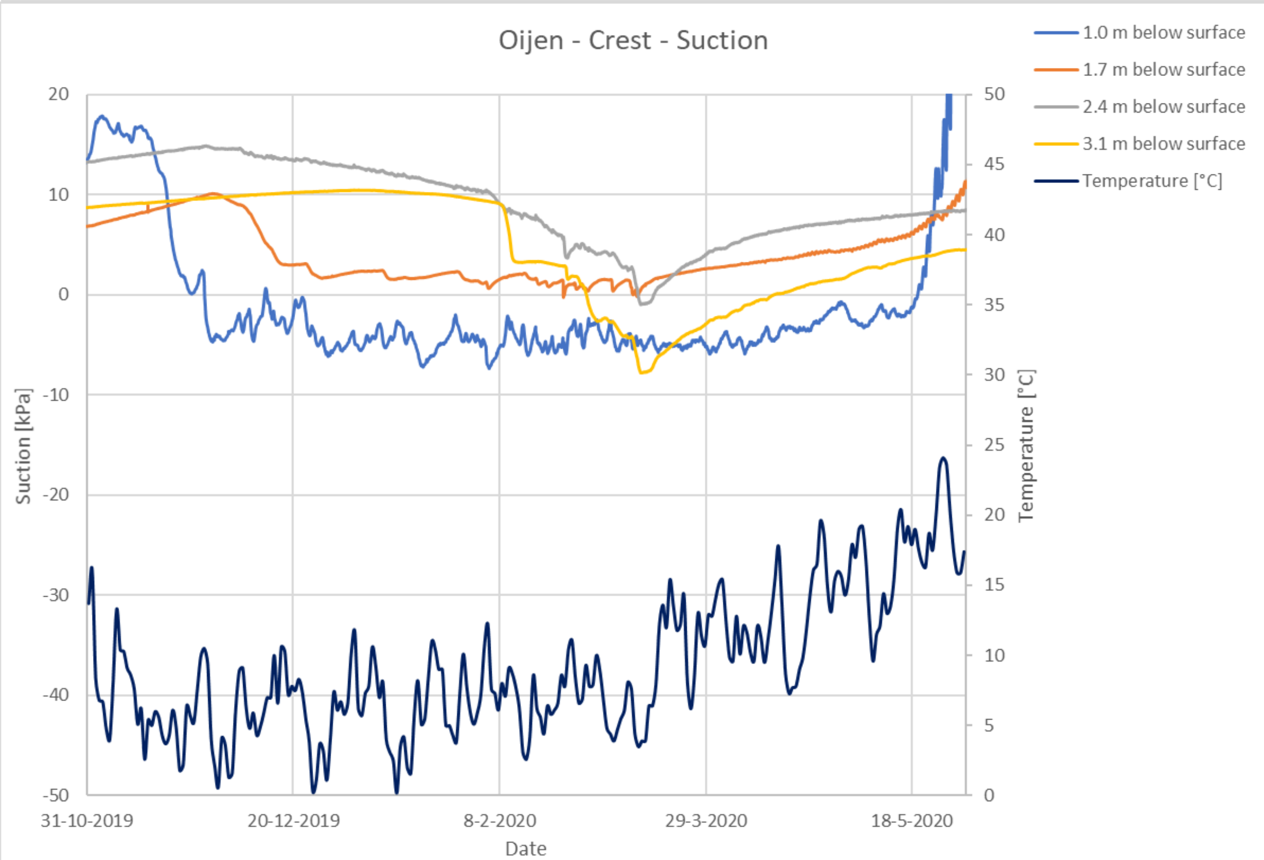

Figure IV-5: The soil suction measured in the crest in Oijen, with the precipitation (upper Figure) or Temperature (bottom Figure).